CELLULAR MECHANISMS REGULATING NEUROMUSCULAR JUNCTION STABILITY AND PLASTICITY IN NORMAL AND DISEASED MICE

by

Julia M. Harrison

Submitted in partial fulfilment of the requirements
for the degree of Doctor of Philosophy

at

Dalhousie University
Halifax, Nova Scotia
November 2019

DEDICATION

To Mom and Dad

Thank you for lifting me up and giving me the courage to pursue my passions. I am a scientist because of you.

TABLE OF CONTENTS

LIST OF TABLES

LIST OF FIGURES

ABSTRACT

The stability of the neuromuscular junction (NMJ) is critical for maintaining independence and quality of life. Therefore, understanding the mechanisms that underlie this stability is of paramount importance to be able to recover function lost due to disease or injury. This thesis seeks to investigate these NMJ stability mechanisms in three states: disease, homeostasis, and repair. First, amyotrophic lateral sclerosis (ALS) is a progressive neurodegenerative disease characterized by distal neuropathy at the NMJ followed by paralysis and motor neuron (MN) death. I found that terminal Schwann cells (TSCs) at a subset of muscle fibres (type IIb, the most susceptible to disease progression in ALS) vanished from denervated endplates after a partial denervation injury in a mouse model of ALS. These endplates were therefore unable to become reinnervated via a compensatory process called collateral reinnervation. I also found that infiltrating macrophages were interacting with these TSCs, and, when inhibited with masitinib, was able to recover TSC loss and reinnervation in ALS mice. Second, I investigated whether muscular BMP4 in a mouse model had similar roles in NMJ homeostasis as had been previously reported in *Drosophila*. NMJs lacking BMP4 had impaired synaptic transmission and fragmented acetylcholine receptor clusters. This resulted in mice with locomotor, strength, and proprioceptive impairments. These results correlate with the previous *Drosophila* literature and provide evidence that the role of this protein at the NMJ is highly conserved. Third, I examined whether muscular BMP4 has a role in neuromuscular reinnervation following Tibial n. crush injury. I found that reinnervated NMJs at muscles lacking BMP4 had impaired reinnervation and delayed withdrawal of polyneuronal innervation. These results were consistent with a delayed maturation phenotype, indicating that BMP4 has similar roles during repair as it does during development. Together, this thesis highlights the complexity of mechanisms that exist at the NMJ to maintain proper function and reveals potential targets to exploit to improve outcomes in ALS as well as following peripheral nerve injury.

LIST OF ABBREVIATIONS AND SYMBOLS USED

α	alpha
AAV	Adeno-associated virus
ACh	Acetylcholine
AChR	Nicotinic acetylcholine receptor
ALS	Amyotrophic Lateral Sclerosis
ALSFRS-R	Amyotrophic Lateral Sclerosis Functional Rating Scale - revised
ATP	Adenosine triphosphate
β	Beta
BDNF	Brain derived neurotrophic factor
bFGF	Basic fibroblast growth factor
BMP4	Bone Morphogenic Protein 4
BMPRI/II	Bone morphogenic protein receptor I/II
BTX	Bungarotoxin
CD68	Cluster of differentiation 68
CGRP	Calcitonin gene-related peptide
ChR2	Channelrhodopsin
CNS	Central nervous system
CRMP	Collapsin response mediator protein
CSA	Cross-sectional area
CTX	Conotoxin
DRG	Dorsal root ganglion
EJP	Excitatory junction potential
EMG	Electromyogram
EPP	Endplate potential
ERK	Extracellular signal-regulated kinase
ES	Embryonic stem
ESCMN	Embryonic stem cell-derived motor neuron
fALS	Familial amyotrophic lateral sclerosis
GAP-43	Growth associated protein 43
gbb	Glass bottom boat
GDNF	Glial cell-derived neurotrophic factor
GSK3β	Glycogen synthase kinase 3
HSA	Human skeletal α-actin
IGF	Insulin-like growth factor
IL-1	Interleukin-1
iPSC	Induced pluripotent stem cell
MN	Motor Neuron
mAChR	Muscarinic acetylcholine receptor
MAP	Microtubule-associated protein
mEPP	Miniature endplate potential
MG	Medial gastrocnemius
NFκB	Nuclear factor kappa-light-chain-enhancer of activated B cells
NCAM	Neural cell adhesion molecule
NMJ	Neuromuscular Junction

NMNAT	Nicotinamide mononucleotide adenyltransferase
Ω	Ohm
PBS	Phosphate Buffered Saline
PD	Partial Denervation
PFA	Paraformaldehyde
PLA	Plantaris
PSD	Postsynaptic Density
sALS	Sporadic amyotrophic lateral sclerosis
SARM1	Sterile Alpha And TIR Motif Containing 1
SC	Schwann Cell
SCG10	Superior cervical ganglion 10
Sema3A	Semaphorin 3A
SNPH	Syntaphilin
SOD1	Superoxide dismutase 1
SOL	Soleus
SMA	Spinal Muscular Atrophy
SV2	Synaptic vesicle protein 2
TA	Tibialis anterior
TC	Tibial nerve crush
TDP-43	Tar DNA binding protein subunit 43
TGF-β	Transforming growth factor beta
TSC	Terminal Schwann Cell
µ	Micro/mu
VAChT	Vesicular acetylcholine transporter
VGluT1	Vesicular glutamate transporter 1
VIP	Vasoactive intestinal peptide
wit	Wishful Thinking
WT	Wild Type

ACKNOWLEDGEMENTS

First, to my supervisor, Dr. Victor Rafuse, who had my best interests at heart throughout this entire journey. Navigating a successful PhD is not easy given the twists and turns that scientific research throws at you, but he was there to provide guidance every step of the way. I hope I absorbed as much of his knowledge as I could over these years.

To the members of the Rafuse lab, past and present, particularly our incredible lab manager, Cindee Leopold, who is an invaluable asset to the Rafuse lab team. Thank you for providing so much support to me over the years. I would also like to thank Borbala Podor for her friendship and assistance on the BMP4 project, as well as Asal Yans, Arul Jude Cline Asainayagam, Ahmad Qureshi, Cameron Penny, Taigan Radomske, and Anna Minarik for help with data acquisition on certain experiments. Earlier students such as Jeremy Toma, Erin Aubrey, Basu Shettar, and Philippe Magown also provided incredible guidance while I was new to the lab.

I specifically want to acknowledge my fellow graduate students over the years. I have gained friends for life, and no one else can relate to graduate school as well as you. Particularly Shannon Hall, Antonios Diab, Alexandria Muise-Hennessey, Emily Capaldo, Lauren Landoni, Stephanie Blandford, Olivier D. Laflamme, and Kaitlin Keller. The support you gave me through our shared experiences was invaluable and I can only hope that I've helped you as well.

To Iain Thompson, you're the one that I want to talk to at the end of a long day. Having you by my side washed away so many of my daily struggles so that I could start each day anew. You kept me sane during a PhD, which is no easy feat.

To my parents, Maxine Langman and Glenn Harrison, not everyone understands the scientific career path. When it was clear that I wouldn't pursue medicine or any of the other professional programs typical of science students, you assured me that I was still on the right path. Since you were both so knowledgeable about the graduate school experience, I was able to dive into this crazy world, unafraid. Every step of the way, from failed (and successful) experiments, to first conferences, to preparing this thesis, you both supported me unconditionally and with wisdom. I cannot thank you enough.

CHAPTER 1: INTRODUCTION

The Motor System

Communication between the nervous system and skeletal muscle is what allows for all voluntary movement that we experience throughout life. Motor commands initiated by upper motor neurons (MNs) in the cerebral cortex are transmitted to lower MNs in the brain stem and spinal cord, which extend axons into the periphery to make synaptic contact with their target muscles at neuromuscular junctions (NMJs). This results in a complex array of possible behaviours, including locomotion, speech, feeding, and tool use. Therefore, the health and function of the motor system and the NMJ are of vital importance to survival and quality of life.

Motor Units

The term given to describe one MN and all the muscle fibres that it innervates is called the motor unit and represents the smallest fraction of muscle force that the central nervous system (CNS) can activate. Early studies in the cat showed that motor unit contractile properties were not homogenous and, in fact, differed substantially with respect to speed of contraction rate and degree of fatigability upon repetitive stimulation (Burke, 1981). Using a combination of contractile speed and fatigue resistance during a repetitive firing fatigability test, Burke and colleagues were able to identify and classify three major classes of motor units: fast fatigable (FF), fast fatigue-resistant (FR), and slow (S) (Burke et al., 1971, 1973; Burke and Tsairis, 1973). Furthermore, the authors showed that each motor unit subtype contained histologically distinct muscle fibre types that were later shown to correspond to different distinct skeletal myosin subtypes (Burke et al., 1971, 1973; Burke and Tsairis, 1973). Finally, subsequent studies later showed that MNs within the different motor unit subtypes differed with respect to rheobase (related to soma size), input resistance (related to excitability) and conduction velocity (related to axon size) (Fleshman et al., 1981; Zengel et al., 1985; Lorenz and Jones, 2014).

In general, MNs within FF motor units have large somas, relatively low input resistances, fast conduction velocities, and they innervate large diameter muscle fibres expressing myosin type IIb (Burke et al., 1971, 1973; Fleshman et al., 1981; Zengel et al.,

1985). FR motor units contain MNs with relatively moderate input resistances, slower conduction velocities, and they innervate a relatively smaller number of smaller diameter muscle fibres expressing myosin type IIa. Finally, MNs with the highest input resistances and slowest conduction velocities are contained within S motor units and they innervate the fewest number of small muscle fibres that express type I myosin. Because the orderly recruitment of motor units is determined, in large part, by their input resistance, S units are typically recruited before FR units, while FF motor units are recruited last during muscle contraction (Henneman et al., 1965a, 1965b). This orderly recruitment of motor units is commonly referred to as the Henneman's size principle (Henneman, 1957; Henneman et al., 1965a). Although, it is important to note that motor units activated by a specific activity may not include S units, with size-ordered recruitment occurring within the population of MNs necessary for the particular movement (Bawa et al., 2014). Finally, because motor unit subtypes have different excitability and fatigability, S units tend to populate postural muscles that tend to be activated throughout the day (and are fatigue resistant) while muscles used for strength tasks tend to be more populated by large, FF motor units.

The Neuromuscular Junction (NMJ)

The NMJ is the name given to the synapse between MNs and a specialized region of the muscle known as the endplate. They are also the largest and most extensively studied synapse in the body (Sanes and Lichtman, 1999). As the communication point between the nervous system and the muscular system, these synapses are critically important in maintaining normal behaviour. Incredibly, NMJs are formed during development and are maintained throughout life, and the mechanisms underlying this stability are fundamental to understanding neuromuscular disease and repair. Therefore, the focus of this thesis is to investigate how mechanisms at the NMJ contribute to the stability/instability of the synapse during 1) disease, 2) homeostasis, and 3) injury.

Considering the experimental accessibility of the NMJ, it was historically the most commonly studied synapse, and formed the foundation of our understanding of synaptic structure and transmission. In 1928, Fernando Tello, working under Santiago Ramon y Cajal, identified the general aspects of NMJ synaptogenesis and repair using

only a light microscope (Cajal, 1928; Sanes and Lichtman, 1999). A few years later, the first in-depth analysis of synaptic transmission utilized the vertebrate NMJ as a model, identifying acetylcholine (ACh) as the neurotransmitter (Dale et al., 1936), later found to be released within vesicular quanta (Katz, 1966). The advent of intracellular recording and electron microscopy technologies in the 1950s yielded further and more detailed analyses of NMJ structure and function (Sanes and Lichtman, 1999). Given the extensive research on the NMJ throughout the 20th century, it is no surprise that the first neurotransmitter receptor ever to be purified and sequenced was the nicotinic ACh receptor (AChR) in the electric organ of *Torpedo californica*; the same receptor found at the mammalian NMJ (reviewed by Duclert and Changeux, 1995).

The NMJ is composed of three cellular components: the MN, muscle fibre, and terminal Schwann cell (TSC; also referred to as the perisynaptic Schwann cell). It is the interplay between these cell types that establishes the NMJ during development, maintains its homeostasis throughout life, and governs its plasticity after an injury (Ogata, 1988; Sanes and Lichtman, 1999). The MN component of the NMJ is called the motor-nerve terminal or synaptic bouton, and it contains large numbers of ACh-filled synaptic vesicles as well as mitochondria to supply the energy necessary for ACh synthesis and release (Sanes and Lichtman, 1999). The vesicles themselves contain various vesicular proteins including synaptic vesicle protein 2 (SV2), synaptobrevin, synaptotagmin, synaptophysin, and the vesicular ACh transporter (VAChT). Also present at the active zone within the MN terminal are voltage-dependent potassium and calcium channels, which respond to membrane depolarizations due to action potentials and are necessary for calcium influx and vesicle fusion (Robitaille et al., 1993; Sugiura et al., 1995; Day et al., 1997).

The presynaptic terminal rests within a depression on the surface of the muscle fibre, which contains the postsynaptic site such that one muscle fibre is associated with one NMJ in the adult. This postsynapse is elaborated into ~1 μm deep junctional folds which increase the surface area available for AChRs (Sanes and Lichtman, 1999). The receptors are located in high density (>10,000/μm) along the peaks of these junctional folds and extend partially down the troughs, which contain high concentrations of sodium channels and neural cell adhesion molecule (NCAM) (Covault and Sanes, 1986; Flucher

and Daniels, 1989; Sanes and Lichtman, 1999). Junctional fold structure and receptor localization are maintained by a complex network of cytoskeletal proteins including rapsyn, utrophin, dystrophin, ankyrin, and α-dystobrevins 1 and 2 (Sealock et al., 1984; Covault and Sanes, 1986; Flucher and Daniels, 1989; Peters et al., 1998; Wood and Slater, 1998). Additionally, a basal lamina surrounds each muscle fibre and extends through each synaptic cleft. Synaptic basal lamina locations contain acetylcholinesterase (Krejci et al., 1997), glycoconjugates (Scott et al., 1988), neuregulin, and agrin; the last two of which are necessary for the clustering and formation of AChRs at the synaptic site (McMahan, 1990; Cohen and Godfrey, 1992; Reist et al., 1992; Goodearl et al., 1995; Loeb and Fischbach, 1995; Sandrock et al., 1997).

The third cell type at the NMJ, the TSC, is the least studied and therefore its role has been historically relatively poorly understood. Each NMJ typically has 2-3 TSC cell bodies whose processes intimately cap and line the presynaptic neuron. These TSCs differ from typical, myelinating SCs. While derived from the same progenitors as SCs, TSCs do not produce myelin or any myelin-associated proteins. Much of the discussion surrounding the role of TSCs at the NMJ have been related to the generic glial role of "support" to the synapse. More recently, studies have revealed that TSCs monitor synaptic transmission in a calcium-dependent manner and respond following its loss to re-establish innervation following denervation (discussed further below) (Reist and Smith, 1992; Reynolds and Woolf, 1992; Georgiou et al., 1994; Son and Thompson, 1995a; Robitaille, 1998; O'Malley et al., 1999; Rochon et al., 2001; Reddy et al., 2003; Colomar and Robitaille, 2004; Feng and Ko, 2008; Rousse et al., 2010; Todd et al., 2010; Darabid et al., 2013).

During development, the three cells of the NMJ have different lineages and must all meet at the synapse. MNs and SCs are both ectodermal in origin, MNs are derived within the developing neural tube while SCs come from migrating neural crest. MNs are born in the ventral neural tube and their axons exit the CNS via the ventral roots or cranial nerves to reach their target muscles. En-route to the periphery, motor axons encounter SCs in, or near, the somites, and then the two components travel together to make contact with muscle fibres (Sanes and Lichtman, 1999). There is some debate as to whether the MN or the SC provides the guidance for this journey during development. It

has previously been shown that motor axon growth cones lead while SCs follow closely behind (however, see Riethmacher et al., 1997). During regeneration, however, it is known that the SC processes provide the direction and scaffold for regenerating neurons (Son and Thompson, 1995b).

Muscle fibres are derived from mesodermal cells, which obtain their myogenic fate within the somites before migrating to sites where they will form muscles (Sanes and Lichtman, 1999). These committed myogenic cells divide at the muscle site and are then referred to as myoblasts. Myoblasts arrange into bundles and begin to fuse to form multinucleated myotubes. During this time, contractile proteins are beginning to be synthesized, though the maturation from myotube to muscle fibre is generally accepted to be when the previously centrally located nuclei become peripherally located (Sanes and Lichtman, 1999). Interestingly, following muscle damage, regenerating muscle in adults also have centrally located nuclei. This is one of countless examples where regenerative phenotypes closely recapitulate observations during development.

Synaptic transmission begins soon after the motor axons and SCs arrive at the developing myotube (Sanes and Lichtman, 1999). The growth cones convert to nerve terminals, and AChRs begin to cluster in the muscle (Sanes and Lichtman, 1999). It appears that the location of the motor axon contact with the muscle induces AChR clustering via agrin, rather than motor axons seeking out previously formed spontaneous AChR clusters, which are eventually lost as the muscle matures (Bennett and Pettigrew, 1976; Anderson and Cohen, 1977; Frank and Fischbach, 1979; McMahan, 1990). Motor axons contact developing myotubes at the nerve entry point to the muscle and the muscle grows symmetrically on both sides, leading, in part, to the stereotypical pattern of NMJ location in a central band across muscle fibres (Zhang and McLennan, 1995).

At the same time as early NMJs are forming, there are extrasynaptic repression mechanisms to limit NMJ patterning outside the immediate synaptic site. A prominent theory is that activity provides a driving force to maintain AChR clustering at the NMJ and limits its expression extrasynaptically (Lomo and Westgaard, 1975; Sanes and Lichtman, 1999). Preventing transmission at the NMJ has been shown to induce AChR synthesis and, correspondingly, electrical stimulation of muscle fibres represses AChR gene expression (Lomo and Westgaard, 1975; Fambrough, 1979; Goldman et al., 1988).

In this way, ACh itself negatively regulates its receptors at a distance, while those receptors located immediately at the synapse appear immune (Sanes and Lichtman, 1999).

At birth, each immature endplate is polyneuronally innervated by several MNs (Redfern, 1970). During the first few postnatal weeks, NMJ structure and function changes rapidly. MNs withdraw from the endplate until a single axon remains and the NMJ morphologically changes from an elliptical plaque of AChRs on the postsynaptic site to a pretzel like structure. While the mechanisms governing this process are not fully understood, regions of low AChR density appear in the plaques in locations not immediately apposed by the motor terminal, likely due to reduced activity at these sites. As these extraneous AChRs are lost, the postsynaptic apparatus takes on the classical pretzel shape associated with mature NMJs (Nystrom, 1968; Steinbach, 1981; Slater, 1982; Balice-Gordon and Lichtman, 1993). As the body grows and muscles elongate, depressions within the muscle fibre at the NMJ begin to appear, which then further invaginate to form junctional folds immediately apposed to active zones in the corresponding nerve terminal (Sanes and Lichtman, 1999). AChRs undergo alterations in subunit composition and become more stable. Whereas their half-life prenatally was on the order of ~ 1 day, perinatally, this increases to more than 10 days (Salpeter and Loring, 1985). AChRs at this time also become increasingly resistant to dispersal (Bloch et al., 1986). This increase in stability could be due to alterations in AChR interactions with the basal lamina or the postsynaptic cytoskeleton. Agrin, which clusters AChRs, binds to dystroglycan which in turn binds to the cytoskeleton. This complex has also been shown to mature postnatally and potentially contributes to AChR stability (Campanelli et al., 1994; Bewick et al., 1996; Namba and Scheller, 1996; Grady et al., 1997; Xu and Salpeter, 1997).

As aforementioned, mature NMJs exist throughout life and only seem to lose their stability with age. Time-lapse imaging of mouse NMJs revealed that the general structure of endplates did not change over the majority of life, although there was a tendency for endplates to enlarge with age (Lichtman et al., 1987; Balice-Gordon and Lichtman, 1990; Balice-Gordon et al., 1990; Wigston, 1990). In support of this theory, the postsynaptic structure of AChRs remains stable long after motor terminals and SCs degenerate

following axotomy, in some cases for over 4 months (Frank et al., 1976). A potential candidate for this stability is the basal lamina, which has been shown to induce post-synaptic patterning in regenerating muscles (Burden et al., 1979; Goldman et al., 1991; Brenner et al., 1992; Jo and Burden, 1992), so it is, therefore, tempting to consider that it plays a role in synapse maintenance. The basal lamina also actively inhibits TSC process extension into the synaptic cleft (Patton et al., 1998). In the absence of the synaptic laminin β2 chain, TSC processes infiltrate the cleft and impair transmission (Noakes et al., 1995). As correct TSC apposition is also essential for a healthy NMJ, the basal lamina plays a key role in maintaining this balance.

The basal lamina, however, is not sufficient to account for NMJ stability considering that nerve terminals do not remain at the NMJ long after muscle degeneration (Rich and Lichtman, 1989a). It also seems as though the nerve terminal requires ongoing retrograde signaling from the muscle to remain present. In a study where researchers injected toxins into otherwise healthy muscle, the nerve terminals quickly withdrew from their NMJs (McCann et al., 2007). Finally, synaptic activity is also stabilizing. Activity becomes increasingly reduced with age, which correlates with a decline in the number of AChRs as well as more terminal sprouts (Courtney and Steinbach, 1981; Rosenheimer and Smith, 1985). These effects of ageing can be slowed with exercise in older animals and accelerated with inactivity (Smith and Rosenheimer, 1982; Fahim, 1989; Pachter and Spielholz, 1990), further supporting that active synaptic transmission itself stabilizes the synapse. Therefore, it seems that all components of the NMJ, including its own function, coordinate to maintain these synapses throughout life.

The concept of NMJ stability is also fundamental to understanding neuromuscular diseases, considering that neuromuscular denervation is a hallmark of many conditions including amyotrophic lateral sclerosis (ALS), spinal muscular atrophy (SMA) muscular dystrophy, and myasthenia gravis. Understanding the mechanisms that underlie homeostatic and injury induced NMJ stability will ultimately allow us to understand how these processes are perturbed during disease progression.

Peripheral Nerve Injury

Peripheral nerves are particularly susceptible to damage due to injury or disease considering their exposure in the body, compared to the relative safety of structures within the CNS. These peripheral nerves lack the structural protection of the cranium, vertebrae, meninges, as well as the chemical protection of the blood brain barrier. As such, peripheral nerve damage can arise from a wide variety of events, from physical trauma such as a crush, stretch, or transection, to non-traumatic causes such as disease, genetics, or drugs (Caillaud et al., 2019). The general mechanisms that govern peripheral nerve degeneration and regeneration have been extensively studied and are outlined below. However, even with this current state of understanding, effective therapies to significantly improve functional outcomes have remained elusive, and the best predictors of recovery are the severity of the injury as well as its proximity to the target tissue relative to the cell body.

Nerve Degeneration

In response to axonal injury, the peripheral nerve segment distal to the injury site undergoes a stereotyped process of degeneration known as Wallerian degeneration, named after the scientist, Augustus Waller, who first observed this process (Waller, 1851). Wallerian degeneration is a structured and organized form of axon degeneration (Stoll et al., 1989). In mice, the distal segment remains intact for about 36 hours, followed by rapid axonal fragmentation and the breakdown of myelin (Beirowski et al., 2005; Ding and Hammarlund, 2019). This debris is cleared by activated macrophages resident in the nerve tissue, in addition to circulating macrophages, attracted to the injury site by monocyte chemoattractant protein-1 produced by SCs (Toews et al., 1998; Caillaud et al., 2019).

Nicotinamide mononucleotide adenyltransferase (NMNAT) is an axonal survival factor. In response to axon transection, NMNAT levels decrease and local calcium levels increase, contributing to the activation of Sterile Alpha and TIR Motif Containing 1 (SARM1), a key regulator of Wallerian degeneration (Osterloh et al., 2012; Girouard et al., 2018). Activated SARM1 drives the fragmentation and degeneration of the distal axon via calpain, which in turn causes the disassembly of the cytoskeleton and impairs

mitochondrial function (Girouard et al., 2018). Importantly, disruption of this pathway, by administering NMNAT, or inhibiting calpain or SARM1, have been shown to delay Wallerian degeneration post injury by two weeks or more (George et al., 1995; Sasaki and Milbrandt, 2010; Girouard et al., 2018; Ding and Hammarlund, 2019).

Degeneration can also occur in response to disease. For instance, peripheral nerve degeneration is a hallmark of ALS, which actually precedes gross observable motor deficits (Frey et al., 2000; Clark et al., 2016). Mechanisms of axon degeneration in ALS are similar to Wallerian degeneration in that there is ultimate cytoskeletal breakdown and axonal fragmentation (Frey et al., 2000). One key difference in ALS, however, is that neuromuscular denervation precedes evidence of axon degeneration and the axon withdraws from the synapse. The pattern of degeneration of the axon thus begins at the terminal and progresses proximally, rather than the case in traditional Wallerian degeneration were degeneration progresses from the injury site distally (Frey et al., 2000). Another difference is that axonal degeneration in ALS is not an all-or-nothing event with the axon suddenly retracting all at once; but rather a progressive process of retraction, regeneration, and sprouting until ultimately the disease takes over (Clark et al., 2016; Martineau et al., 2018). There is also evidence that early axon degeneration in ALS is associated with protein aggregation within the axon (Frey et al., 2000), which is not the case in injury-induced, Wallerian degeneration.

Nerve Regeneration

While the distal axon segment undergoes Wallerian degeneration following injury, the proximal nerve segment prepares for regeneration (Girouard et al., 2018). Primarily, the cut axon must transform into a growth cone to allow for successful axonal extension (Bradke et al., 2012). For this to occur, extensive remodeling of the cytoskeleton takes place, including the breakdown and restructuring of microtubules, neurofilaments, actin, spectrin, and ankyrin (Kamakura et al., 1983; Malik et al., 1983; Yoshida et al., 1984; Schlaepfer and Zimmerman, 1985; Billger et al., 1988; Roberts-Lewis et al., 1994; Spira et al., 2003; Verma et al., 2005; Schafer et al., 2009; Girouard et al., 2018). Neurons also produce numerous proteins and neuropeptides associated with growth during the few days following injury, including brain-derived neurotrophic factor (BDNF), glial cell

line-derived neurotrophic factor (GDNF), c-jun, growth-associated protein 43 (GAP-43), calcitonin gene-related peptide (CGRP), vasoactive intestinal peptide (VIP), substance P, and somatostatin, all of which contribute to growth cone formation during the first week following injury (Caillaud et al., 2019). The developing growth cone also produces proteases to help eliminate collagen-containing scar tissue, which would impede the path of the regenerating axon (Geraldo and Gordon-Weeks, 2009).

Formation of new growth cones in invertebrate models have also been shown to depend on calcium-dependent calpain signaling (Geraldo and Gordon-Weeks, 2009), which, interestingly, has a different role in the distal axon segment (Girouard et al., 2018). Research into the role of calcium on new growth cone formation in vertebrate models is less advanced, although it has been shown that there is an early influx of calcium following injury that is correlated with greater recovery potential (Williams et al., 2014). In contrast, limiting influx later during degeneration is beneficial (Ribas et al., 2017). Therefore, calcium plays key roles in both the proximal and distal nerve segments following injury, both promoting growth cone formation and degradation, respectfully.

This concept of one factor having dual roles in both degeneration and regeneration is not unique to calcium/calpain. Other proteins involved in both processes include superior cervical ganglion 10 (SCG10) or stathmin 2, and Collapsin Response Mediator Protein (CRMP) family proteins (Girouard et al., 2018). SCG10 regulates microtubule dynamics and neurite outgrowth in developing sensory neurons (Sugiura and Mori, 1995; Morii et al., 2006; Shin et al., 2014). In peripheral nerve injury, SCG10 accumulates at the injury site in the proximal nerve segment and promotes the microtubule reassembly necessary for regeneration, while SCG10 depletion in the distal segment accelerates axon fragmentation (Riederer et al., 1997; Mason et al., 2002; Shin et al., 2014). CRMP proteins are also associated with microtubules and overexpression promotes regeneration in injured MNs (Fukata et al., 2002; Suzuki et al., 2003). CRMP2 activity is regulated by glycogen synthase kinase 3 (GSK3β), which is inactivated in regenerating axons, thus, promoting microtubule polymerization by CRMP2 (Wakatsuki et al., 2011; Xiong et al., 2013; Liz et al., 2014). Conversely, in the degenerating segment, activation of GSK3β leads to the phosphorylation of CRMP2, which in turn accumulates in axons undergoing Wallerian degeneration (Wakatsuki et al., 2011).

Another key factor necessary for successful axon regeneration are mitochondria, which provide the necessary energy required for new protein synthesis, growth cone formation, and axon outgrowth. Increasing mitochondrial density in the proximal segment of an injured axon improves axon regeneration in *C. elegans* (Han et al., 2016). Mitochondria have also been observed to accumulate naturally in MNs following injury (Kiryu-Seo et al., 2016). Promoting mitochondrial motility after injury in mammalian axons by knocking out its anchoring protein, syntaphilin (SNPH), also enhances axon regeneration (Zhou et al., 2016). Considering the high energy demand of regeneration, this accumulation of mitochondria is not surprising.

Outside the axon itself, SC and fibroblast activation is also necessary for regeneration. SCs are stimulated to proliferate by interleukin-1 (IL-1), transforming growth factor β (TGFβ), and insulin-like growth factor (IGF), which are secreted by macrophages that have entered the injury site to phagocytose debris (Baichwal et al., 1988; Zochodne, 2000; Ronchi et al., 2009). This proliferation reaches peak levels around 3-4 days following injury (Caillaud et al., 2019). SCs, in turn, secrete nerve growth factor (NGF), which, as its name suggests, stimulates regeneration in the proximal segment of the axon as well as further SC proliferation (Lunn et al., 1990). SCs and fibroblasts infiltrate the injury site and form a tissue bridge between the proximal and distal segments, called a neuroma (Caillaud et al., 2019). Proliferating SCs also align themselves along the distal axon segment into interdigitating bands along the endoneurium (known as bands of Büngner) that ultimately guide the regenerating axon (Son and Thompson, 1995b; Burnett and Zager, 2004). Finally, these SCs also secrete basal lamina along the endoneurium, filled with fibronectin and laminin, that promotes growth cone adhesion (Lunn et al., 1990). SC extension seems to be the limiting factor to axon regeneration, further confirming that axon regeneration is dependent on SCs (Son and Thompson, 1995b).

As the regenerating axon approaches its target in the following weeks after injury, the new axon segment must now mature to make a functional connection (Caillaud et al., 2019). At this time, SC proliferation is no longer necessary and they make the switch to a pro-myelinating phenotype, responding to axonal release of neuregulin-1 type I and III, ATP, and ACh (Birchmeier and Nave, 2008; Vrbova et al., 2009). Approximately five

weeks after injury, there is a decreased expression of metabolic growth and signaling proteins, while the expression of proteins involved in lipid metabolism and other pro-myelinating proteins increases, indicating that the maturation process has begun (Jimenez et al., 2005). Once the axon is myelinated, normal neurotransmission can occur, though it is not for some months before all signs of regeneration have diminished. For instance, the regeneration of the mature perineurium is still ongoing about three months after injury (Caillaud et al., 2019).

Collateral Reinnervation

Under some circumstances, an injury or disease can lead to the degeneration of a subset of MNs within a muscle (partial denervation), leaving other MNs within the same muscle unaffected. The process by which these remaining MNs compensate for the loss of their neighbours is called collateral reinnervation or sprouting. This process results in an up to four-fold increase in size (i.e. number of muscle fibres innervated by each MN) of the remaining motor units as each MN becomes responsible for more muscle fibres (Rafuse et al., 1992; Tam et al., 2001; Tam and Gordon, 2003).

Early studies on partial denervation injuries in experimental animals revealed that muscle strength is quickly recovered following injury, even without regeneration of the cut nerve (Hines et al., 1945; Van Harreveld, 1945; Weiss and Edds, 1946). Further work in the following years revealed that this recovery of muscle strength is due to the branching of new axonal sprouts of neighbouring intact axons to re-innervate the orphaned endplates (Edds, 1950; Hoffman, 1950; Van Harreveld, 1952; Morris, 1953).

This phenomenon was described both in the context of injury, but also in diseases such as poliomyelitis and ALS (Wohlfart and Hoffman, 1956; Wohlfart, 1957). In the former, collateral branches are observed regularly, as early as nine days post paralysis-onset in a mouse Theiler's encephalomyelitis model. The majority of branches were observed distally within the muscle itself, typically from nodes of Ranvier or intact NMJs (Wohlfart and Hoffman, 1956). Immature branches were even observed in later disease stages, indicating that the recovery process was still ongoing and was not limited to the immediate time period following paralysis-onset (Wohlfart and Hoffman, 1956). In ALS, signs of collateral sprouting and nerve regeneration are often observed in patients, and it

was hypothesized that collateral reinnervation could be contributing to the fasciculation phenotype observed in this disease (Wohlfart, 1957). However, there is an ongoing battle between degeneration and regeneration such that regenerative mechanisms are overwhelmed by the degenerative ones. With the advent of transgenic models to study ALS approximately forty years later, conflicting evidence of the sprouting capacity of these mice, compared to previous human studies, revealed a challenge in ALS research that persists to this day (Schaefer et al., 2005). The findings of sprouting capacity in ALS animal models are outlined in more detail below.

It wasn't until 1995 when work by Son and Thompson revealed that collateral reinnervation is regulated by TSCs, the non-myelinating glia residing at the endplate and contribute to NMJ maintenance and plasticity. This was the first evidence to suggest that mechanisms outside the MN itself drive this regenerative process. They showed that following muscle denervation and prior to collateral sprouting, TSCs at denervated NMJs extend processes into the surrounding muscle parenchyma to encounter nearby innervated NMJs (Son and Thompson, 1995a, 1995b). The TSC processes then induce the motor axon to sprout and are used as guides to direct axonal sprouts to denervated endplates, leading to an increase in motor unit size (Son and Thompson, 1995a, 1995b). Evidence to confirm that motor axons more or less blindly follow TSC processes comes from the observation that in cases where TSC processes extended past the immediate area of a previously denervated endplate, the new motor axon would also grow along these processes, indicating that the motor axons do not stop growing after innervating a new endplate (Son and Thompson, 1995b). SCs along peripheral nerves behave in a similar fashion following nerve transection with SC growth preceding the regenerating axon and limiting the rate of axonal regeneration (Son and Thompson, 1995b). More recently, there is evidence to support the view that TSCs are intimately aware of synaptic transmission at the NMJ, and this response to denervation is likely a response to the loss of synaptic transmission (Robitaille, 1998; Colomar and Robitaille, 2004; Rousse et al., 2010; Todd et al., 2010; Arbour et al., 2015).

Amyotrophic Lateral Sclerosis

ALS is a MN disease characterized by neuromuscular denervation followed by the death of lower MNs in the brain stem and spinal cord, and ultimately upper MNs in the brain (Statland et al., 2015). It is a rapidly progressive neurodegenerative disease with death typically within 3-5 years of diagnosis and an incidence of about 2/100,000 individuals (Chancellor and Warlow, 1992; Traxinger et al., 2013; Statland et al., 2015). By the end-stage of the disease, paralysis of respiratory muscles results in the need for respiratory assistance; consequently, respiratory complications are the most common cause of death in people with ALS (Statland et al., 2015).

There are two major classes of ALS: familial (fALS), where there is a known inherited genetic cause for the disease, accounting for only about 10% of cases; and sporadic (sALS), where there is no family history or known gene mutation associated with the disease, which accounts for about 90% of cases. Both sALS and fALS have similar patterns of degeneration and disease course (Horton et al., 1976), though cases of fALS are often more rapidly progressive.

Another way to classify ALS cases is by the location of paralysis onset. Individuals with limb onset ALS experience their earliest symptoms distally in the upper or lower extremities, typically one side before the other, with paralysis progressing inwards towards the trunk (Statland et al., 2015). These individuals experience gross motor deficits as a result of their paralysis, although often retain the use of their head and neck muscles until much later in the disease. In contrast, bulbar-onset patients experience initial paralysis in their neck or facial muscles, often affecting speech early in the disease (Statland et al., 2015). These individuals retain ambulatory control longer during the disease but will have trouble speaking or holding their head upright.

ALS models

The first genetic mutation linked to the development of fALS was the glycine to alanine substitution at position 93 of the gene encoding Cu,Zn superoxide dismutase 1 (SOD1), referred to as the $SOD1^{G93A}$ mutation. Overexpression of this human transgene in mice led to the discovery of the first ALS disease model in 1994, the $SOD1^{G93A}$ mouse (Gurney et al., 1994), which continues to be the most commonly studied model in ALS

research, including this thesis. These mice display muscle specific denervation as early as P40, prior to MN loss from the spinal cord (Hegedus et al., 2007). This is followed by hindlimb weakness by 3 to 4 months of age, which accelerates to paralysis and severe deterioration of gait by 5 months, at which point mice were typically moribund (Gurney et al., 1994). As disease progresses, there is a loss of MNs and denervation-induced atrophy of skeletal muscle (Gurney et al., 1994). There are currently many variations of the $SOD1^{G93A}$ mouse, which vary predominantly in terms of their background and copy number of the mutant transgene, both of which impact the time course and severity of the disease.

In addition to the $SOD1^{G93A}$ mutation, there have been numerous other SOD1 mutations that have been found to cause ALS, impacting various aspects of SOD1 function. More recently, TDP-43-positive inclusions observed in cases of human sALS, as well as mutations of its gene discovered in fALS cases, led to the development of new ALS models surrounding TDP-43. Finally, the most recent major discovery in terms of ALS models was the discovery that repeat expansions in C9orf72 are responsible for the majority of ALS cases (DeJesus-Hernandez et al., 2011; Renton et al., 2011). However, development of models using these mutations has been challenging considering their complexity, and many of them do not recapitulate the human disease as well as the $SOD1^{G93A}$ mouse.

Some critiques of the $SOD1^{G93A}$ mouse have questioned whether an overexpression of the mutant human gene in a mouse accurately represents the human condition. Though all major hallmarks of human ALS align with the disease of $SOD1^{G93A}$ mice, the time course of the mouse model is largely accelerated compared to human cases, even when considering the relative lifespans of humans versus mice. This led to the development of more slowly progressing ALS models, such as the $SOD1^{G37R}$ mouse, which have a much later disease onset in addition to a more prolonged disease course. Consequently, models like these have the additional challenge of laboratory efficiency and length of studies required to observe a progressive degenerative disease.

Another drawback of the transgene overexpression in $SOD1^{G93A}$ mice is the question of whether the high copy number itself leads to an unnatural amount of the mutation that has additional complications to the mutation itself. It has been shown that

severity of disease phenotype correlates with the degree of protein overexpression (Gurney et al., 1994; Alexander et al., 2004; Wang et al., 2009). This agrees with the findings that mutant SOD1 likely takes on a toxic gain of function, rather than loss of function, to cause ALS, considering that a loss of SOD1 dismutase activity does not cause the disease (Reaume et al., 1996). Furthermore, studies on these transgenic mice have revealed that the normal dismutase activity of SOD1 is not lost (Gurney et al., 1994; Wong et al., 1995). However, SOD1 mutations have been generated in *Drosophila* that recapitulate many hallmarks of the disease without overexpression of the transgene, indicating that high copy number is not necessary for the ALS phenotype (Şahin et al., 2017). These findings also suggest that it is not the high copy number alone but, rather, a gain of toxic activity, that causes ALS in traditional overexpression mutations of SOD1.

Muscle fibre-type susceptibility

There is a well-documented, predictable pattern of neuromuscular denervation in ALS disease progression whereby the first endplates to be denervated are associated with type IIb, or fast-fatigable muscle fibres (Frey et al., 2000; Hegedus et al., 2007). The next to succumb to the disease are the type IIa, fast-fatigue-resistant muscle fibres (Frey et al., 2000; Hegedus et al., 2007). The last muscle fibres to be denervated are the type I, or slow, muscle fibres, which are the most resilient to ALS disease progression (Frey et al., 2000; Hegedus et al., 2007). Similarly, the regenerative capacity in FF motor units is limited in ALS while the slow motor units have displayed the greatest regenerative capacity (Schaefer et al., 2005; Sharp et al., 2018). This pattern of degeneration and regenerative capacity has raised the question among researchers why different muscle fibres are more vulnerable than others.

Interestingly, the fast-twitch extraocular muscles never become denervated during ALS and, despite some alterations, remain remarkably spared (Ahmadi et al., 2010; Harandi et al., 2014). One explanation for this phenomenon is that extraocular muscles are often multiply innervated, meaning if one MN were to withdraw innervation, the muscle would remain innervated. Another theory lies in our understanding of the relative activity of fast vs slow-twitch muscles. Unlike most fast-twitch muscles, which tend to be infrequently recruited, slow-twitch muscles are used throughout the day. This led to the

prominent hypothesis that neuromuscular activity, and not the MN or muscle fibre-type *per se*, dictates which endplates become denervated first. Since most IIb muscle fibres are only recruited when a great deal of force needs to be generated, they are relatively inactive, in contrast with the type I fibres, responsible for postural control, which are continuously active. Therefore, one hypothesis is that the activity in the S motor units is protective against ALS disease progression and helps to stabilize the NMJ.

In accordance with the activity hypothesis, Gordon and colleagues postulated that a forced increase in activity of these vulnerable motor units should prevent neuromuscular denervation. They partially denervated the hindlimbs of $SOD1^{G93A}$ mice by L4 or L5 spinal nerve avulsion at P40 and measured muscular and motor unit forces at P90. They found that induced over-activity of the remaining neurons of the partially denervated muscles resulted in reduced disease-related denervation. They also found that in typically fast-twitch muscles, partial denervation led to an increased proportion of slower muscle fibre types (type IIa and IId/x) than unoperated controls. They concluded that these vulnerable, fast-twitch motor units were saved by "functional overload" of their neuromuscular activity, which consequently converted them to more fatigue-resistant motor units (Gordon et al., 2010). Further, sciatic nerve crush experiments have shown that regenerated axons of S motor units were more resilient to disease progression even than intact S units (Sharp et al., 2018).

The question that remains with the activity hypothesis is whether physical activity (i.e. exercise) is beneficial as a treatment for ALS. Studies in ALS mouse models have had somewhat conflicting results. While swimming has been reported to improve survival, muscle strength, and muscle energy and glucose metabolism (Desseille et al., 2017; Flis et al., 2018, 2019), prolonged running has been shown to accelerate deterioration in ALS mice (Garbugino et al., 2018). A recent clinical trial on exercise in ALS reported that all exercise types (resistance, endurance, and flexibility) were safe and tolerated well by patients, however, there was no evidence that exercise delayed functional decline, though it did not exacerbate disease (Clawson et al., 2018). In a recent survey of physicians and healthcare professionals, only about half reported that they were likely to prescribe exercise to ALS patients, citing a need for further evidence (Jones et

al., 2019). Therefore, more research is needed to determine the relative benefits of different types of exercise vs MN stimulation as a therapy for ALS.

It has also been shown that early synaptic alterations occur prior to NMJ denervation in a motor unit-dependent manner. In a study utilizing a slow-progressing ALS mouse line, the $SOD1^{G37R}$, synaptic and morphological changes were observed at multiple time points throughout the lifespan of the mice (Tremblay et al., 2017). The authors found that long before disease onset (P180 in these mice), NMJs of FF motor units already had reduced quantal content compared with S motor units, which had increased quantal content with respect to wild type (WT) controls at this age. These differences persisted throughout disease course until the clinical phase of the disease (visible behavioural impairments around P450), when quantal content eventually decreased in the slow motor units as well. However, by this late stage, there was also extensive denervation and MN loss. Therefore, early synaptic changes are occurring long before the onset of NMJ denervation, which either reflect or contribute to NMJ instability in ALS in a muscle fibre-type-dependent manner.

Glial Cells in ALS

ALS is understood to be a non-cell autonomous disease, such that pathological activity of multiple cell types, in addition to MNs, contributes to the disease. Glial cells, the "support cells" of the nervous system, have particularly been shown to contribute to ALS pathogenesis both *in vitro* and *in vivo*.

Early results to support this concept came from a study where WT MNs were cultured in the presence of astrocytes or microglia expressing a SOD1 mutation. MNs cultured in the presence of either of these mutant glia had significantly decreased survival and altered electrophysiological properties, consistent with MNs that express the SOD1 mutation (Xiao et al., 2007; Meyer et al., 2014; Glajch et al., 2016; Song et al., 2016; Massenzio et al., 2018).

In the periphery, at the NMJ, the resident glia are TSCs. The roles of TSCs are relatively poorly understood, however, they are known to facilitate reinnervation of denervated endplates following injury or disease via a process called collateral reinnervation (see above). Studies in mice suggest that the sprouting response is limited

in SOD1^{G93A} mice, particularly during early disease onset, meaning that this typical self-repair mechanism is impaired in ALS (Frey et al., 2000; Schaefer et al., 2005). Studies with human ALS patients have shown enlarged electromyogram (EMG) recordings indicative of MN sprouting and motor unit enlargement (McComas et al., 1971; Pinelli et al., 1991). Interestingly, there appears to be two populations of MNs in SOD1^{G93A} mice; those that can sprout and those that cannot (Schaefer et al., 2005; Gould et al., 2006; Hegedus et al., 2007). Furthermore, motor unit studies on fast and slow-twitch muscles in SOD1^{G93A} mice suggest that FF motor units have a much lower capacity to sprout compared to the smaller S units (Hegedus et al., 2007). This differential capacity to sprout is unusual considering all subtypes of MNs have the same sprouting capacity after a partial nerve injury (Rafuse et al., 1992). Whether different MN subtypes in ALS patients have a differential capacity to sprout is currently unknown. This a complex issue because by the time a patient is diagnosed with ALS, they are already displaying symptoms of paralysis. We know from studies on SOD1^{G93A} mice that by the time motor dysfunction is clearly apparent, neuromuscular denervation has already progressed significantly in fast twitch muscles due to the loss of FF motor units and lack of compensatory sprouting (Hegedus et al., 2007). If the largest MNs in ALS patients cannot sprout it seems reasonable to assume that increasing this limited capacity could lead to possible early therapy as sprouting may help to maintain some of the motor function and improve the quality of life for patients.

Since TSCs are responsible for initiating sprouting, their pathology may underlie this early sprouting insufficiency that contributes to ALS disease progression in animal models of ALS and in patients with the disease. TSCs monitor synaptic transmission at the NMJ in a Ca^{2+}-dependent manner, allowing the TSCs to alter their behaviour from maintenance to repair in the event of an injury (Reist and Smith, 1992; Robitaille, 1998; Rochon et al., 2001; Colomar and Robitaille, 2004; Rousse et al., 2010; Todd et al., 2010; Darabid et al., 2013). In particular, muscarinic AChRs (mAChRs) regulate TSC gene expression and, thus, their tendency towards homeostasis or repair (Reynolds and Woolf, 1992; Georgiou et al., 1994). Activation of mAChRs, such as that from normal synaptic transmission, keep TSCs in a maintenance phenotype while at the same time suppressing the expression of genes necessary for repair (Arbour et al., 2015). In a study of the slow-

progressing SOD1^{G37R} mouse model of ALS, the ability of TSCs to interpret synaptic transmission as normal or abnormal was found to be impaired by increased mAChR activation (Arbour et al., 2015). This indicates that TSCs would be unable to initiate repair mechanisms or a sprouting response because they would be insensitive to the alterations in synaptic transmission that occur prior to NMJ denervation in ALS.

These alterations in TSCs in response to denervation have also been observed in terms of their morphology. Carrasco et al (2016) reported that as early as P30 in SOD1^{G93A} mice, approximately 50% of endplates in the mixed fibre-type medial gastrocnemius (MG) did not have the typical placement of TSC cell bodies on the endplate itself, but, rather, the TSC processes covered the endplates. By P60, about 25% of endplates were denervated in the MG and lacked TSC cell bodies, in addition to a large proportion of denervated endplates. These observations were only observed to a minimal degree in the slow-twitch soleus muscle. Together, their results indicate that abnormal TSC morphology preceded NMJ denervation in normally progressing SOD1^{G93A} ALS in a muscle fibre-type-dependent manner. These observations were further corroborated as being a hallmark of SOD1 ALS by confirming these TSC abnormalities in SOD1^{G85R} mice, as well (Carrasco et al., 2016b).

There is also evidence to suggest that TSC pathology in ALS is linked to motor unit type susceptibility to degeneration. Neuromuscular synapses of different motor units have differing regenerative capacities in healthy controls, outside the context of ALS. During development, reinnervation and toxin-induced paralysis, the axon repellent Semaphorin 3a (Sema3A) is selectively expressed by TSCs associated with type IIb fibres and not type I or IIa muscle fibres, indicating a possible explanation for limited plasticity at these synapses (De Winter et al., 2006). Furthermore, in SOD1^{G93A} ALS mice, Sema3A is selectively expressed at type IIb/x NMJs as early as P35, around the time of the earliest evidence of fast-fatigable muscle fibre denervation (De Winter et al., 2006; Hegedus et al., 2007). Considering Sema3A expression at these endplates is a hallmark of the normal response to denervation, it is likely only a contributing factor explaining limited stability at these endplates in ALS. However, Sema3A expression is higher during presymptomatic and disease-onset stages of ALS than during the later stages of the disease, indicating it could play a role early on in ALS disease progression

(De Winter et al., 2006). Considering these findings were the first evidence of molecular differences between TSCs residing at NMJs of different muscle fibre types, it is tempting to speculate that further differences exist that could be contributing to the role that TSCs play in the stability of different NMJ types in ALS.

Inflammation in ALS

Following NMJ denervation, either due to injury or in the context of ALS, peripheral macrophages infiltrate the muscle and phagocytose cellular debris from the degenerating axon (Sakaguchi et al., 2014; Trias et al., 2017, 2018). These macrophages release neurotrophic factors, IL-1, and TGF-β, contributing to a pro-inflammatory environment in the muscle and around the degenerating nerve (Deng et al., 2018). This immune response is necessary for successful nerve regeneration. However, in ALS, there is conflicting evidence whether macrophage recruitment is reduced or enhanced, leading to a debate as to whether limited beneficial inflammation, or excessive aberrant inflammation, contributes to disease pathogenesis.

Deng et al in 2018 examined the peripheral nerves of $SOD1^{G93A}$ mice at varying points throughout disease progression. They reported that in P120 mutant mice, the expression of CD68, a marker of activated macrophages, was elevated during the inflammatory response, in addition to the mRNAs of other inflammatory factors such as Mcp-1, Cd86, and TGF-β. In contrast, in the same study, sciatic nerve crush experiments at P30 revealed that $SOD1^{G93A}$ mutant mice had significantly less macrophage recruitment compared to WT littermates 7 days after injury. These findings were correlated with declines in the number of S100-positive cells and proliferating cells in $SOD1^{G93A}$ mice (Deng et al., 2018).

Another study has further reported that enhancing immune activation in peripheral axons delays disease progression. In a comparison between two $SOD1^{G93A}$ strains that had the same amount of transgene, but differed in the time course of disease, they found that the slow-progressing strain had dramatically more infiltrating macrophages and higher levels of immune molecules compared to the fast progressing mice (Nardo et al., 2016). The researchers concluded that these differences in immune cell activation

actually impacted the time course of these different strains by actively delaying muscle denervation in the slow-progressing mice (Nardo et al., 2016).

Furthermore, it is debatable whether the peripheral immune response that occurs in ALS is beneficial or contributing to axon degeneration. There is evidence that macrophages and mast cells accumulate in muscle in both rodent and human ALS (Trias et al., 2017, 2018). Inhibition of these cell types in $SOD1^{G93A}$ rats via a tyrosine kinase inhibitor, masitinib, led to reductions in axon pathology, demyelination, and rescued some muscle fibre atrophy. These results indicated that, in this case, immune cell infiltration was deleterious and exacerbates disease progression (Trias et al., 2016, 2017, 2018).

Overall, it seems that immune cells accumulate in muscle and peripheral nerves over the course of ALS disease progression, while the activation of immune cells following injury in ALS may be impaired. Differences between these studies could be accounted for by the differences between the models used as well as the disease stage examined. It is possible that early on in ALS disease progression (or in slow-progressing ALS), the immune response is more effective at delaying axonal degeneration, while at later stages (or in fast-progressing ALS) other contributing pathological mechanisms make it difficult for the immune system to protect against NMJ denervation.

Bone Morphogenic Protein 4 (BMP4)

To better understand NMJ stability in the disease or injury condition, we must first determine the processes that govern NMJ stability in homeostasis. In this way, we can better determine what processes are disrupted. Various proteins and signaling pathways have been thoroughly studied in NMJ stability. One candidate that has not been evaluated extensively in vertebrate models is bone morphogenic protein 4 (BMP4), which contributes to the formation, stability, and function of the *Drosophila* NMJ (Aberle et al., 2002; Marqués et al., 2002; McCabe et al., 2003). Also of interest, BMP4 dysregulation has been implicated in ALS (Duval et al., 2014; Deshpande et al., 2016). Therefore, I sought to determine how BMP4 contributes to mouse NMJ stability.

BMP Signaling

Bone morphogenic proteins (BMPs) belong to the TGF-β superfamily and are widely expressed during development and in postnatal life. They were initially described in the context of bone formation but have since been shown to have roles in many different systems throughout the body. During development, BMP signaling is known to contribute to dorsoventral patterning, organ and tissue specification, and central nervous system development (Osses and Henriquez, 2015).

Two classes of transmembrane receptors are involved in BMP signaling, type I and II, which together form heteromeric complexes that are required for functional signal transduction (Yamashita et al., 1994; Liu et al., 1995). There are three different type I (ActRIA, BMPRIA, and BMPRIB) or type II (ActRIIA, ActRIIB, and BMPRII) receptors, all of which are serine/threonine kinases (Osses and Henriquez, 2015). BMP binding to a complex of BMPRI and BMPRII initiates a Smad-dependent signaling cascade resulting in the regulation of transcription of various target genes. After a BMP ligand binds to this receptor complex, BMPRII phosphorylates and thus activates BMPRI, which in turn phosphorylates receptor (R)-Smad-1, 5, or 8. These activated Smads will then form heteromeric complexes with Smad-4 and translocate to the nucleus (Shi and Massagué, 2003; Nohe et al., 2004; Miyazono et al., 2005; Osses and Henriquez, 2015). BMPs are also capable of signaling via MAP kinases, ERK, NFkB, and phosphoinositide 3-kinase, which allows for their wide range of activities (Sieber et al., 2009; Bragdon et al., 2011). Smad-dependent and independent signaling pathways have both been implicated in the variety of roles that BMPs play in the nervous system including: neural tube formation and patterning; neural stem cell proliferation and cell fate determination; neurite growth; and synapse formation and stabilization, including the NMJ (Gámez et al., 2013; Osses and Henriquez, 2015).

BMP4 at the NMJ

BMPs are expressed throughout the developing nervous system and act as retrograde, trans-synaptic signals that influence the development and function of presynaptic terminals, both centrally and at NMJs (Berke et al., 2013). At the NMJ, BMP4 is produced both in muscle and TSCs, while its receptor BMPRII is expressed in MNs

(Chou et al., 2013). Our understanding of the role of BMP4 at the NMJ comes primarily from studies in *Drosophila* that have revealed key roles for BMP4 signaling in synaptic growth, stability, and plasticity.

Mutation of the *Drosophila* BMPRII homolog, *wishful thinking* (*wit*), results in impaired morphology and function of the NMJ during development, a pathology that can be rescued by postnatal induced expression of *wit* (Aberle et al., 2002; Marqués et al., 2002). Specifically, disruption of this *wit* pathway at the *Drosophila* NMJ results in severe motor defects, impaired synaptic transmission, decreased NMJ size and reduced lifespan (Aberle et al., 2002; Marqués et al., 2002). Synaptic deficits in these flies include reductions in the size and frequency of spontaneous transmitter release, reduced evoked responses, and consequent decreases in quantal content (Aberle et al., 2002; Marqués et al., 2002). *Wit* mutations also result in MN retraction from the NMJ (Marqués et al., 2002; Lee et al., 2016). Mutations in other BMP ligands, receptors, or downstream effectors similarly impair NMJ growth and function. For instance, mutations in the *Drosophila* homolog of BMP4, *Glass bottom boat (gbb)*, severely impairs NMJ development (McCabe et al., 2003). BMP4 signaling in the presynaptic neuron is, therefore, vital in ensuring the health and normal function of the *Drosophila* NMJ (Osses and Henriquez, 2015). However, it is currently unclear whether BMP4 retains similar roles at the vertebrate NMJ.

The few studies that have examined BMP4 function in vertebrate muscle suggest that it plays a role in maintaining NMJ morphology and muscle homeostasis. For example, homozygous null mutations in zebrafish *gdf6a*, a BMP-family encoding gene, results in fish with decreased endurance and altered NMJ morphology (Duval et al., 2014). In mice, BMP4 has been shown to be expressed at the NMJ both in muscle and in TSCs, and is taken up and transported by MNs, which express BMPRII (Chou et al., 2013).

During muscle development, muscle precursor cells, called myoblasts, fuse to create multinucleate mature muscle fibres. A subpopulation of these myoblasts do not differentiate and remain dormant in the mature muscle (Chargé and Rudnicki, 2004). These cells are called satellite cells, and, upon muscle injury, they are recruited to differentiate and repair the damaged site (Chargé and Rudnicki, 2004). Activated satellite

cells have been shown to express phosphorylated Smad1/5/8 following injury in the Tibialis anterior (TA) of adult mice, indicating that Smad-dependent BMP4 signaling happens in response to muscle injury (Ono et al., 2011). Specifically, BMP4 causes an increase in the size of the committed satellite cell population but suppresses the number of differentiating cells. Accordingly, blocking BMP4 signaling results in increased differentiation (Ono et al., 2011). BMP4 signaling in injured muscle seems to simultaneously maintain the satellite cell pool while preventing precocious myoblast differentiation during regeneration (Ono et al., 2011).

BMP/Smad-dependent signaling has also been shown to contribute to muscle mass homeostasis by promoting hypertrophy and preventing atrophy (Sartori et al., 2013; Winbanks et al., 2013). Genes encoding various BMPs are induced in mouse skeletal muscle as a result of denervation, and activation of the Smad pathway is proposed to be critical in preventing atrophy following denervation (Sartori et al., 2013; Winbanks et al., 2013). Many BMP genes and receptors are also expressed predominantly in innervated muscles, indicating that MN activity and apposition at the NMJ is necessary for some muscle-derived BMP signaling (Sartori et al., 2013; Winbanks et al., 2013).

It is possible that agrin, a MN-derived organizer of postsynaptic receptors, is involved in controlling BMP activity in skeletal muscle. BMP4 binding to agrin inhibits BMP4 signaling by sequestering it away from the extracellular domain of the BMPRIA, functionally preventing it from binding to its receptor (Bányai et al., 2010). Agrin administration to C2C12 muscle cultures also causes a dose-dependent increase in BMP4 mRNA expression (Chou et al., 2013). Furthermore, BMP4 staining in mouse soleus muscle appears to be localized around the perimeter of the postsynaptic densities (PSDs) at NMJs, and denervated soleus muscles lose this BMP4 immunoreactivity (Chou et al., 2013). Together, this corroborates the idea that BMP4 activity in muscle is MN-dependent. There is evidence to suggest that this localization of BMP4 around the perimeter of the PSDs at NMJs could function to prevent the clustering of AChRs outside the synaptic site. In addition to BMP4 at these sites, there is also polymerized f-actin and the protein LL5β; activity associated with both of which has been implicating in breaking up and limiting AChR clustering (Kishi et al., 2003; Lee et al., 2010). Therefore, this location of BMP4 at the NMJ could contribute both to maintain the BMP4 ligand in the

vicinity of its presynaptic receptors, as well as to contain AChRs at the synapse site (Osses and Henriquez, 2015).

Although these studies clearly indicate roles for BMP4 signaling at the NMJ, it is still unknown to what extent muscle-derived BMP4 regulates normal and pathological physiology at the NMJ in vertebrates. This thesis will therefore, in part, seek to reproduce the physiological findings in *Drosophila* in a mouse model, in the absence of muscular BMP4 signaling.

BMP4 in Injury

BMP4 signaling in MNs has also been linked to axon outgrowth and regeneration following injury (Zhong and Zou, 2014). Inhibition of BMP4 with noggin has been shown to limit neurite outgrowth in culture and noggin is downregulated following dorsal root ganglion (DRG) injury *in vivo* (Ma et al., 2011). In an *in vitro* study on DRG neurons, a downstream effector of BMP4 (Smad1) was upregulated in response to axotomy and prior to new axon outgrowth (Zou et al., 2009). They also showed that axon outgrowth was impaired in neurons after knockdown of Smad1. Furthermore, administration of BMP4 prior to axotomy significantly improved neurite outgrowth, suggesting that BMP4-dependent Smad1 signaling is required for axon outgrowth following axotomy (Zou et al., 2009).

In vivo, similar results have shown that Smad1 activation is responsible for both axon outgrowth during development, and for regeneration following spinal cord injury (Parikh et al., 2011; Kelly et al., 2013). Mice harboring a conditional knockout mutation of Smad1 in DRG neurons had impaired axonal regeneration following dorsal column transection injury. This phenotype could be rescued with intrathecal AAV administration of BMP4 following the injury, in a more clinically relevant scenario (Parikh et al., 2011). Together, these studies highlight the necessity of BMP4/Smad1 signaling in promoting axon outgrowth following injury.

BMP4 in ALS

As mentioned above, NMJ stability is a likely a key contributor to degeneration in ALS, with the less stable synapses becoming affected earlier during disease progression. Given the evidence supporting that BMP4 signaling is a key regulator of NMJ homeostasis, it has been speculated that alterations in BMP4 signaling could contribute to ALS pathogenesis at the NMJ. In a *Drosophila* study investigating mutant TDP-43, reduced BMP signaling was reported at the NMJ (Deshpande et al., 2016). This study further determined that mutations in TDP-43 caused BMP receptors to move from early to recycling endosomes, and for these receptors to be abnormally localized outside of the NMJ site (Deshpande et al., 2016).

Increasing BMP signaling has also been shown in *Drosophila* to rescue both early and late-disease pathologies. Transgenic expression of the fly homolog, *gbb*, in a subset of neurons (including MNs) in $SOD1^{G85R}$ flies, improved NMJ structure in end-stage individuals where alterations in axon branching and reductions in terminal bouton number are typically observed (Held et al., 2019). In this model, there were also corresponding improvements in NMJ function as evidenced by a rescue of mEPP frequency (Held et al., 2019). $SOD1^{G85R}$ flies expressing *gbb* also had improved leg extension and reductions in MN degeneration (Held et al., 2019). These mutant fly larvae also have locomotor impairments long before disease end-stage, which is improved with *gbb* expression. This study further identified that these early locomotor deficits were not a result of NMJ structural or functional impairments (such as at end-stage), but, rather, by a defect in sensory feedback, which was rescued by increasing BMP signaling in proprioceptor neurons (Held et al., 2019). Improving BMP signaling early in the life of these $SOD1^{G85R}$ flies also led to a partial rescue of late-disease pathologies and improved lifespan (Held et al., 2019).

Additional evidence to support the role of BMP4 in ALS comes from a zebrafish study where BMP-family knockdown resulted in an ALS-like phenotype. Mutant zebrafish displayed a progressive reduction in endurance, a reduced number of spinal MNs, and reduced lifespan, similar to ALS (Duval et al., 2014). Co-expression of this BMP family mutation and mutant SOD1 in zebrafish exacerbated this phenotype, with fish displaying further reduced motor performance and neuromuscular innervation. They

concluded that BMP-family mutation sensitizes mutant SOD1 zebrafish to develop ALS symptoms (Duval et al., 2014), though it is unclear whether these fish have two separate, comorbid motor defects, or whether these two processes are mechanistically linked.

Another study investigating the role of astrocytosis in ALS discovered that BMP4 was consistently upregulated in reactive astrocytes in the rat ventral spinal cord (Shijo et al., 2018). Inhibition of BMP4 with noggin resulted in reduced motor disfunction, muscle atrophy, and extended survival in these ALS rats, even when treatment with noggin was initiated after symptom onset. Noggin treatment also prevented harmful astrocyte hypertrophy and neuroinflammation in the spinal cord, indicating that aberrant BMP4 signaling could be contributing to astrocytosis that exacerbates ALS disease progression (Shijo et al., 2018).

Using an unbiased proteomic screen, several Smad proteins down-stream of BMPRII activation were recently identified as being differentially regulated between TDP-43 mutant embryonic stem cell-derived MNs (ESCMNs) and WT ESCMNs. As an upstream effector of Smad activity, BMP4 activity is therefore likely altered in this ALS mutant cell line. This finding, along with results from previous studies, informed our hypothesis that alterations in BMP4 signaling could be contributing to NMJ instability in ALS. However, we first needed to better understand how BMP4 contributes to normal NMJ homeostasis in mice.

Summary of Objectives

The unifying theme of this thesis is NMJ stability. As the communication interface between the nervous and muscular systems, the NMJ and its stability are fundamental to understanding normal behaviour as well as neuromuscular diseases such as ALS. Much of our understanding of the NMJ is MN-centric, with limited understanding how the other key cell types, muscle fibres and TSCs, contribute to homeostasis and plasticity. This thesis, therefore, seeks to address the concept of NMJ stability and how these other cell types contribute to disease, healthy function, and response to peripheral nerve injury.

Chapter 2: To investigate the role of TSCs in muscle fibre-type susceptibility and impaired sprouting response in the SOD1^{G93A} mouse model of ALS.

Chapter 3: To characterize the anatomy and physiology of the NMJ in an adult onset skeletal muscle specific BMP4 knockdown model, in mice, to determine whether mammalian BMP4 contributes to NMJ structure and function.

Chapter 4: To examine the role of muscular BMP4 in neuromuscular reinnervation following a tibial nerve crush.

CHAPTER 2: MUSCLE SPECIFIC RESPONSE TO PARTIAL DENERVATION IN SOD1^{G93A} MICE

Abstract

Amyotrophic lateral sclerosis (ALS) is an adult-onset disease characterized by the progressive death of MNs and denervation of muscle fibres. To restore motor function, surviving MNs in partially denervated muscles typically sprout axons to reinnervate denervated endplates. However, studies on ALS rodent models indicate that sprouting is significantly limited in fast, but not slow, twitch muscles when the largest MNs die at disease onset. This limitation hastens the rate of muscle weakness and loss of motor function. Although the causes of this limitation are unknown, neuromuscular junction (NMJ) pathologies are likely involved because NMJ instability precedes MN death, terminal Schwann cells (TSCs) at endplates regulate sprouting and muscle fibre phenotypes differ between subpopulations of MNs that sprout and those that do not. To test this, we compared the sprouting capacity of MN subtypes by partially denervating the fast twitch plantaris (composed of type IIa/IIb muscle fibres) and slow twitch soleus muscles (contains type I/IIa fibres) at P30 in SOD1^{G93A} and WT mice. We found that only MNs innervating the SOD1^{G93A} plantaris had a limited sprouting capacity, which was correlated with the selective loss of TSCs at IIb fibres and increase in macrophage infiltration. Treating SOD1^{G93A} mice with a macrophage inhibitor significantly reduced infiltration, prevented TSC loss and increased sprouting capacity to normal. These results suggest that TSCs at denervated type IIb muscle fibres are aberrantly targeted by infiltrating macrophages in SOD1^{G93A} mice, and their loss accounts for the compromised sprouting capacity of the largest MNs during early stages of ALS.

Introduction

ALS is a fatal, adult-onset neurodegenerative disorder characterized, in part, by the progressive dysfunction and death of lower motor neurons innervating skeletal muscle fibres. While most cases of ALS are sporadic, approximately 10% have an inherited form, one of which is caused by a mutation in the SOD1 gene (Rosen et al., 1993; Ajroud-Driss and Siddique, 2015). Transgenic mice over-expressing human mutant SOD1 with a glycine to alanine conversion ($SOD1^{G93A}$) develop several pathologies typical of ALS including progressive spinal and cortical MN loss, cortical MN dendritic spine loss, NMJ denervation, and motor dysfunction (Gurney et al., 1994; Chiu et al., 1995; Fogarty et al., 2015, 2016).

To compensate for the loss of innervation, surviving MNs sprout terminal branches to reinnervate previously denervated endplates (McComas et al., 1997; Shefner et al., 2006). Sprouting is mediated by TSCs that are closely associated with NMJs (Son and Thompson, 1995a). Following denervation, TSCs grow processes from denervated endplates to innervated NMJs where they act as bridges to guide axonal sprouts back to the denervated NMJs (Son and Thompson, 1995a; Lee et al., 2017). Functional compensation due to MN loss can be remarkable since each MN can expand its field of innervation by up to four times its normal size if more than 80% of its original innervation is removed due to injury (Brown and Ironton, 1978; Rafuse et al., 1992). Interestingly, several studies have indicated that sprouting is limited in $SOD1^{G93A}$ mice, particularly by the largest MNs early on in disease progression (Frey et al., 2000; Gordon et al., 2004; Schaefer et al., 2005; Gould et al., 2006; Pun et al., 2006; Hegedus et al., 2007; Carrasco et al., 2016b). Because of this limitation, muscle fibres become denervated sooner leading to an earlier onset of muscle weakness and loss of motor function. The cellular basis for reduced sprouting capacity in ALS is poorly understood.

A clue to identifying the mechanisms underlying the limited sprouting capacity comes from the pattern of MN death in ALS. It is well established that the largest, least active MNs innervating type IIb skeletal muscle fibres die first, followed by smaller, more active MNs innervating type IIa fibres, and, finally, by the most active and smallest MNs innervating type I fibres (Frey et al., 2000; Pun et al., 2006; Hegedus et al., 2007, 2008). Prior to MN cell death, axons withdraw from endplates (Fischer et al., 2004;

Arbour et al., 2017; Martineau et al., 2018), in part, because there is abnormal TSC decoding at NMJs (Arbour et al., 2015; Carrasco et al., 2016a, 2016b). Because TSCs mediate synaptic stability and initiate sprouting, it seemed reasonable to investigate whether TSC pathologies underlie the impaired sprouting response observed by a subset of MNs in SOD1^{G93A} mice during disease progression and, if abnormalities are observed, explore means to reverse them.

Here, we compared the sprouting capacity of MN subtypes innervating type IIb, IIa and I fibres by partially denervating the fast twitch plantaris and slow twitch soleus muscles prior to disease onset in SOD1^{G93A} and WT mice. We found that only MNs innervating the SOD1^{G93A} plantaris had a limited sprouting capacity, and that this limitation was correlated with the selective loss of TSCs at IIb fibres and an overall increase in macrophage infiltration. Furthermore, treating SOD1^{G93A} mice with masitinib, a macrophage inhibitor, significantly reduced macrophage infiltration, reversed the loss of TSCs at IIb fibres, and restored the sprouting response to normal. These results suggest that TSCs at denervated type IIb muscle fibres are aberrantly targeted by infiltrating macrophages in SOD1^{G93A} mice and their removal accounts for the reduced sprouting capacity of MNs in fast twitch muscles.

Methods

Mice

The hemizygous B6.Cg-Tg(SOD1-G93A)1Gur/J (Jackson Laboratory; hereafter referred to as SOD1^{G93A}) mouse model of ALS was used in this study. These mice display extensive MN cell death and progressive skeletal muscle weakening due to neuromuscular denervation because they have a high copy number of the human SOD1 gene carrying a glycine to alanine transition at position 93 (Gurney et al., 1994). SOD1^{G93A} mice have a shortened life expectancy with mean survival at 161±10 days (Heiman-Patterson et al., 2011). Onset of muscle denervation begins at approximately P40 and continues throughout life with first visible motor deficits beginning at approximately P90 (Hegedus et al., 2007). Hemizygous mice were bred and genotyped shortly after birth so that age-matched littermates, not expressing the mutant gene, could

be used as WT controls. All experiments were conducted in accordance to the guidelines of the Canadian Council on Animal Care and the policies of Dalhousie University.

Surgeries

All surgeries were performed under aseptic conditions on P30 mice. Animals were anesthetized with a mixture of isoflurane (Baxter) and oxygen throughout surgery. For partial denervation of plantaris and soleus muscles, a small (~1.5 cm) incision was made in the skin, left of the dorsal midline at the level of, and rostral to, the iliac crest. Another incision was then made along the border between the spinalis muscles and fat layer parallel to the spine to expose the L4-S1 spinous processes. The L5 transverse process was removed and a 10-0 suture was used to ligate and gently lift the dorsal L5 root and to cut it distal to the suture. The ligation ensured that regeneration of the nerve was prevented. Mice were allowed 1, 2, 3, 14, or 30 days of recovery, after which they were killed by isoflurane inhalation and cervical dislocation.

In some experiments, the plantaris and soleus muscles were completely denervated by cutting the tibial nerve. Briefly, under isoflurane anesthesia, a small incision (~1 cm) was made along the rostral/caudal axis of the lower hindlimb behind the knee. The underlying layer of fat was carefully separated to expose the branching point of the tibial nerve. A suture (7-0 to 10-0) was used to ligate the tibial nerve prior to its branching point to the triceps surae muscles. The nerve was then cut distal to the ligation. Mice recovered for 3 days and then killed by isoflurane inhalation and cervical dislocation.

Preparation and administration of masitinib mesylate

A 100 mg/ml stock solution of masitinib mesylate (AdooQ Bioscience) was prepared by dissolving 50 mg masitinib mesylate powder in 500 µl distilled water (dH_2O). This solution was aliquoted and stored at -20 °C. The amount of masitinib stock was calculated per mouse for the desired 30 mg/kg dose and diluted to 150 µl in 10% dextrose solution. The masitinib and dextrose mixture was fed to mice using a syringe with a

blunted needle. Mice were administered masitinib three days prior to the partial denervation surgery and daily after surgery until the final acute experiment.

Ex vivo *isometric tension recordings*

Mice were anesthetized with a mixture of isoflurane and oxygen. The plantaris, or soleus muscle, was rapidly dissected free along with its supplying nerve and placed into carbogenated (95% O2, and 5% CO2) Tyrode's solution containing the following: 125 mM NaCl, 24 mM $NaHCO_3$,5.37 mM KCl, 1 mM $MgCl_2$, 1.8 mM CaCl2, and 27.75 mM dextrose. The proximal muscle tendon (soleus) or hindlimb bones (plantaris) were securely pinned in a Sylgard (Dow Corning)-coated recording chamber that was continuously perfused with carbogenated Tyrode's. Thread was tied to the distal end of each muscle and connected to a force transducer (FT 03; Grass Technologies). A fine-tipped, fire polished glass stimulated suction electrode (World Precision Instruments, Inc.) was used to deliver electrical current (0.05 – 0.1 ms duration) to the innervating nerve via an S88 stimulator (Grass Technologies) that was isolated from ground using a stimulus isolation unit (PSIU6; Grass Technologies). Muscle length was adjusted to maximal isometric contraction. Tetanic forces were recorded at 50 Hz (1 s duration) using a Digidata 1322A analog-to-digital board and AxoScope version 10.2 software (Molecular Devices).

Immunofluorescence and imaging

*S*oleus and plantaris muscles from partially denervated, completely denervated, and contralateral unoperated limbs were dissected from the lower hindlimb immediately after euthanasia and transferred to phosphate buffered saline (PBS). Muscles were then pinned at physiological length and fixed in 4% paraformaldehyde (PFA) for 15-20 minutes. Next, they were washed in PBS, permeabilized in -20 °C methanol for 6 min, washed again in PBS, and then securely pinned in a Sylgard dish immersed in PBS under a dissecting microscope. One tendon was removed so the muscle fibres could be carefully teased into bundles using forceps.

To visualize pre-synaptic structures at the NMJs, muscle fibre bundles were incubated overnight in in 0.3% Triton-PBS containing 10% normal goat serum and a cocktail of primary antibodies described in Table 1. The next day, muscles were washed in PBS and then incubated for 1 hr in 0.3% Triton/PBS with the appropriate secondary antibody solutions, including goat anti-mouse Alexa Fluor 488/Cy2 (1:500; Invitrogen/Jackson Laboratories), goat anti-rabbit Alexa Fluor 647 (1:500; Invitrogen), and goat anti-rat Cy3 (1:500; Jackson Laboratories). To visualize post-synaptic acetylcholine receptors (AChRs), all fibres were labeled with either rhodamine (1:500) or Alexa Fluor 647-conjugated α-bungarotoxin (BTX; 1:250; Invitrogen) in 0.3% Triton in PBS. Muscles were finally rinsed in PBS and mounted on slides using 50% glycerol/PBS and 0.03 mg/ml ρ-phenylenediamine to prevent fading.

Teased muscles immunostained for muscle fibre-types were pre-blocked for 30 min in 0.01% Triton-PBS containing 10% normal goat serum. Muscle fibres were then incubated overnight at room temperature in 0.01% Triton-PBS containing primary antibodies against different myosin isoforms (Table 1), washed in PBS and finally incubated for 2 hr in 0.01% Triton-PBS containing BTX (1:250 or 1:500, depending on the fluorophor) and the appropriate secondary antibodies including goat anti-mouse Cy3 IgG (1:500; Jackson ImmunoResearch), Alexa Fluor 594 IgM (1:500; Invitrogen) and goat anti-rabbit Alexa Fluor 488 (1:500; Invitrogen). Muscles were mounted on slides as described above.

Z-stacks were acquired with a laser-scanning confocal microscope (Zeiss Microimaging) utilizing Zeiss Zen 2009 software (Zeiss Microimaging). Three-dimensional rendering was achieved on a subset of z-stacks using the surfaces function in Imaris software (Oxford Instruments).

Classification of innervation, terminal sprouts, terminal Schwann cell presence, and macrophage density

For quantification of endplate innervation, BTX-positive zones of AChRs were located and visualized by focusing up and down using an upright fluorescence microscope (Leica Instruments). For any given BTX-positive zone, it was determined whether it was

innervated, partially innervated, or denervated by the presence, or lack thereof, of presynaptic structures imaged on a different fluorescence channel. If presynaptic structures (either SV2 alone, or SV2 and TUJ1 together) were present in the same configuration as the postsynaptic structure (BTX), it was termed innervated. Endplates with partial colocalization of presynaptic structures were classified as partially innervated, while endplates without any discernible presynaptic structures were classified as denervated. TSCs were characterized as S100β^{+} cells overlying BTX^{+} post-synaptic AChRs and their presence at the NMJ was classified in the same fashion as described for innervation (above). Approximately 150 endplates/muscle were quantified for the presence of presynaptic innervation and TSC presence at the NMJ.

Whole mounted muscles stained for BTX and immunolabeled for Tuj1 were used to quantify terminal sprouts. Endplate-rich regions were chosen at random and both the total number of terminal sprouts and number of sprouts extending from an innervated endplate to previously denervated endplate (termed successful sprouts), were quantified. Terminal sprouts were clearly identifiable as small caliber axons extending from terminals innervated by a larger caliber axon (Schaefer et al., 2005; Chipman et al., 2014a). A minimum of 250 endplates were counted per muscle, and the proportions of total and successful sprouts were represented as a percentage of the endplates counted.

Whole mounted muscles immunostained for CDllb, S100β and labeled with BTX were used to determine macrophage density (cells/mm^2) at 6 endplate-rich regions/muscle. Four muscles were analyzed per group.

Experimental Design and Statistical Analysis

Two-way ANOVAs were performed to examine the differences between group over time and Mann–Whitney tests were used to compare between groups. Data were analyzed using GraphPad Prism 5 software and were considered statistically significant at $p<0.05$.

Results

L5 spinal nerve transection partially denervates plantaris and soleus muscles in WT and SOD1^{G93A} mice to the same extent

To examine whether MNs innervating type I, IIa, and IIb muscle fibres in SOD1^{G93A} mice have the same capacity to sprout as their WT littermates prior to disease onset (i.e. P30; Hegedus et al., 2007), we partially denervated the fast twitch plantaris and slow twitch soleus muscles by cutting and ligating the L5 ventral root (Fig 2.1A). We chose those muscles because they are innervated by different MN subtypes based on their muscle fibre type composition. More specifically, the plantaris muscle contains 50% type IIb, 25% IIa fibres, and 0% type I fibres, while the soleus contains 50% type I fibres and only 3% IIb fibres (Bloemberg and Quadrilatero, 2012). In addition, both muscles are innervated by the same spinal nerves.

However, before examining whether MN subtypes have differential capacities to sprout after partial denervation, we first needed to ascertain whether the relative distribution of plantaris and soleus MNs in the L4 and L5 spinal nerves differed between WT and SOD1^{G93A} mice. To determine this, we partially denervated both muscles in WT and SOD1^{G93A} mice by cutting and ligating the L5 spinal nerve at P30 and then quantified the degree of partial denervation using *ex vivo* tetanic force recordings upon tibial nerve stimulation three days later. Contralateral muscles in each mouse served as unoperated controls. As shown in the tetanic force recordings (Fig. 2.1B,C), cutting the L5 spinal nerve caused approximately 40% reduction in plantaris muscle contractile force in both the WT and SOD1^{G93A} mice (Fig. 2.1B,D). Transecting the L5 spinal nerve caused a 50% loss of force in the soleus muscle compared to the contralateral control in the WT and SOD1^{G93A} mice (Fig. 2.1C,D). To examine whether the extent of NMJ denervation in plantaris and soleus muscles was comparable to the loss in contractile forces, we characterized the degree and pattern of endplate innervation using BTX staining and SV2 immunohistochemistry to identify post-synaptic AChRs and synaptic vesicles, respectively, in the innervating MN. As shown in Figure 2.1E, the pattern of innervation, when present, occasionally differed, and, thus, we sub-characterized endplate innervation based on the extent of co-labeling between pre- and post-synaptic markers. NMJs

exhibiting ~100% co-localization were considered fully innervated, while endplates with limited contact with pre-synaptic markers were identified as partially innervated. Endplates with a complete absence of pre-synaptic markers were considered denervated (Fig. 2.1E). Using this classification scheme, we found that both the plantaris (Fig. 2.1F) and soleus muscles (Fig. 2.1G) were equally denervated in the WT and SOD1^{G93A} mice after transection of the L5 spinal nerve, and the extent of denervation was similar to the loss of force. These results indicate that the degrees of partial denervation caused by cutting the L5 spinal nerve were similar between the two muscles, and that the SOD1^{G93A} mutation does not alter the relative distribution of soleus and plantaris MNs in the L4 and L5 spinal nerves prior to P30.

Reinnervation via axonal sprouting is limited following partial denervation of SOD1^{G93A} plantaris muscles

To ascertain whether MNs innervating plantaris and soleus muscles have the same capacity to sprout and innervate denervated fibres prior to disease onset, we transected the L5 spinal nerve at P30 and examined endplate innervation 14 days later. As before, unoperated, contralateral muscles were used as internal controls. The examples in Figure 2.2A show that some endplates in partially denervated soleus and plantaris muscles in WT and SOD1^{G93A} mice remained denervated, or partially innervated, 14 days after spinal nerve transection (Fig. 2.2A; arrowheads and asterisks, respectively). When quantified, we observed that the number of innervated endplates was higher 14 days after spinal nerve transection compared to 3 days after (yellow lines in Figs. 2.2B,C indicate degree of innervation after 3 days) in partially denervated soleus and plantaris muscles in WT mice. However, while the degree of innervation was the same in partially denervated SOD1^{G93A} and WT soleus muscles (Fig. 2.2C), partially denervated SOD1^{G93A} plantaris muscles contained significantly fewer innervated endplates ($p=0.0079$) compared to partially denervated WT plantaris muscles (Fig. 2.2B). These results suggest that axonal sprouting occurs normally in partially denervated soleus muscles in SOD1^{G93A} mice but is significantly compromised in SOD1^{G93A} plantaris muscles.

To further examine whether this is the case, we immunolabeled partially denervated WT and SOD1^{G93A} soleus and plantaris muscles 30 days after spinal nerve transection to examine endplate innervation and axonal sprouts. Figure 2.3A shows examples where dual immunolabeling with Tuj1 and SV2 revealed several endplate phenotypes including fully denervated endplates (arrowheads), partially innervated endplates (arrows), endplates innervated by axonal sprouts (asterisks) and axonal sprouts that did not contact an endplate (+). As observed 14 days after spinal nerve transection, the percentage of innervated endplates in partially denervated WT and SOD1^{G93A} soleus was the same (Fig. 2.3C; yellow lines indicate degree of innervation at 3 days). In contrast, endplate innervation remained significantly lower in partially denervated SOD1^{G93A} plantaris muscles compared to WT plantaris (Fig. 2.3B). Interestingly, the degree of endplate denervation was the same in the unoperated and partially denervated SOD1^{G93A} plantaris muscle 30 days after spinal nerve transection. This was not due to an increase in innervation in the partially denervated muscles because the percentage of innervation remained unchanged from the mean 3-day values (Fig. 2.3B; yellow lines indicates 3-day values). Rather, the observed endplate denervation in the unoperated plantaris likely reflects progression denervation that is known to occur in SOD1^{G93A} fast twitch muscles between P30 and P60 (Hegedus et al., 2007).

To characterize the various sprouting phenotypes between different muscle groups, we quantified the percentage of endplates with terminal sprouts (Fig. 2.3D) and the percentage of axonal sprouts that successfully contacted a denervated endplate (Fig. 2.3E). We found that the percentage of endplates with terminal sprouts was the same in partially denervated soleus muscles in SOD1^{G93A} and WT mice. In contrast, this percentage was significantly lower in partially denervated SOD1^{G93A} plantaris muscles compared to their WT counterparts (Fig. 2.3D). Furthermore, the percentage of axonal sprouts that successfully reinnervated an endplate was the same in partially denervated WT and SOD1^{G93A} soleus muscles. In contrast, the number of successful sprouts was significantly lower ($p=0.006$) in partially denervated plantaris muscles in SOD1^{G93A} mice compared to the same muscle in WT mice (Fig. 2.3E). Together with the innervation results, this data suggests that the impairment in endplate reinnervation following partial

denervation of the SOD1^{G93A} plantaris muscle, but not SOD1^{G93A} soleus, is most likely due to a reduction in sprouting competence.

TSCs at denervated endplates in SOD1^{G93A} plantaris muscles decline over time following partial denervation

It is well established that TSCs are essential for initiating and facilitating collateral reinnervation by neighbouring MNs following partial denervation (Son and Thompson, 1995a, 1995b). Because there was a reduced number of successful sprouts and endplate reinnervation in SOD1^{G93A} plantaris muscles, compared to SOD1^{G93A} soleus and WT muscles following partial denervation, we next sought to investigate if there were differences in TSC morphology between muscle groups. TSCs and endplates were visualized in whole mounted muscle fibres labeled with BTX and immunostained for presynaptic markers Tuj1/SV2, and S100β to visualize all SCs, including TSCs. We chose to examine muscles one, two, and three days after partial denervation, as this corresponds to the time TSCs extend from denervated endplates (Son and Thompson, 1995b). Figure 2.4A shows representative labeling in the four muscle groups three days after partial denervation. Denervated endplates associated with TSCs are indicated by arrows while denervated endplates not associated with a TSC are demarcated by an arrowhead (Fig. 2.4A). When quantified, >80% of the denervated endplates in WT plantaris and soleus muscles were associated with TSCs 1 to 3 days after partial denervation (Fig. 2.4B). In contrast, while >90% of denervated endplates in partially denervated SOD1^{G93A} soleus muscles were associated with TSCs one to three days after spinal nerve transection, there was a significant decline in the percentage of endplates in SOD1^{G93A} plantaris muscles associated with TSCs over the same time-period (Fig. 2.4C). By three days, the number of endplates associated with TSCs was significantly less in the SOD1^{G93A} plantaris muscles (40.9 ± 26.2%) compared to the soleus in the same SOD1^{G93A} mice (94.1 ± 6.97%).

A subset of endplates become disassociated with TSCs in completely denervated SOD1^{G93A} plantaris muscles

To further investigate whether all denervated endplates in SOD1^{G93A} plantaris muscles lose TSCs, we completely denervated the soleus and plantaris muscles by cutting and ligating the tibial nerve (Fig. 2.5A). The presence of TSCs at endplates was then quantified three days later. As shown in Figure 2.5B, most endplates (>80%) in denervated WT soleus and plantaris muscles, as well as denervated SOD1^{G93A} soleus muscles, were associated with TSCs. In contrast, significantly fewer endplates (52.2 ± 11.7%) in completely denervated SOD1^{G93A} plantaris muscles were associated with TSCs three days after denervation.

TSCs loss is muscle fibre-type specific

The observation that approximately 50% of the endplates in completely denervated SOD1^{G93A} plantaris muscles had lost TSCs is intriguing considering the mouse plantaris is composed of approximately 50% type IIb fibres (Bloemberg and Quadrilatero, 2012). Based on this correlation, and the fact that endplates on IIb muscle fibres are the first to withdraw in SOD1^{G93A} mice (Frey et al., 2000), we decided to examine whether this aberrant loss of TSCs was associated with IIb muscle fibres in SOD1^{G93A} plantaris muscles following partial denervation. As such, we partially denervated plantaris muscles in WT and SOD1^{G93A} mice at P30 and immunostained teased muscle fibres with antibodies against myosin heavy chain isoforms IIa and IIb, S100β and labeled endplates with BTX, three days later. Two representative images of endplates in SOD1^{G93A} plantaris muscles immunostained for myosin IIa or IIb shows TSCs associated with two endplates on type IIa fibres (Fig. 2.6A) while the endplate on the IIb fibre was not in contact with a TSC (Fig. 2.6C; arrowhead). When quantified, we found that virtually none of the endplates on type IIa muscle fibres in WT and SOD1^{G93A} plantaris muscles lacked a TSC (Fig. 2.6B). Likewise, none of the endplates associated with type IIb fibres in WT plantaris muscles lacked TSCs (Fig. 2.6D). In contrast, only 64.7 ± 5.56% of endplates on type IIb muscle fibres had TSCs (Fig. 2.6D). Taken together, our results reveal that a population of TSCs associated with type IIb muscle fibres in SOD1^{G93A}

plantaris muscles are lost 3 days post partial denervation. As a result, these endplates are unable to participate in the reinnervation process because they cannot guide axonal sprouts to the denervated endplates.

Macrophages infiltrate partially denervated muscles and interact with TSCs in SOD1^{G93A} plantaris muscles

Macrophages infiltrate and populate denervated muscles in order to clear cellular debris and contribute to inflammation and recovery (Sakaguchi et al., 2014). Macrophage infiltration also occurs in humans with ALS and in animal models of the disease (Trias et al., 2017, 2018). Macrophages and microglia are also known to phagocytose myelin debris after peripheral and central nerve injury (Gaudet et al., 2011). Based on these previous observations, we reasoned that macrophages, recruited into partially denervated muscles, could interact with TSCs at type IIb muscle fibres and contribute to their morphological changes and ultimate removal from endplates.

Figure 2.7A shows representative examples of intramuscular CD11b^{+} macrophages in WT and SOD1^{G93A} plantaris and soleus muscles three days after partial denervation. Quantification of macrophage density near endplate-rich regions showed that SOD1^{G93A} plantaris and soleus muscles were infiltrated by significantly more macrophages compared to their WT counterparts, although neither WT nor SOD1^{G93A} plantaris contained as many macrophages as the partially denervated soleus muscles (Fig. 2.7B). Interestingly, when the distribution of macrophages around TSCs was examined closely, we noticed clear differences in their patterning. As shown in the computer rendering images in Figure 2.7C, macrophages were often in direct contact with TSCs in SOD1^{G93A} plantaris muscles while they were diffusely distributed around the endplates in SOD1^{G93A} soleus muscles, as well as in WT muscles (data not shown).

Masitinib administration reduces macrophage infiltration, TSC loss and improves reinnervation in partially denervated SOD1^{G93A} plantaris muscles

The close association between macrophages and TCSs in the SOD1^{G93A} plantaris muscles provides some evidence that they contribute to their removal from denervated endplates.

To investigate this possibility further, we administered masitinib mesylate to WT and SOD1^{G93A} mice for three days before partially denervating the plantaris muscle, and daily there after. Masitinib mesylate was chosen because it is a selective tyrosine kinase inhibitor that prevents proliferation and migration of hematopoietic cells such as macrophages, and been shown to decrease macrophage infiltration in SOD1^{G93A} rat extensor digitalis longus (EDL) muscles after the onset of paralysis (Trias et al., 2017). Figure 8A shows representative examples of masitinib treated and untreated WT and SOD1^{G93A} plantaris muscles immunolabelled with CD11b two weeks after partial denervation. When quantified, we observed that partially denervated SOD1^{G93A} plantaris muscles from untreated mice had significantly more macrophages present in endplate-rich areas compared to WT mice (183±17.38 vs 76.8±28.2 macrophages/mm^2) (Fig. 2.8B). Interestingly, masitinib administration had little effect on reducing macrophage infiltration in partially denervated plantaris muscles in WT mice. However, plantaris muscles in masitinib treated SOD1^{G93A} mice had a significantly lower density of macrophages at endplate rich regions compared to non-treated SOD1^{G93A} mice (Fig. 2.8B). Furthermore, there was no difference in macrophage density between masitinib treated SOD1^{G93A} and masitinib treated WT mice (Fig. 2.8B).

We next quantified the percentage of denervated endplates with TSCs in masitinib treated and untreated WT and SOD1^{G93A} mice to determine whether reduced macrophage infiltration led to an increased maintenance of TSCs at denervated endplates. Figure 2.8C shows that masitinib administration significantly increased the percentage of TSCs at denervated endplates in SOD1^{G93A} plantaris muscles to WT levels three days after partial denervation. Finally, we wanted to determine whether preventing TSC loss at denervated endplates was sufficient to rescue the observed impairment in reinnervation 14 days after partial denervation. Figure 2.8D shows that the number of reinnervated endplates in plantaris muscles was significantly higher in masitinib treated SOD1^{G93A} mice compared to untreated mice, although the percentage was not as high as masitinib treated WT mice.

Taken together, this data strongly suggest that macrophage infiltration contributes to the loss of TSCs in SOD1^{G93A} plantaris muscles, and that this loss prevents axonal sprouting and reinnervation of denervated endplates after partial denervation in muscles

containing type IIb fibres. Furthermore, these results indicate that the lack of sprouting is not solely an anomaly of SOD1^{G93A} MNs, but rather it is due, in part, to TSC pathology.

Discussion

Here, we demonstrate that TSCs associated with type IIb fibres aberrantly vacate denervated endplates prior to disease onset in SOD1^{G93A} mice when muscles are partially denervated by spinal nerve transection. This pathology was correlated with reduced collateral sprouting from neighboring MNs and the reinnervation of denervated type IIb muscle fibres. In addition, macrophages infiltrated partially denervated muscles in all mice, but were more closely associated with TSCs near endplates on type IIb fibres compared to endplates at type IIa and I fibres in in SOD1^{G93A} mice. To reduce macrophage infiltration, we administered the macrophage migration inhibitor, masitinib mesylate, prior to partially denervating the plantaris muscles in SOD1^{G93A} and WT mice at P30. We found that masitinib treatment reduced macrophage infiltration, prevented TSC loss at denervated endplates on type IIb fibres in SOD1^{G93A} mice, and restored collateral reinnervation to near WT values. These findings indicate that erroneous macrophage mediated removal of TSCs at denervated type IIb fibres underlies, at least in part, the differential sprouting response motor unit types have during early disease progression in SOD1^{G93A} mice.

Our observation that axonal sprouting is compromised in SOD1^{G93A} plantaris, but not soleus muscles, is consistent with previous studies examining sprouting in fast and slow twitch muscles in rodent models of ALS (Frey et al., 2000; Schaefer et al., 2005; Pun et al., 2006; Hegedus et al., 2007). For example, electrophysiological studies on slow twitch soleus and fast twitch extensor digitalis longus (EDL) muscles in SOD1^{G93A} mice showed a progressive decline in motor unit numbers between P40 and P80 in the EDL, but not soleus muscles (Hegedus et al., 2007). Because EDL muscle forces declined in parallel with motor unit numbers, no functional compensation by sprouting was observed. Similarly, Caroni and colleagues (Pun et al., 2006) reported an abrupt loss of MNs innervating type IIb fibres (fast fatigable units, FF) with little sign of sprouting during disease progression in SOD1^{G93A} mice while MNs innervating type I fibres (Slow units, S) sprouted and maintained enlarged motor units until the animals died. Taken together,

our study along with these are consistent with the existence of large MNs with a low sprouting capacity and smaller MNs that sprout efficiently (Schaefer et al., 2005; Arbour et al., 2017).

Somewhat surprisingly, we did not observe further denervation in the partially denervated SOD1^{G93A} plantaris between P30 and P60 (Fig. 2.3B) even though additional MNs would have died during that time period (Hegedus et al., 2007). This lack of additional denervation could be due to sprouting and reinnervation of previously denervated endplates by FR and S MNs (Pun et al., 2006). Additionally, it has been shown that partially denervating muscles in SOD1^{G93A} mice leads to functional hyperactivity of the remaining MNs and that this increased activity protects them from further denervation (Gordon et al., 2010; Sharp et al., 2018). Either response could explain the lack of progressive denervation in the SOD1^{G93A} plantaris in our study.

Our results showing abnormal TSC behaviour at denervated endplates on type IIb fibres are consistent with previous publications documenting irregularities in TSC morphology and activity during disease progression in rodent models of ALS (Arbour et al., 2015; Carrasco et al., 2016b, 2016a). For example, TSCs were found to be unusually disorganized at endplates in the fast twitch medial gastrocnemius muscle prior to denervation in SOD1^{G93A} and SOD1^{G85R} mice and later, as the disease progressed, became absent from denervated NMJs (Carrasco et al., 2016b). Electron microscopy later confirmed the absence of TSCs at endplates 7 days after denervation leading Pinter and colleagues (Carrasco et al., 2016a) to suggest that this abnormality could hinder reinnervation from neighboring MNs. Using a slowly progressing model of ALS (SOD1^{G37R} mice), Robitaille and colleagues (Arbour et al., 2015) showed TSCs had an abnormally elevated activity-dependent increase in intracellular Ca^{2+} levels prior to disease onset and that this elevation was associated with an increased level of neurotransmitter release. Furthermore, the authors reported a larger than normal contribution of muscarinic AChR activation of TSCs during synaptic transmission pre-disease onset in SOD1^{G37R} mice (Arbour et al., 2015). This, in turn, could alter TSC gene expression causing them to lose the ability to stabilize/remodel the synapse (Kang et al., 2014; Arbour et al., 2015, 2017; Martineau et al., 2018) or become susceptible to phagocytosis (Vilalta and Brown, 2018).

Although ALS is not initiated by immune alterations, disease progression is amplified by activated microglia and inflammatory responses in the central nervous system (CNS) (Thonhoff et al., 2018; Beers and Appel, 2019). Inflammatory responses, including intramuscular infiltration of skeletal muscles with macrophages, have also been documented outside the CNS in animal models of ALS and in patients with the disease (Martinez-Muriana et al., 2016; Van Dyke et al., 2016; Trias et al., 2017; Wang et al., 2017; Beers and Appel, 2019). Furthermore, interventions reducing intramuscular macrophage infiltration attenuate the rate of endplate denervation (Martinez-Muriana et al., 2016; Van Dyke et al., 2016; Trias et al., 2017, 2018; Wang et al., 2017) and improve the overall sprouting capacity caused by the loss of TSCs at type IIb fibres (present study).

While little is known about macrophage-SC interactions in ALS, a great deal is known about the role of macrophages in Wallerian degeneration. Following a peripheral injury, SCs produce monocyte chemoattractant proteins which contributes to the recruitment of macrophages to the injury site, where they work to phagocytose axonal and myelin debris produced by the degenerating distal nerve segment (Stoll et al., 1989; Toews et al., 1998; Caillaud et al., 2019). Indeed, macrophage-SC dynamics are essential for normal axonal regeneration and remyelination after a peripheral nerve injury (Barrette et al., 2008; Stratton et al., 2018). Therefore, it is not intuitively obvious why intramuscular macrophages would change from a cell required for axonal repair to one detrimental to it in ALS. However, gene expression is known to be altered as early as P40 in the spinal cord and muscle of $SOD1^{G93A}$ mice (de Oliveira et al., 2013; Saris et al., 2013). It is therefore conceivable that altered gene expression in TSCs could make them more susceptible to phagocytosis. Interestingly, studies by Rotshenker and colleagues suggest that myelin in the CNS and peripheral nervous system normally down-regulate their own phagocytosis by sending a “do not eat me” message to macrophages by expressing CD47 on their cell surface (Gitik et al., 2011, 2014). It is possible that the $SOD1^{G93A}$ mutation alters CD47 expression and/or its function in TSCs in $SOD1^{G93A}$ mice causing the cells to be targeted and degraded by infiltrating macrophages. However, if true, it still doesn’t explain why TSCs associated with denervated type IIb endplates are more likely to be selectively targeted.

However, there is precedence for targeting and degradation of specific neuronal subtypes by glia in ALS (Nagai et al., 2007; Di Giorgio et al., 2008) indicting that distinct cell recognition and subsequent degradation can take place. In addition, it is well recognized that distinct subclasses of MNs with differing activation patterns selectively innervate discrete subtypes of muscle fibres. Because Ca^{2+} responses in TSCs discriminate between patterns of activity and regulate presynaptic plasticity (Todd et al., 2010) it seems plausible that different subclasses of TSCs exists to match MN activation patterns and muscle fibre contractile properties. Evidence for different TSC subtypes comes from the study by De Winter et al., (2006) where they showed semaphorin 3A (Sema3A), an inhibitor of axonal regeneration, is selectively upregulated in TSCs associated with type IIb muscle fibres in $SOD1^{G93A}$ mice (De Winter et al., 2006). Whether other proteins such as CD47 are selectively expressed or repressed in TSCs at denervated type IIb fibres in $SOD1^{G93A}$ mice remains to be determined.

To what extent our findings are applicable to human ALS is unknown. Evidence that they may be comes from a recent randomized clinical trial where masitinib, combined with riluzole, slowed Amyotrophic Lateral Sclerosis Functional Rating Scale-Revised (ALSFRS-R) decline in patients with ALS to a clinically meaningful degree (Mora et al., 2019). Furthermore, clinical improvement was greater when the masitinib/riluzole treatment was initiated at a less severe stage of the disease (Mora et al., 2019). These clinical findings are consistent with our study because we would predict better outcomes if masitinib was administered early in disease progression when larger MNs innervating type IIb fibres are still functioning and capable of sprouting. Improved sprouting capacity would maintain motor function longer and slow the ALSFRS-R decline. Finally, while more research is clearly warranted, this study highlights the NMJ as early therapeutic target to improve MN function and enhance quality of life for patients with ALS.

Chapter 2 Tables and Figures

Table 2.1. Primary Antibodies

Antiserum	Host Species	Dilution	Clonality	Source
Beta III tubulin (Tuj1)	Mouse	1:500	Monoclonal	BioLegend, San Diego, CA
CD11b	Rat	1:250	Monoclonal	Invitrogen, UK/Rockford IL
Myosin heavy chain type IIa (SC-71)	Mouse	1:5	Monoclonal	Developmental Studies Hybridoma Bank, Iowa City, IA
Myosin heavy chain type IIb (BF-F3)	Mouse	1:5	Monoclonal	Developmental Studies Hybridoma Bank, Iowa City, IA
S100	Rabbit	1:500	Polyclonal	Dako, Denmark
SV2	Mouse	1:500	Monoclonal	Developmental Studies Hybridoma Bank, Iowa City, IA

Figure 2.1. Quantification of endplate denervation after spinal nerve section. **A,** Schematic illustration showing site of spinal nerve transection (red x) used to partially denervate the plantaris and soleus muscles in WT and $SOD1^{G93A}$ mice. **B,C** Representative tetanic recordings (mN) from partially denervated (PD) and unoperated (unop) plantaris (B) and soleus muscles (C) in WT and $SOD1^{G93A}$ mice 3 days post-surgery. **D,** Mean (± SD) maximum tetanic force of partially denervated WT and $SOD1^{G93A}$ plantaris and soleus muscles shown as a percentage of force generated from the unoperated muscles in the contralateral limb ($p=0.5000$ for plantaris and 0.2226 for soleus, Mann-Whitney test). **E,** Representative confocal images, stained for synaptic vesicle protein 2 (SV2) and R-BTX, show different NMJ innervation patterns. **F,G** Percent endplate innervation (mean ± SD) in unoperated and partially denervated WT and $SOD1^{G93A}$ plantaris (F) and soleus (G) three days post-spinal nerve transection ($p=0.0571$ and $p=0.2000$ for plantaris and soleus muscles, respectively, $n=4$; Mann-Whitney test). ns, not significant; unop, unoperated; PD, partially denervated; SOL, soleus; PLA, plantaris. Scale bar = 25 μm.

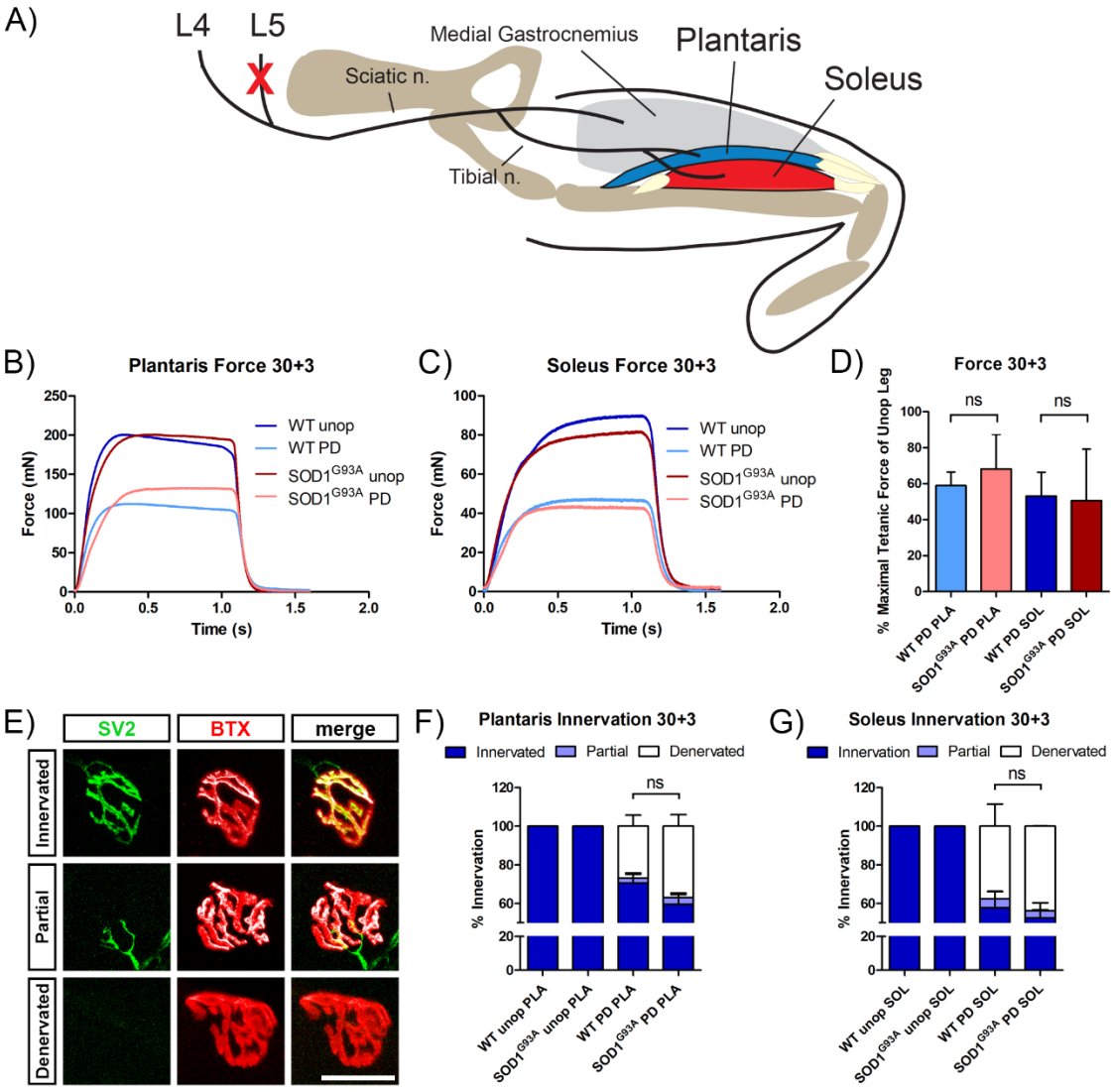
A)
L4
L5
Medial Gastrocnemius
Plantaris
Sciatic n.
Soleus
Tibial n.
B)
Plantaris Force 30+3
Force (mN)
Time (s)
WT unop
WT PD
SOD1G93A unop
SOD1G93A PD
C)
Soleus Force 30+3
Force (mN)
Time (s)
WT unop
WT PD
SOD1G93A unop
SOD1G93A PD
D)
Force 30+3
% Maximal Tetanic Force of Unop Leg
ns
ns
WT PD PLA
SOD1G93A PD PLA
WT PD SOL
SOD1G93A PD SOL
E)
SV2
BTX
merge
Innervated
Partial
Denervated
F)
Plantaris Innervation 30+3
Innervated
Partial
Denervated
% Innervation
ns
WT unop PLA
SOD1G93A unop PLA
WT PD PLA
SOD1G93A PD PLA
G)
Soleus Innervation 30+3
Innervation
Partial
Denervated
% Innervation
ns
WT unop SOL
SOD1G93A unop SOL
WT PD SOL
SOD1G93A PD SOL

Figure 2.2. Endplate reinnervation is compromised in SOD1^{G93A} plantaris muscles 14 days after partial denervation. **A,** Representative confocal images of NMJs in unoperated and partially denervated plantaris and soleus muscles in SOD1^{G93A} and WT mice 14 days after spinal nerve transections. Sections were immunostained for SV2 and labeled with R-BTX. Arrowheads indicate denervated endplates and asterisks indicate partially innervated endplates **B,C** Percentage of endplates innervated (mean ± SD) in unoperated and partially denervated plantaris (B) and soleus muscles (C) 14 days after nerve section. **p=0.0079 and ns p=0.5000, for the plantaris and soleus muscles, respectively (Mann-Whitney test). Abbreviations as in Figure 1. Scale bar = 50 μm.

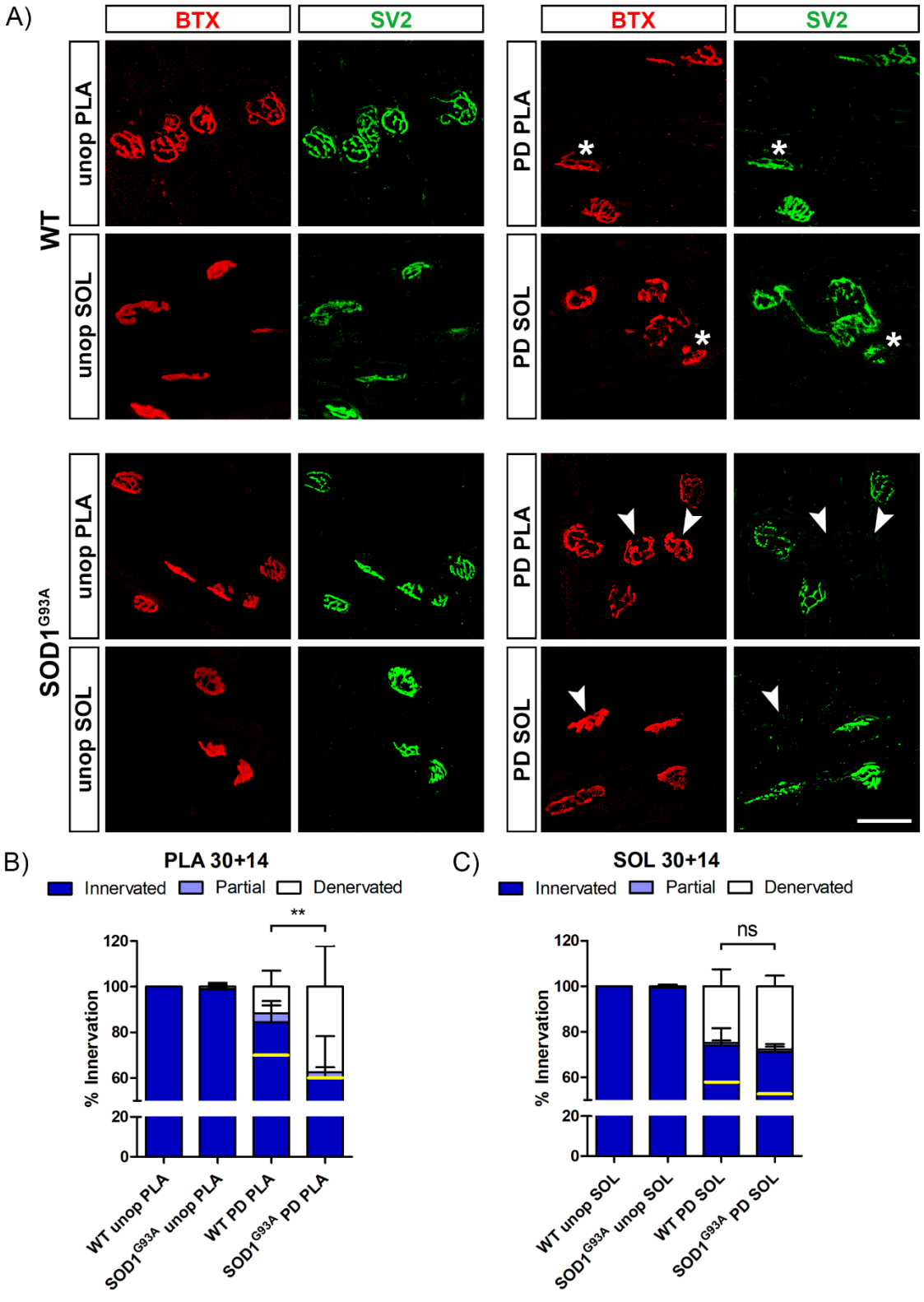
A)
BTX
SV2
BTX
SV2
WT
unop PLA
unop SOL
PD PLA
PD SOL
SOD1G93A
unop PLA
unop SOL
PD PLA
PD SOL
B)
PLA 30+14
Innervated
Partial
Denervated
**
% Innervation
120
100
80
60
20
0
WT unop PLA
SOD1G93A unop PLA
WT PD PLA
SOD1G93A PD PLA
C)
SOL 30+14
Innervated
Partial
Denervated
ns
% Innervation
120
100
80
60
20
0
WT unop SOL
SOD1G93A unop SOL
WT PD SOL
SOD1G93A PD SOL

Figure 2.3. Endplate innervation and axonal sprouting in compromised in SOD1^{G93A} plantaris muscles 30 days after partial denervation. **A,** Representative confocal images of NMJs in unoperated and partially denervated plantaris and soleus muscles in SOD1^{G93A} and WT mice 30 days after spinal nerve transections. Sections were immunostained for SV2/TUJ1 (green) and labeled with R-BTX (red); co-localization appears yellow. Partially denervated muscles contained denervated endplates (arrowheads), partially innervated endplates (arrows) and endplates reinnervated by a collateral sprout (asterisks). In some cases, axonal sprouts did not contact an endplate (+). **B,C** Percentage of endplates innervated (mean ± SD) in unoperated and partially denervated plantaris (B) and soleus muscles (C) 30 days after nerve section. *p=0.0133 for unop plantaris, *p=0.05 for PD plantaris, and p=0.2000 for PD soleus (Mann-Whitney tests). **D,** Percent endplates (mean ± SD extending terminal sprouts. *p=0.0476, Mann-Whitney test. **E,** Percent of terminals sprouts (mean ± SD) contacting an endplate (successful sprouts). **p=0.0060, Mann-Whitney test. Abbreviations as in Figure 1. Scale bar = 50 μm.

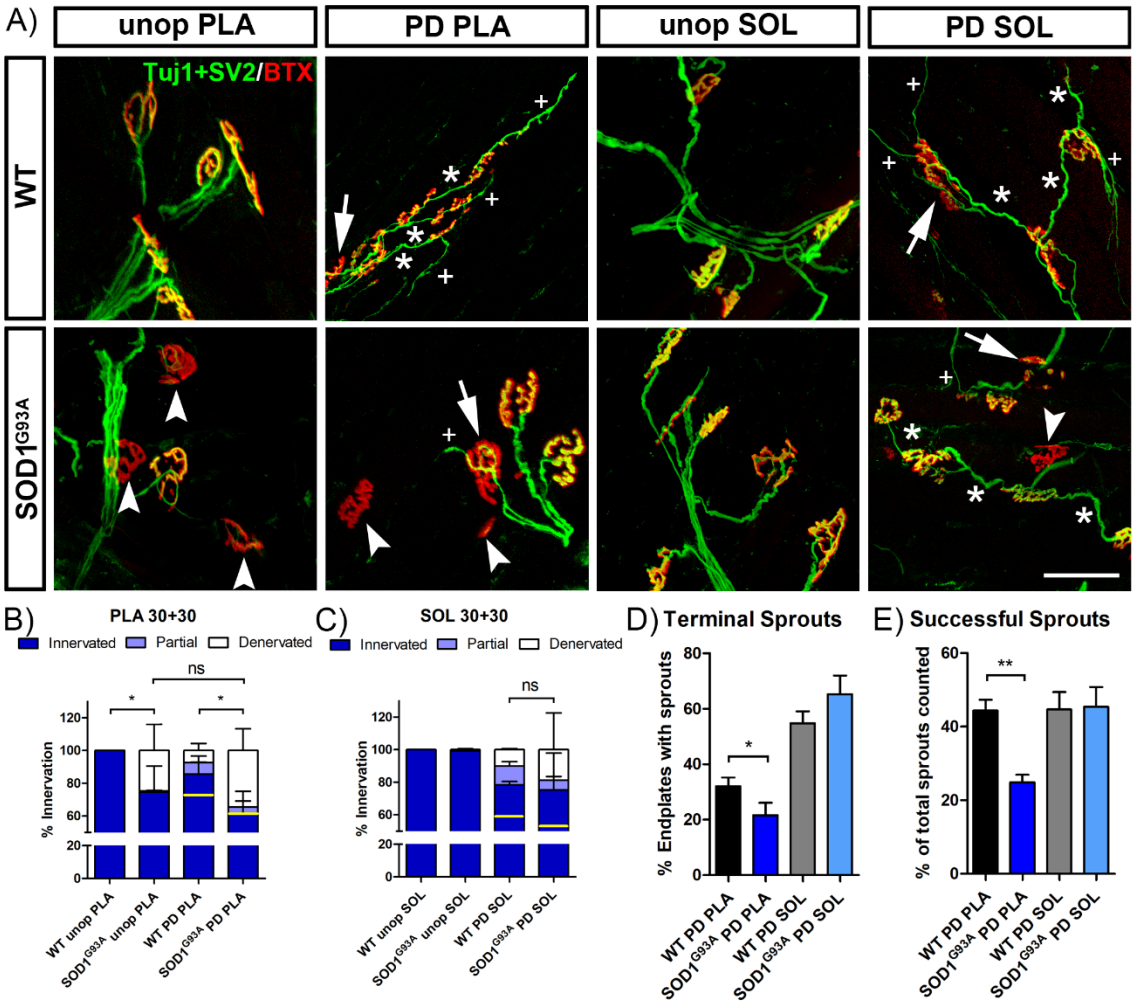
A)
unop PLA
PD PLA
unop SOL
PD SOL
WT
SOD1G93A
Tuj1+SV2/BTX
B)
PLA 30+30
Innervated
Partial
Denervated
% Innervation
ns
*
*
WT unop PLA
SOD1G93A unop PLA
WT PD PLA
SOD1G93A PD PLA
C)
SOL 30+30
Innervated
Partial
Denervated
% Innervation
ns
WT unop SOL
SOD1G93A unop SOL
WT PD SOL
SOD1G93A PD SOL
D) Terminal Sprouts
% Endplates with sprouts
*
WT PD PLA
SOD1G93A PD PLA
WT PD SOL
SOD1G93A PD SOL
E) Successful Sprouts
% of total sprouts counted
**
WT PD PLA
SOD1G93A PD PLA
WT PD SOL
SOD1G93A PD SOL

Figure 2.4. Denervated endplates in SOD1^{G93A} plantaris muscles lose TSCs over time post partial denervation. **A,** Representative confocal images of NMJs in WT and SOD1^{G93A} plantaris and soleus muscles 3 days after partial denervation labeled with R-BTX (red) and immunostained with Tuj1/SV2 (green) and S100β (white). Arrowheads indicate denervated endplates with TSCs, arrows indicate denervated endplates without TSCs, and asterisks indicate sprouts. **B,C** Percentage of denervated endplates (mean ± SD) with a TSC in WT (B) and SOD1^{G93A} (C) plantaris and soleus muscles 1-3 days post partial denervation. *$p<0.05$, **$p<0.001$ (Two-way ANOVA). Abbreviations as in Figure 1. Scale bar = 50 μm.

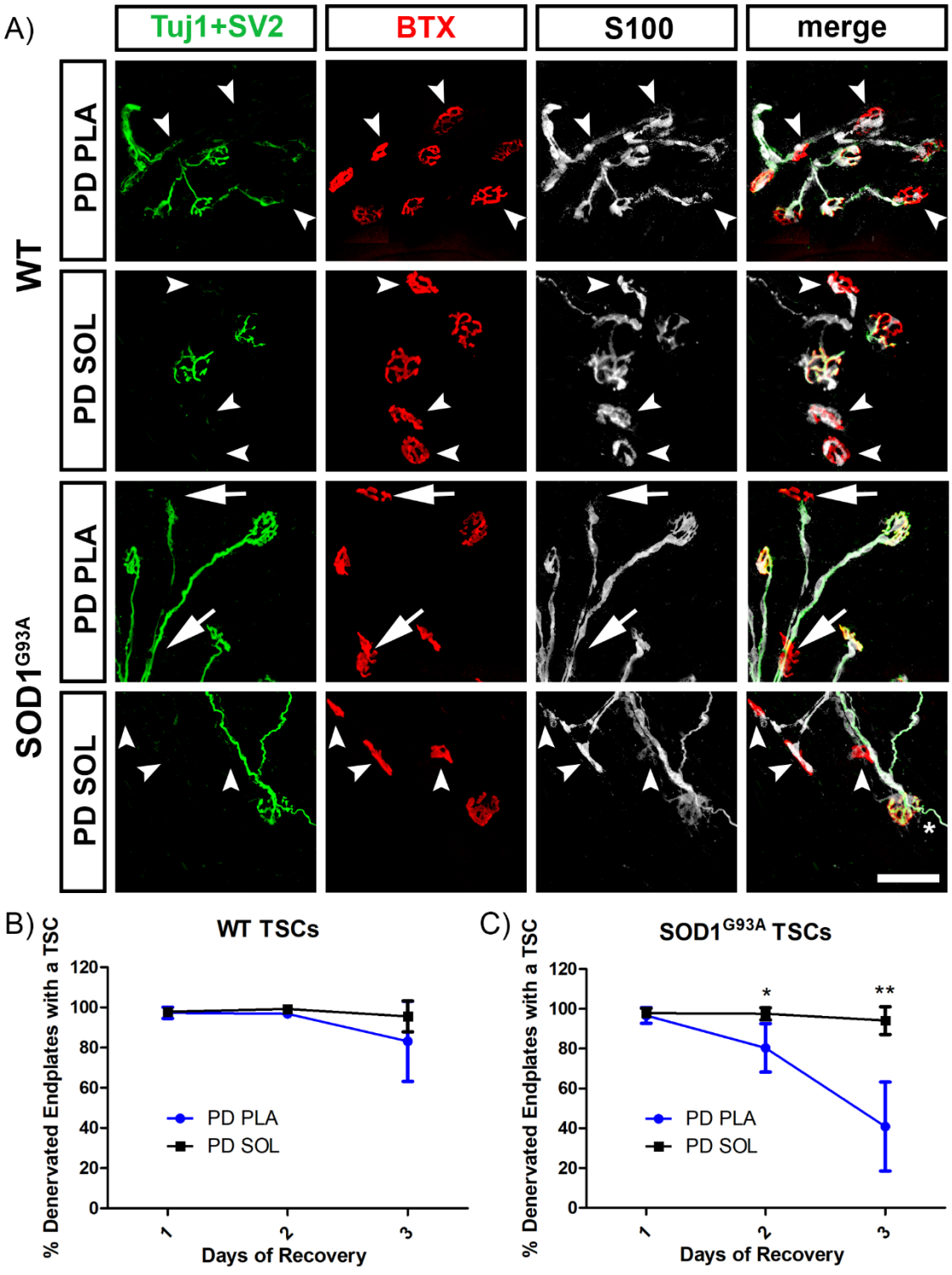
A)
Tuj1+SV2
BTX
S100
merge
WT
SOD1G93A
PD PLA
PD SOL
PD PLA
PD SOL
B)
WT TSCs
% Denervated Endplates with a TSC
120
100
80
60
40
20
0
PD PLA
PD SOL
1
2
3
Days of Recovery
C)
SOD1G93A TSCs
% Denervated Endplates with a TSC
120
100
80
60
40
20
0
*
**
PD PLA
PD SOL
1
2
3
Days of Recovery

Figure 2.5. TSCs are absent at a subset of endplates in completely denervated $SOD1^{G93A}$ plantaris muscles. **A,** Schematic illustration showing complete denervation surgery. Red 'x' indicates where the tibial nerve was section and ligated. **B,** Quantification of TSC presence at denervated endplates (mean ± SD) in WT (n=4) and $SOD1^{G93A}$ (n=6) mice 3 days following complete denervation. **p=0.0011 (Mann-Whitney test). Abbreviations as in Figure 1.

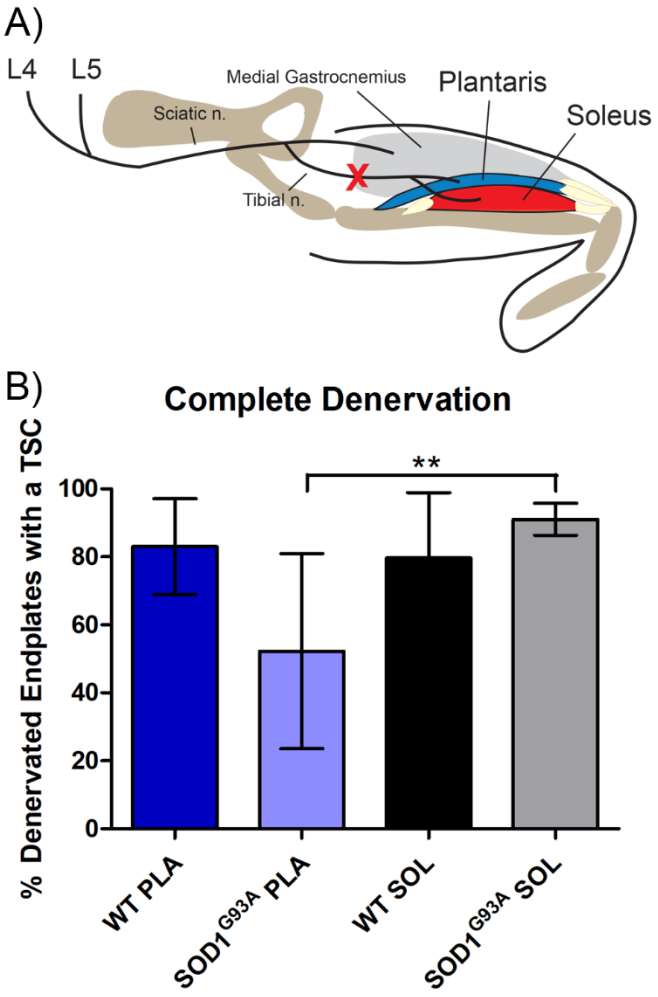
A)
L4
L5
Medial Gastrocnemius
Plantaris
Soleus
Sciatic n.
Tibial n.
X
B)
Complete Denervation
% Denervated Endplates with a TSC
**
100
80
60
40
20
0
WT PLA
SOD1G93A PLA
WT SOL
SOD1G93A SOL

Figure 2.6. Muscle fibre-type specific absence of TCSs at endplates in SOD1^{G93A} plantaris muscles. **A,C** Confocal images of endplates on plantaris muscles fibres in SOD1^{G93A} mice labeled with BTX and immunostained for S100β and myosin IIa (A) or IIb (C). **B,D** Quantification of TSC presence (mean ± SD) at endplates on type IIa (B) and IIb (D) plantaris muscle fibres in WT and SOD1^{G93A} mice. $p = 0.3223$ and $p = 0.0133$ for IIa and IIb, respectively (Mann-Whitney test). Scale bar = 50 μm.

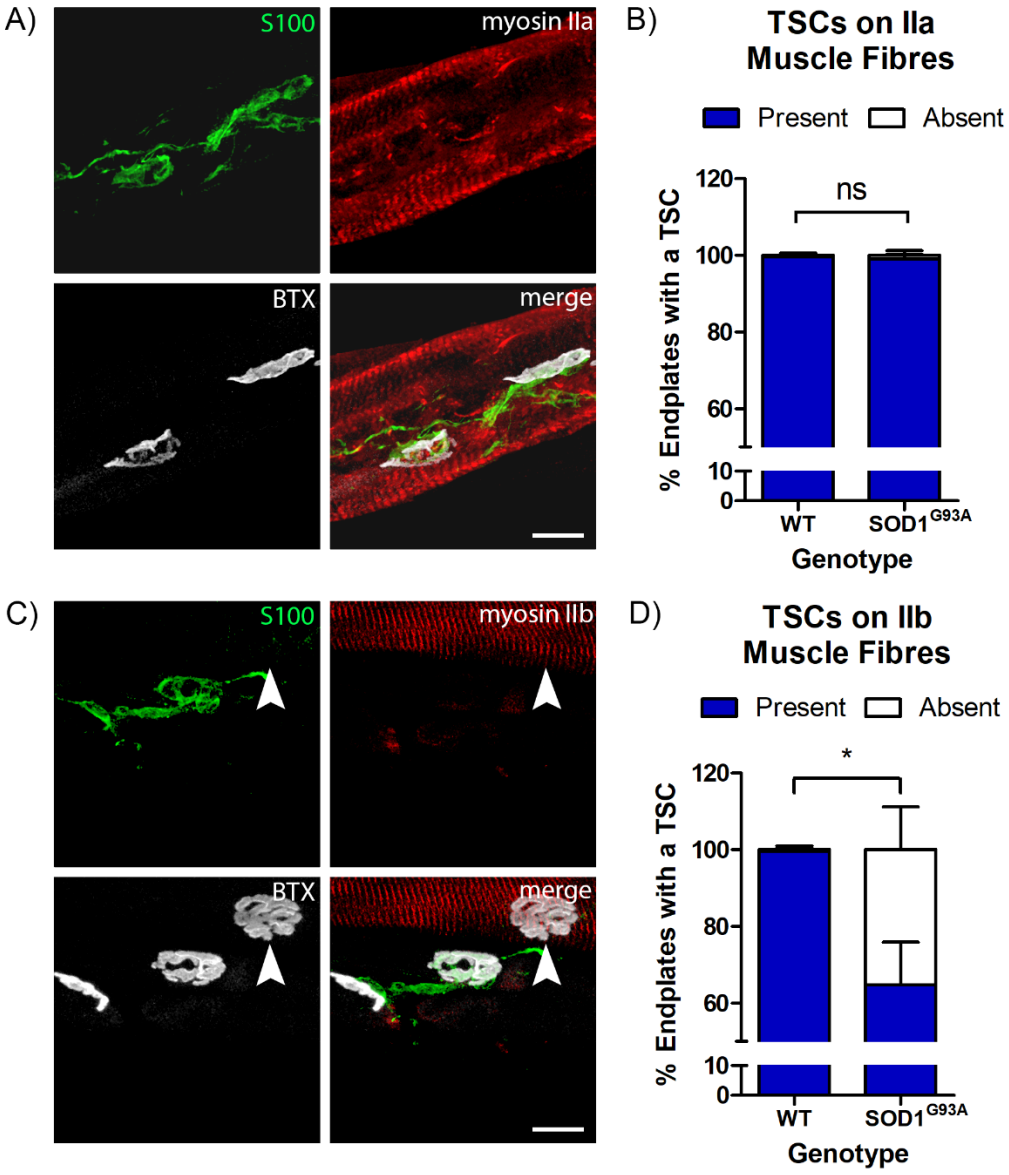
A)
S100
myosin IIa
BTX
merge
B)
TSCs on IIa Muscle Fibres
Present
Absent
ns
% Endplates with a TSC
120
100
80
60
10
0
WT
SOD1G93A
Genotype
C)
S100
myosin IIb
BTX
merge
D)
TSCs on IIb Muscle Fibres
Present
Absent
*
% Endplates with a TSC
120
100
80
60
10
0
WT
SOD1G93A
Genotype

Figure 2.7. Macrophages infiltrate partially denervated muscles and appear to interact with more closely with endplates in plantaris muscles in $SOD1^{G93A}$ mice. **A,** Representative confocal images of partially denervated plantaris and soleus muscles in WT and $SOD1^{G93A}$ mice 3 days after surgery. Muscles were labelled with R-BTX and immunostained for CD11b. **B,** Macrophage density (mean ± SD) around endplates on plantaris and soleus muscles in WT and $SOD1^{G93A}$ mice (*p=0.0143; Mann-Whitney test). **C,** Imaris three-dimensional renderings of confocal images taken of endplates on plantaris and soleus muscle fibres in $SOD1^{G93A}$ mice two days of surgery showing S100 (green), macrophages (CD11b – red), and BTX (white). $SOD1^{G93A}$ PLA scale bars = 5 µm; $SOD1^{G93A}$ SOL left scale = 20 µm, right scale = 10 µm.

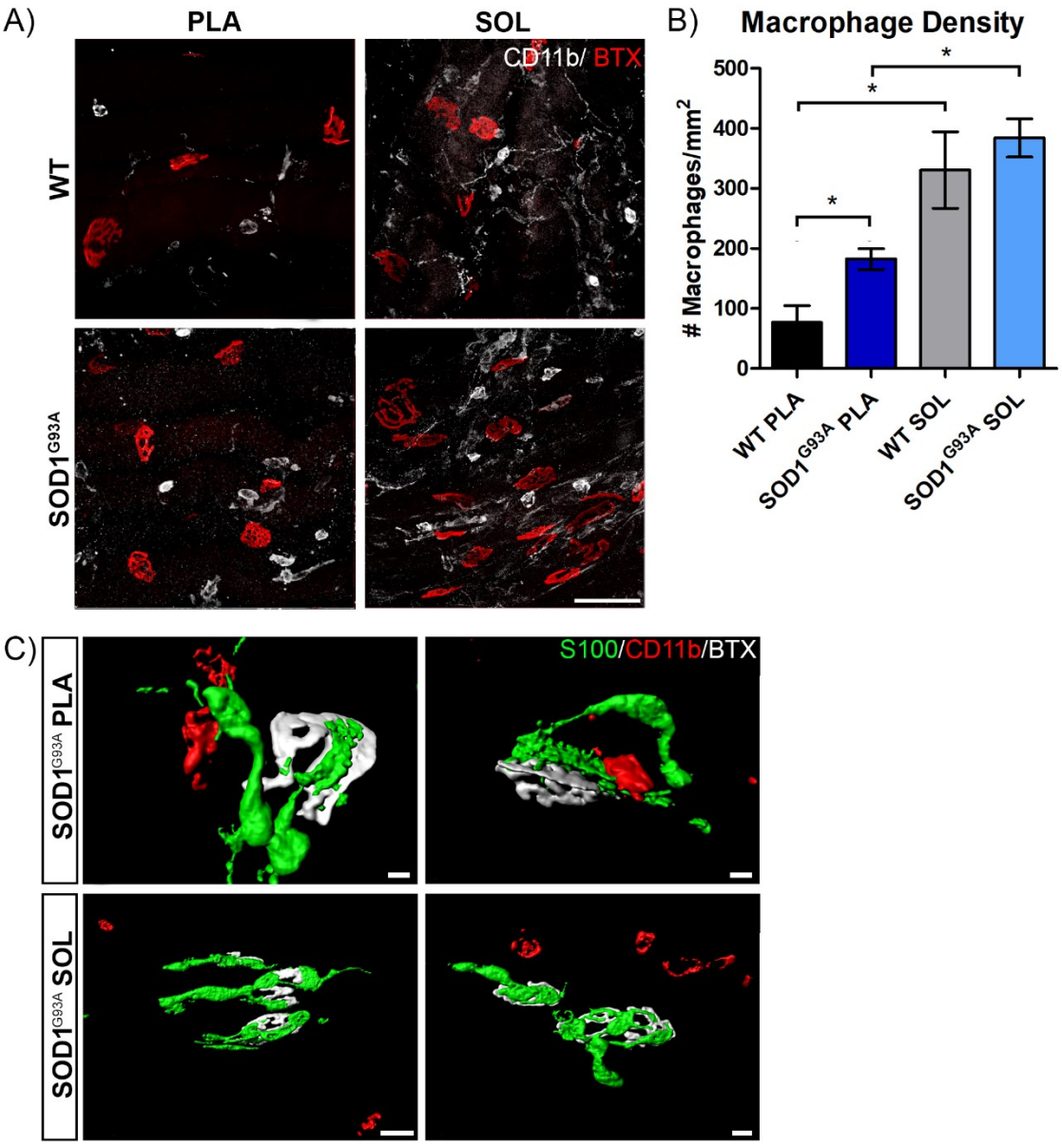
A)
PLA
SOL
CD11b/ BTX
WT
SOD1G93A
B)
Macrophage Density
Macrophages/mm2
500
400
300
200
100
0
*
*
*
WT PLA
SOD1G93A PLA
WT SOL
SOD1G93A SOL
C)
S100/CD11b/BTX
SOD1G93A PLA
SOD1G93A SOL

Figure 2.8. Macrophage inhibition reduces macrophage density, increases TSC presence and innervation in partially denervated SOD1^{G93A} plantaris muscles. **A,** Representative confocal images of partially denervated WT and SOD1^{G93A} plantaris muscles 3 days after surgery. Muscles were labeled with R-BTX and immunostained for CD11b. **B,** Mean (± SD) macrophage density at endplates in WT and SOD1^{G93A} plantaris muscles from mice treated, or not treated, with masitinib. (*p=0.0143). **C,** Mean (± SD) percentage of denervated endplates with TSCs in partially denervated plantaris muscles from WT and SOD1^{G93A} mice that were treated or not treated with masitinib (n=4). *p=0.0278, WT PD PLA untreated vs SOD1^{G93A} PD PLA untreated; *p=0.0159, WT PD PLA untreated vs WT PD PLA + masitinib; **p=0.0079, SOD1^{G93A} PD PLA untreated vs SOD1^{G93A} PD PLA + masitinib; and **p=0.0079, SOD1^{G93A} PD PLA untreated vs WT PD PLA + masitinib. **D,** Mean (± SD) percent innervation of endplates in partially denervated WT and SOD1^{G93A} plantaris muscles 14 days of surgery. Mice were treated or not treated with masitinib 3 days prior to the partial denervation (WT untreated n=5, masitinib treated n=4; SOD1^{G93A} untreated n=4, masitinib treated n=4). *p=0.0143, SOD1^{G93A} PD PLA untreated vs SOD1^{G93A} PD PLA + masitinib; *p=0.0286, SOD1^{G93A} PD PLA + masitinib and WT PD PLA + masitinib; **p=0.0079, SOD1^{G93A} PD PLA untreated vs WT PD PLA untreated; ns p=0.0556, WT PD PLA untreated vs SOD1^{G93A} PD PLA + masitinib (Mann-Whitney tests for all). Scale bar = 50 μm.

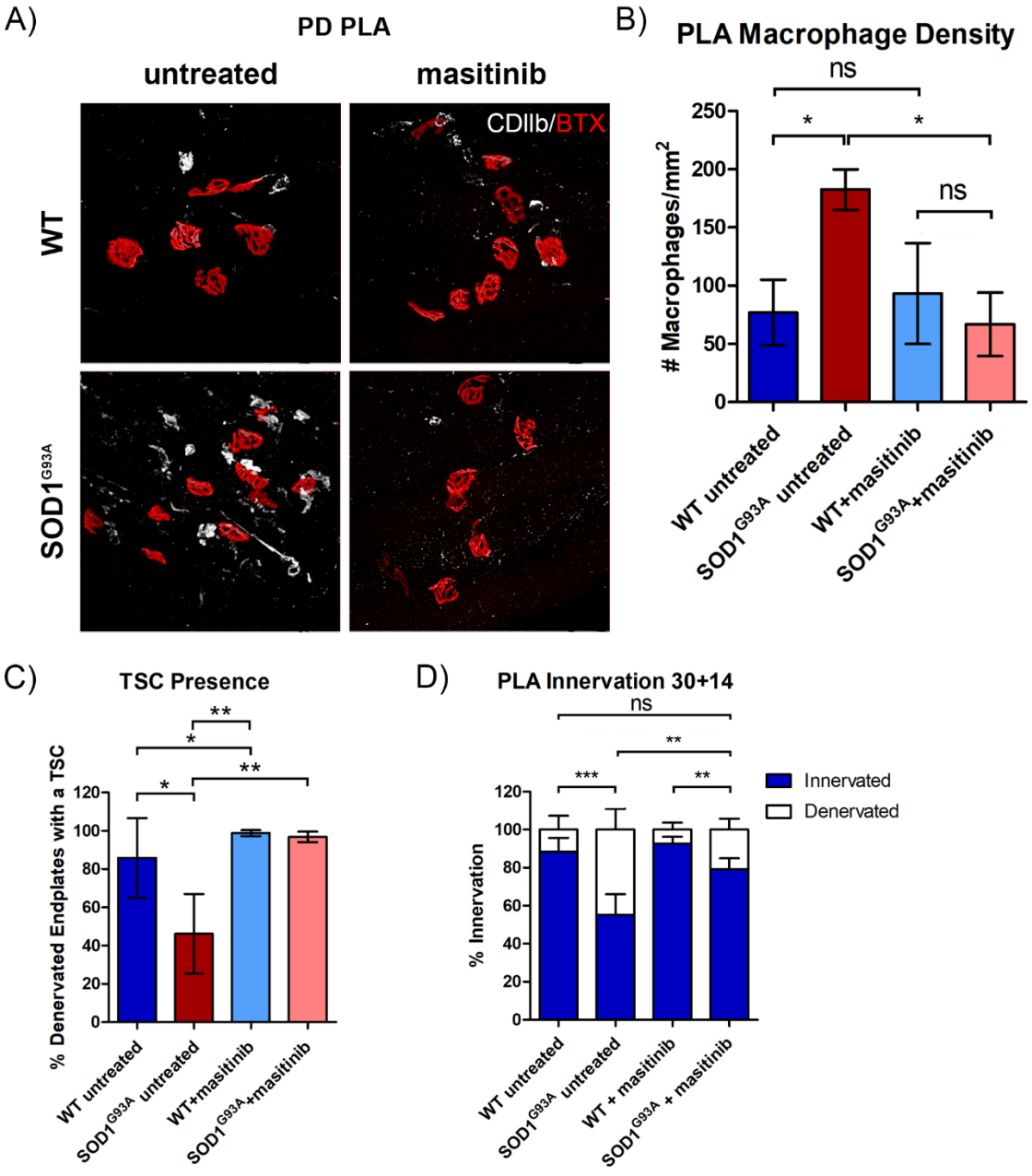
A)
PD PLA
untreated
masitinib
WT
SOD1G93A
CDIIb/BTX
B)
PLA Macrophage Density
Macrophages/mm2
ns
*
*
ns
WT untreated
SOD1G93A untreated
WT+masitinib
SOD1G93A+masitinib
C)
TSC Presence
% Denervated Endplates with a TSC
D)
PLA Innervation 30+14
% Innervation
Innervated
Denervated
WT + masitinib
SOD1G93A + masitinib

CHAPTER 3: CHARACTERIZATION OF A NOVEL MOUSE MODEL OF BMP4 LOSS IN SKELETAL MUSCLE

Abstract

Growth factors are well known to regulate morphological and electrophysiological properties of synapses including the NMJ. For example, in *Drosophila*, mutants lacking proteins in the Bone Morphogenic Protein 4 (BMP4) signaling pathway have abnormally small muscle fibres, smaller NMJs with ultrastructure synaptic defects, smaller evoked excitatory junctional potentials, reduced frequency of spontaneous neurotransmitter release and an ~ 4-fold decrease in quantal content. Whether BMP4 signaling has a similar role at vertebrate NMJs is currently unknown. To examine this question, we generated doxycycline inducible, muscle-specific BMP4 null mice by crossing HSA-rtTA/TRE-Cre mice with mutant mice where exon 4 of the BMP4 gene is flanked by *loxP* sites (referred to here as $HSA^{Cre}BMP4^{fl/fl}$ mice). Doxycycline induced knock-down of BMP4 expression in muscle was initiated at three months of age. Motor behaviour tasks were examined pre- and post-doxycycline administration while electrophysiological and morphological characteristics of the NMJ were recorded 2 and 4 months after BMP4 knock-down. We found that $HSA^{Cre}BMP4^{fl/fl}$ mice had a reduced latency to fall on the rotarod turning at 40 rpm compared to wildtype (WT) littermates 14 days after doxycycline administration. *Ex vivo* contractile force recordings indicated that soleus muscles in $HSA^{Cre}BMP4^{fl/fl}$ mice were significantly weaker than their WT counterparts by 4 months. Morphologically, type I, but not type IIa muscle fibre cross-sectional areas in soleus muscles were significantly smaller in $HSA^{Cre}BMP4^{fl/fl}$ mice 4 months after doxycycline administration. Interestingly, NMJs were larger in $HSA^{Cre}BMP4^{fl/fl}$ mice compared to the controls due to a significant increase in acetylcholine receptor cluster number and distribution. Electrophysiological studies showed that the amplitude and frequency of miniature endplate potentials (mEPPs) were significantly smaller in $HSA^{Cre}BMP4^{fl/fl}$ mice compared to their WT littermates. Similarly, evoked EPP amplitude and quantal content were also significantly smaller in $HSA^{Cre}BMP4^{fl/fl}$ mice while the number of neurotransmission failures at high stimulus frequencies was significantly higher in muscles lacking BMP4. Finally, muscle spindle structure and

function were significantly compromised in $HSA^{Cre}BMP4^{fl/fl}$ animals. Consequently, as observed in *Drosophila*, these results indicate that muscle-derived BMP4 regulates morphological and electrophysiological attributes of the NMJ in mice. We are currently exploring the possibility that abnormalities caused by the loss of muscle-derived BMP4 are associated with an accelerated, premature ageing phenotype.

Introduction

The formation and maturation of the NMJ is regulated by a multitude of coordinated anterograde and retrograde signals between the innervating MN and post-synaptic muscle fibres, as well as the TSCs that cap the synapse (Sanes and Lichtman, 2001; Wu et al., 2010). Incredibly, once established, NMJs become stable and persist throughout life. Indeed, constant stability of the NMJ is essential for normal skeletal muscle function. Conditions causing NMJ instability can lead to a cessation of neurotransmission, motor axon withdrawal, muscle weakness and even paralysis.

One condition known to cause NMJ instability leading to motor axon withdrawal and MN death is ALS (Fischer et al., 2004; Gould et al., 2006; Moloney et al., 2014; Arbour et al., 2017; Martineau et al., 2018). Results from animal models of ALS indicate that axon withdrawal occurs independently to the activation of the cell death pathway in MNs (Kostic et al., 1997; Gould et al., 2006). As a result, ALS is considered a multifaceted disease with numerous modifiers, including those that lead to NMJ instability/axon withdrawal and those that cause MN cell death (Moloney et al., 2014). Consequently, understanding the cellular mechanisms underlying NMJ instability could eventually lead to combination therapies aimed to promote synaptic stability and enhance MN survival.

Several pre- and postsynaptic components of the NMJ have been shown to be involved in its stability, including extracellular matrix proteins, cell adhesion molecules, and growth factors (Bloch-Gallego, 2015). With respect to ALS, the transforming growth factor superfamily molecule, BMP, has recently been shown to be involved in NMJ stability in zebrafish (Duval et al., 2014). Zebrafish mutants harboring homozygous null mutations in the BMP-family gene, *gdf6a*, have a shorter lifespan, reduced endurance in a swimming task, disrupted NMJ morphology, and a 50% reduction in spinal MNs by nine months of age (Duval et al., 2014). Interestingly, these phenotypes were exacerbated in zebrafish with mutations in *gdf6a* and SOD1, a mutation known to cause ALS (Rosen et al., 1993), suggesting that *gdf6a* could be a modulator of the disease (Duval et al., 2014).

Our primary understanding of the role of BMPs in NMJ function comes from studies in *Drosophila* larvae with mutations in glass bottom boat (*gbb*) and wishful thinking (*wit*), the *Drosophila* homologs to BMP4 and its receptor, BMPRII (Aberle et

al., 2002; Marqués et al., 2002; McCabe et al., 2003, 2004; Goold and Davis, 2007). Taken together, these studies revealed that mutations in the BMP4 signaling pathway cause pre- and postsynaptic pathologies, including reduced frequency of spontaneous transmitter release, reduced amplitude of evoked postsynaptic potentials, reduced quantal content, and abnormally small NMJs and muscle fibres.

The role of BMP4 signaling at the NMJ in higher vertebrates is not as well understood. In adult mice, BMPRII, the receptor for BMP4 is expressed in adult MNs (Chou et al., 2013) while BMP4 is found in muscle fibres and Schwann cells (Son and Thompson, 1995a; Chou et al., 2013). It is also transported both retrogradely and anterogradely along motor axons (Chou et al., 2013). Additionally, BMP4 signaling pathways, downstream of BMPRII activation, control muscle fibre mass in adult mice (Sartori et al., 2013; Winbanks et al., 2013). Whether BMP4 expression regulates neurotransmission and morphology of the NMJ in adult mice, like its homolog in *Drosophila,* is currently unknown.

Here, we generated inducible, muscle specific, BMP4 null mice ($HSA^{cre}BMP4^{fl/fl}$) to genetically inhibit its expression at P30. Using behavioural, electrophysiological, and anatomical approaches, we found that muscle-specific knock out of BMP4 causes significant motor task deficits, abnormal neurotransmission, and increased fragmentation of endplates over time. Surprisingly, contractile force and muscle fibre cross-sectional areas were only modestly attenuated in $HSA^{cre}BMP4^{fl/fl}$ mice compared to their WT littermates. To reconcile this disparity, we performed a horizontal ladder task and found that $HSA^{cre}BMP4^{fl/fl}$ mice performed poorly, suggesting that the motor deficit was partially due to impaired proprioception. Together, these results indicate that muscle-derived BMP4 in vertebrates is required for normal NMJ structure and function in the adult, similar to that reported previously in *Drosophila* larvae.

Methods

Mice

Skeletal muscle specific, doxycycline inducible, BMP4 knockout mice (referred to as $HSA^{Cre}BMP^{fl/fl}$ mice) were generated by crossing B6;C3-Tg(ACTA1-rtTA,tetO-

cre)102Monk/J mice (Rao and Monks, 2009) (Jackson Labs) with B6;129S4-Bmp4tm1Jfm/J mice (Liu et al., 2004) (Jackson Labs). Skeletal muscle specific, doxycycline inducible tdTomato mice were generated by crossing B6;C3-Tg(ACTA1-rtTA,tetO-cre)102Monk/J mice with B6.Cg-Gt(ROSA)26Sortm9(CAG-tdTomato)Hze/J (Madisen et al., 2010) (Jackson Labs) to generate $HSA^{cre}tdTomato^{fl/+}$ mice (referred to as $HSA^{cre}ROSATomato^{fl/fl}$ mice throughout). Cre recombinase activity, under control of the tetO, tetracycline-responsive regulatory element, was induced in both strains following administration of doxycycline in food pellets (Bio-Serv). Because human skeletal α-actin (HSA) is selectively expressed in skeletal muscles fibres (Leu et al., 2003; Rao and Monks, 2009), induction of Cre recombinase activity caused selective loss of BMP4 expression, and production of tdTomato, in the skeletal muscle of $HSA^{Cre}BMP^{fl/fl}$ and $HSA^{Cre}ROSATomato^{fl/fl}$ mice, respectively. HSAcre-negative littermates were used as controls and are referred to as WT throughout. Male and female mice were included in all data sets considering no sex differences were observed following post-hoc analysis. All experiments were conducted in accordance to the guidelines of the Canadian Council on Animal Care and the policies of Dalhousie University.

Behavioural tests

Mice were trained on the rotarod (Ugo Basile) (designated as baseline) prior to doxycycline administration. Three days later (designated "day 1"), rotarod testing was initiated on a semi-daily basis for 30 days. On each day of testing, mice randomly performed three trials at 20 rpm and four trials at 40 rpm with five-minute breaks between trials. Latency to fall was recorded for each trial with a maximum time of 100 seconds. Grip strength measurements were taken using a Grip Strength test (Bioseb – In Vivo Research Instruments), where mice held onto a horizontal bar with their forelimbs while the tail was gently pulled (parallel to the floor) until they released their grip. Grip force was recorded from five consecutive trials per mouse. Baseline grip strength was assessed prior to doxycycline administration and then after 5, 12, 19 and 26 days. The same researcher performed all grip strength measurements to ensure consistency. Horizontal ladder experiments were performed prior to feeding with doxycycline, and additionally after five days of doxycycline administration. $HSA^{cre}BMP4^{fl/fl}$ (n=6) and WT

(n=6) mice were filmed while performing three passes across a horizontal ladder, and the number of hindlimb mis-steps (i.e. steps between rungs), per pass, were counted during a post-hoc analysis of the videos.

Ex vivo *isometric force recordings*

Mice were anesthetized with a mixture of isoflurane and oxygen. Under aseptic conditions, the soleus muscle and nerve supply were quickly removed and transferred to a Sylgard–coated (Dow Corning) recording chamber that was continuously perfused with carbogenated (95% O^2 and 5% CO^2) Tyrodes solution containing 125 mM NaCl, 24 mM $NaHCO_3$,5.37 mM KCl, 1 mM $MgCl_2$, 1.8 mM CaCl2, and 27.75 mM dextrose. A knot was tied around the proximal tendon and secured in place with an insect pin. A suture (6-0) was tied around the distal tendon and attached to a force transducer (FT 03; Grass Technologies). A fine-tipped glass stimulating suction electrode was used to deliver electrical current (0.05 ms duration) to the innervating nerve via an S88 stimulator (Grass Technologies) that was isolated from the ground using a stimulus isolation unit (PSIU6; Grass Technologies). Muscle length was adjusted to maximal isometric contraction. Tetanic forces were recorded at 50 Hz (1 s duration) using a Digidata 1322A analog-to-digital board and AxoScope version 10.2 software (Molecular Devices).

Intracellular NMJ physiology

Mice were anesthetized with an isoflurane/oxygen mixture to remove the soleus muscle and supplying nerve. The muscle was pinned in a Sylgard coated recording chamber perfused with carbogenated Tyrode solution containing 125mM NaCl, 5.37mM KCl, 24mM NaHCO3, 1 mM MgCl2, 1.8 mM CaCl2 and 5% dextrose. The muscles were then pre-incubated for 90 minutes in well-oxygenated Tyrode solution containing 5μM conotoxin (CTX) GIIIB (Alomone Labs, Jerusalem, Israel) to block nerve evoked muscle contractions (Bewick et al., 2004) and then returned to Tyrode solution without CTX for intracellular recordings.

Intracellular recordings of NMJs were performed using sharp recording electrodes (15-30 MΩ) filled with 3M KCl. Spontaneous miniature endplate potentials (mEPPs) and

nerve-evoked transmitter release (endplate potentials; EPPs) were recorded with a MultiClamp 700B amplifier and digitized with MultiClamp Digidata 1140A. Nerve-evoked transmitter release was induced by stimulating the soleus nerve with a fine tip glass suction electrode using a Grass S88 stimulator that was isolated from ground using a SIU5 stimulus isolation unit. Data were acquired with Clampex 10.2 software (Molecular Devices) and analysed using MiniAnalysis software (Synaptosoft). Quantal content (m) was determined by the direct method (m=mean EPP amplitude/mean mEPP amplitude) from EPPs collected at a 1Hz stimulation rate and mEPPs recorded over one minute. Failures were identified as a stimulus without a subsequent change in resting membrane potential. Resting membrane potentials were -55 mV to -85 mV and data were eliminated if the resting membrane potential changed by >10% of its initial value by the end of the recording.

Immunofluorescence and imaging

Soleus muscles were pinned at physiological length in cryostat molds and immersed in a 1:2, 20% sucrose to O.C.T Compound (Tissue Tek) mixture. Muscles were then flash-frozen in a pool of isopentane cooled in liquid nitrogen and then stored at -80 °C at least overnight. Muscles were sectioned (20 μm) using a cryostat (Leica) and mounted onto microscope slides. All sections, except those to be immunostained for S58, were fixed in 4% PFA for 15 minutes, rinsed three times ten minutes in PBS, and then incubated overnight in PBS containing 0.3% triton (PBS-T), 10% goat serum and select number of primary antibodies including rabbit anti DsRed (Clontech, 1:1000), rabbit anti BMP4 (Abcam, 1:250), mouse anti SC-71 (Developmental Studies Hybridoma Bank, 1:5) and mouse anti S58 (Developmental Studies Hybridoma Bank, 1:5). Sections immunolabeled with S58 were incubated without pre-fixation and were fixed prior to incubation in secondary antibodies, as above. All sections were then washed in PBS and incubated with the appropriate secondary antibodies at 1:500 including Cy3 goat anti rabbit (Jackson Laboratories), Cy2 goat anti mouse (Jackson Laboratories) Cy3 goat anti mouse (Jackson Laboratories), DyLight 594 goat anti-mouse IgA (Abcam). Sections were also labeled with rhodamine-conjugated α-bungarotoxin (BTX; Invitrogen, 1:500) or Alexa Fluor 647-conjugated α-bungarotoxin (Invitrogen, at 1:250) for two hours. Slides were rinsed in

PBS and mounted in a mixture of 50% Glycerol in PBS containing 0.03 mg/ml phenylene diamine to prevent fading.

NMJ morphology and innervation were characterized using muscle whole-mount preparations. Briefly, muscles were pinned at physiological length in cryostat molds on cork and fixed in 4% PFA for 15 minutes. Muscles were then rinsed in PBS, permeabilized in cold methanol for 6 minutes, rinsed, and submerged in PBS in a Sylgard-coated dish. The proximal tendons were secured in place with insect pins and distal tendons removed. Bundles of muscle fibres were then carefully teased apart using fine forceps under a dissecting microscope (Zeiss). Teased muscle bundles were then incubated and shaken overnight in PBS-T containing 10% goat serum and goat anti-mouse SV2 antibody (Developmental Studies Hybridoma Bank). Sections were then rinsed and incubated in PBS-T containing 10% goat serum and goat anti mouse Cy2 (1:500) and BTX (1:500) for one hour. The remaining tendon was removed, and the muscle bundles were transferred to microscope slides and coverslipped in 50% Glycerol in PBS containing 0.03 mg/ml phenylenediamine.

Imaging was performed either on an upright microscope (Leica) utilizing ZenBlue (Zeiss) software or a laser scanning confocal microscope (Zeiss) utilizing Zen 2009 (Zeiss) software. Images were incorporated into figures using either Adobe Photoshop or Imaris (for fragments) software.

BMP4 fluorescence intensity measurements

Cross-sections of WT soleus muscle immunostained for BMP4 and labeled with BTX were viewed on a Leica upright microscope. To determine an appropriate, consistent exposure time across sections, 10 sections were visualized, at random, using the auto-exposure setting in ZenBlue software (Zeiss). The mean auto-exposure time was calculated and then manually applied to all sections used for fluorescence intensity measurements. Fluorescent intensity measurements were taken at muscle membranes and BTX^{+} endplates from $HSA^{Cre}BMP4^{fl/fl}$ and WT soleus muscle sections. The final fluorescence intensities at these locations were determined following subtraction of the background fluorescence.

Quantification of endplate size and fragmentation

Endplate area measurements were performed on longitudinal sections of WT and $HSA^{Cre}BMP4^{fl/fl}$ soleus muscle labeled with BTX and imaged using an upright microscope (Leica). The area of 50 BTX^+ endplates/muscle were quantified by delineating a circumferential line encompassing all individual AChR fragments within a single endplate using the contour function in ZenBlue software (Zeiss). Z-stacks through entire endplates in whole-mounted WT and $HSA^{Cre}BMP4^{fl/fl}$ muscles were imaged with a confocal microscope (Zen 2009 software, Zeiss). The number of individual fragments making up an endplate were quantified from three-dimensional reconstruction of BTX^+ fragments (Imaris, surface function).

Quantification of endplate innervation was determined by focusing up and down on BTX^+ endplates using an upright fluorescence microscope (Leica). For any given BTX^+ site, it was determined to be fully innervated or partially innervated based on the degree of overlap in SV2 immunostaining. If SV2 immunostaining was present in the same configuration as the BTX labelling, it was termed to be fully innervated. Endplates with partial colocalization of SV2 and BTX were classified as partially innervated. Denervated endplates were those with no SV2 colocalization at a BTX^+ site.

Cross-sectional area measurements

Whole soleus muscle cross-sectional area measurements were obtained from the midbelly (largest) sections of each muscle. Cross-sectional areas of soleus type I ($S58^+$) and type IIa ($SC\text{-}71^+$) muscle fibre types were quantified from 50 fibres/muscle at endplate-rich regions in WT and $HSA^{Cre}BMP4^{fl/fl}$ mice. Muscle fibre number was estimated by dividing the average soleus muscle cross-sectional area with the average cross-sectional areas of the individual muscle fibres.

Statistical Analysis

Two-way ANOVAs were performed to examine the differences between groups over time while Bonferroni, Unpaired t, and Mann–Whitney tests were used to compare

differences between individual groups. Data were analyzed using GraphPad Prism 5 software and were considered statistically significant at $p<0.05$.

Results

BMP4 expression in WT and HSA^{Cre}BMP4$^{fl/fl}$ mice

Prior to studying the function of BMP4 in skeletal muscle, we first wished to reconfirm its expression pattern in adult mouse soleus muscle. As reported by Chou et al. (2013), we found that BMP4-immunoreactivity was detected along the sarcolemma and at AChR-rich, BTX^{+} endplates in soleus muscle fibre cross-sections (Fig. 3.1A). Using immunofluorescence intensity to quantify relative expression levels, we found that BMP4 was more highly expressed at the NMJ compared to non-endplate regions (Fig. 3.1A,B, $p<0.0001$; see also Chou et al., 2013). Taken together, these results support those by Chou et al. (2013), indicating that BMP4 is expressed along the sarcolemma, at the NMJ.

To selectively knock-out BMP4 expression in adult skeletal fibres, we bred doxycycline inducible HSA^{cre} mice with BMP4$^{fl/fl}$ mice to generate HSA^{cre}BMP4$^{fl/fl}$ mice. We chose this cross because Cre recombinase activity is highly expressed in skeletal muscles when mice are administered doxycycline, as shown by the ROSATomato expression in the soleus muscle cross-section taken from an induced HSA^{cre}ROSATomato$^{fl/fl}$ mouse (Fig. 3.1C). To show that BMP4 expression is eliminated from skeletal muscle fibres after doxycycline administration, we immunostained soleus muscle cross-sections from WT and HSA^{cre}BMP4$^{fl/fl}$ mice for BMP4. As shown in Figure 3.1D, BMP4 was highly expressed in the WT and absent in the HSA^{cre}BMP4$^{fl/fl}$ soleus muscle. Taken together, these results reconfirm that BMP4 is expressed in adult skeletal muscles and its expression can be eliminated in doxycycline induced HSA^{cre}BMP4$^{fl/fl}$ mice.

HSA^{Cre}BMP4$^{fl/fl}$ mice display motor deficits after doxycycline administration

To assess the role of BMP4 in skeletal muscle function, we first conducted forelimb grip strength and rotarod performance tests before, and after, daily administration of doxycycline to P90 WT and HSA^{cre}BMP4$^{fl/fl}$ mice. As shown in Figure 3.2A, forelimb

grip strength declined over time in HSA^{cre}BMP4$^{fl/fl}$ compared to WT mice ($p<0.0001$, two-way ANOVA) even though the strength at base line (i.e. prior to doxycycline treatment) was the same. In addition to lost grip strength, motor performance was also reduced in HSA^{Cre}BMP4$^{fl/fl}$ mice compared to their WT littermates. While HSA^{Cre}BMP4$^{fl/fl}$ mice had rotarod scores like their WT littermates when the bar was rotated at 20 rpm (Fig. 3.2B), they we significantly worse over time (i.e. latency to fall off) when the rotation was increased to 40 rpm (Fig. 3.2C; $p>0.0001$, two-way ANOVA). Post hoc analysis (Bonferroni test) showed significant differences between genotypes at 12, 23, 26 and 29 days, further confirming the poorer rotarod performance by the HSA^{Cre}BMP4$^{fl/fl}$ mice compared to WT mice.

HSA^{Cre}BMP4$^{fl/fl}$ soleus strength becomes weaker over time since doxycycline administration

To determine to what extent the decline in rotarod performance in the HSA^{Cre}BMP4$^{fl/fl}$ mice was due to a decrease in skeletal muscle strength, we used *ex vivo* recordings to compare contractile forces of soleus muscles from HSA^{Cre}BMP4$^{fl/fl}$ and WT mice 2- and 4-months post doxycycline administration. As shown in the representative twitch contractile recordings (Fig. 3.3A), we found that twitch force was significantly reduced by ~27% and ~26% in HSA^{Cre}BMP4$^{fl/fl}$ mice at 2 and 4 months, respectfully, compared to WT values (Fig. 3.3A,B; $p=0.0338$ and $p=0.0164$ for 2 and 4 months, respectively). Unlike twitch force, there was no significant difference between tetanic forces recorded during a train of stimuli (50 Hz, 1 sec duration) two months after doxycycline treatment (Fig. 3.3C,D; $p=0.1080$). However, there was a significant reduction in tetanic forces generated by soleus muscles from HSA^{Cre}BMP4$^{fl/fl}$ muscles compared to their WT littermates 4 months after doxycycline administration (Fig. 3.3C,D; $p=0.0371$).

To examine whether the fatigability changes in muscles lacking BMP4, we conducted fatigue tests on soleus muscles from HSA^{Cre}BMP4$^{fl/fl}$ and WT mice after 2 and 4 months of doxycycline treatment. As shown in Figure 3.3E, all muscles at both time points had the same fatigue index, indicating that the loss of BMP4 expression did not noticeably alter whole muscle fatigability ($p=0.2534$ and $p=0.1555$ for 2 and 4 months,

respectively). Together, these results suggest that the loss of BMP4 in adult muscle fibres causes a modest, but significant, loss in contractile force overtime and it does not alter muscle fatigability.

Muscle fibre-type specific atrophy in HSA^{Cre}BMP4$^{fl/fl}$ mice

Muscle contractile force is determined by its cross-sectional area and specific tension (force exerted by fibres per unit area). Whole muscle cross-sectional area, in turn, is determined by the number and cross-sectional area of each muscle fibre. Consequently, the small, but significant, loss of force observed by HSA^{Cre}BMP4$^{fl/fl}$ soleus muscles could be due to a decrease in one or more of these factors. To examine whether there were changes in these factors, we fixed and froze each muscle at physiological lengths after the conclusion of the tension recording experiments. Muscles were then cut for immunohistochemical and anatomical analysis. Figures 3.4A and 3.4B show that the average whole muscle cross-sectional area and estimated muscle fibre number did not differ between WT and HSA^{Cre}BMP4$^{fl/fl}$ soleus muscles, respectively. However, when cross-sectional areas of different fibre types (Fig. 3.4C) were quantified separately, we found that the cross-sectional area of the type I, but not type IIa, fibres were significantly smaller in HSA^{Cre}BMP4$^{fl/fl}$ soleus muscles compared to their WT counterparts (Fig. 3.4D; $p=0.4426$ and $p=0.4314$, respectfully). Taken together, these results indicate that the loss of BMP4 in adult skeletal muscle fibres has a modest, but significant, decrease in contractile force and type I cross-sectional area. However, it seems unlikely that these modest changes alone account for the loss of motor function observed in rotarod performance test (see below).

The loss of BMP4 causes postsynaptic disorganization in HSA^{Cre}BMP4$^{fl/fl}$ mice

Previous studies in *Drosophila* larvae reported morphological alterations at the NMJ, such as decreased NMJ size and bouton number, when *gbb* was functionally mutated during development (McCabe et al., 2003). To determine whether similar abnormalities occur at vertebrate NMJs when BMP4 expression is removed in the adult, we quantified NMJ area by labeling HSA^{Cre}BMP4$^{fl/fl}$ and WT soleus muscles with BTX after conducting the *ex vivo* force recordings (i.e. 4 months after doxycycline administration)

(Fig. 3.5A). The size of the NMJs (delineated by a circumferential line encompassing all individual AChR fragments; Fig. 3.5A) in $HSA^{Cre}BMP4^{fl/fl}$ mice were significantly larger than those in WT mice (Fig. 3.5B). However, when three-dimensional reconstructions of individual endplates were performed, we noticed that endplates in $HSA^{Cre}BMP4^{fl/fl}$ mice were abnormally fragmented (Fig. 3.5C). Indeed, when quantified, endplates in $HSA^{Cre}BMP4^{fl/fl}$ mice were found to be significantly more fragmented compared to their WT littermates (Fig. 3.5D; $p<0.0001$). Consequently, the overall increase endplate size was due to increased fragmentation and spreading of individual AChR clusters within individual NMJs.

To determine whether the highly fragmented endplates in the $HSA^{Cre}BMP4^{fl/fl}$ mice were accompanied by presynaptic modifications, we immunostained and labeled teased muscle fibres from both genotypes with SV2 and BTX. Interestingly, we found that significantly fewer NMJs in $HSA^{Cre}BMP4^{fl/fl}$ soleus muscles were innervated 4 months after doxycycline administration (Fig. 3.5E, $p=0.0143$). Furthermore, a significantly higher number of soleus NMJs in $HSA^{Cre}BMP4^{fl/fl}$ mice ($p=0.0286$) were only partially innervated, as defined by the degree of overlap between the pre- and postsynaptic structures (Fig. 3.5F; see Methods for details). Taken together, these results indicate that BMP4 expression in adult muscle fibres is required for the normal organization of pre- and postsynaptic structures.

Synaptic transmission is altered in $HSA^{Cre}BMP4^{fl/fl}$ mice

Neurotransmission deficits indicative of presynaptic abnormalities have been reported in *Drosophila* larvae with mutations in *wit* (Aberle et al., 2002; Marqués et al., 2002) or *gbb* (McCabe et al., 2003). To determine whether similar deficits occur in mice when BMP4 expression is excised from muscle fibres in the adult, we conducted sharp electrode electrophysiological recordings of soleus NMJs in $HSA^{Cre}BMP4^{fl/fl}$ and WT mice four months after doxycycline administration. Spontaneous neurotransmitter release was recorded in normal saline containing μ-conotoxin to block muscle contraction (Fig. 3.6A). We found that the amplitude (Fig. 3.6A,B) and frequency of mEPPs (Fig. 3.6A,C) were significantly reduced in the mutants ($p=0.0004$ and 0.0005, respectively). In addition, rise time of mEPPs was significantly longer in the $HSA^{Cre}BMP4^{fl/fl}$ muscles

compared to WT (Fig. 3.6D; p=0.0025), possibly because of asynchronous activation of AChRs due to the increased amount of fragmentation or because many endplates were only partially innervated.

Evoked neurotransmitter release was recorded by stimulating the innervating nerve at 1 Hz while recording from the NMJs (Fig. 3.7A). Similar to the mEPPs, EPP amplitudes were significantly reduced in $HSA^{Cre}BMP4^{fl/fl}$ mice soleus muscles compared to their WT littermates (Fig. 3.7A,B; p=0.0001). Furthermore, quantal content was also significantly smaller in the mutant mice (Fig. 3.7C; p=0.0011). When plotted as a frequency histogram (Fig. 3.7D, left panel), or a cumulative distribution (Fig. 3.7D, right panel), quantal content values recorded from $HSA^{Cre}BMP4^{fl/fl}$ mice shifted almost in parallel to the WT values indicating that the entire population of NMJs in the mutant mice had smaller quantal content.

Previous studies on *Drosophila* larvae mutants lacking *wit* showed a reduction in neurotransmitter release during repetitive stimuli as indicated by an increased rate of failures at low extracellular [Ca^{2+}] (Marqués et al., 2002). To determine whether neurotransmission is compromised at high rates of activation, we analyzed the percentage of failures in $HSA^{Cre}BMP4^{fl/fl}$ and WT soleus muscles during a 1 sec stimulus train at 5, 10, 20, 50, and 100 Hz. While no failures were observed at frequencies between 5-50 Hz, there was a significant increase in the percentage of failures per cell (15.4%) in $HSA^{Cre}BMP4^{fl/fl}$ soleus muscle fibres compared to WT (2.86%) at 100 Hz (Fig. 3.7E,F). Taken together, the intracellular recordings indicate that neurotransmission at the NMJ is compromised when BMP4 expression is excised from adult skeletal muscle fibres.

BMP4 is required for normal muscle spindle structure and proprioception

While significant, the anatomical and physiological deficits observed in the $HSA^{Cre}BMP4^{fl/fl}$ mice cannot completely account for the ~50% reduction in the rotarod performance test considering neurotransmission was not severely impaired (Fig. 3.2C). The rotarod performance test assesses numerous aspects of motor function including proprioception. Because HSA (the cre recombinase promoter used in this study) is expressed in nuclear bag and chain fibres of muscle spindles (Leu et al., 2003) it is possible that the decline in rotarod performance was due, in part, to a loss of BMP4

expression in intrafusal fibres. This loss, in turn, could lead to reduced proprioception and poorer rotarod performance.

To examine this possibility, we performed a horizontal ladder task. The horizontal ladder task assesses sensory feedback from muscle spindles and can be quantified by measuring the incidence of rear-foot drop (i.e. stepping between rungs) rate while walking along the ladder (Akay et al., 2014). We performed baseline ladder experiments on uninduced $HSA^{Cre}BMP4^{fl/fl}$ mice compared to WT and found no difference in mis-steps between groups (Fig. 3.8A). Five days after doxycycline administration, we found that $HSA^{Cre}BMP4^{fl/fl}$ mice had a significantly higher number of foot-drops compared to their WT littermates (Fig. 3.8B; $p=0.0426$). Together, these results provide evidence to suggest that BMP4 signaling contributes to normal muscle spindle structure and function and may underlie, in part, the poorer performance in the rotarod test.

Discussion

Together, these results indicate muscle-derived BMP4 contributes to the morphological and electrophysiological stability of the adult vertebrate NMJ. In its absence, motor performance during a rotarod test declines, muscles become significantly weaker, neurotransmission at the NMJ is compromised, endplates fragment, and mice perform worse during a motor task designed to assess proprioceptive function.

Our results showing BMP4 expression in adult muscle fibres and SCs agrees with previous work by Chou et al. 2013 where BMP4 mRNA expression was detected in differentiated C2C12 skeletal muscle cells, and not in neurons. Although mRNA for the BMP4 receptor, BMPRII, was expressed both in a neuronal cell line and in laser captured spinal MNs. BMP4 was also found to be transported retrogradely and anterogradely along the sciatic nerve, suggesting that it has a signaling role in the cell body and NMJ (Chou et al., 2013). Although the function of BMP4 was not determined, their results showing increased expression in muscle fibres and sciatic nerve after a peripheral nerve injury, along with *in vitro* data showing BMP4 promoting MN survival, suggests that it may act as a muscle-derived neural trophic factor after injury (Chou et al., 2013).

Our findings of declining rotarod performance in $HSA^{Cre}BMP4^{fl/fl}$ mice after doxycycline administration agrees with previous studies conducted in *Drosophila* and in

zebrafish. Disruption of *gbb* signaling in *Drosophila* by mutating its receptor, *wit,* results in flies with severe impairments at escaping the pupal case, with many individuals dying during the larval stages (Marqués et al., 2002). Even after removal from the pupal case, only a portion of the animals survived, and those that did, only displayed sporadic leg movements and never opened their wings (Marqués et al., 2002). Zebrafish with homozygous null mutations of the BMP family gene, *gdf6a,* performed significantly worse during an endurance motor task and they also had a reduced maximum sprint speed (Duval et al., 2014). Thus, while the severity of motor deficits differs between species, these results indicate that BMP4 expression in muscle fibres is required normal motor control.

Results reported here that the frequency of mEPPs, amplitude of EPPs, and quantal content were all reduced in $HSA^{Cre}BMP4^{fl/fl}$ mice after doxycycline administration agree with those reported in *Drosophila* larvae with mutations in *wit* or *gbb*, the *Drosophila* homologs to vertebrate BMPRII and BMP4, respectively (Aberle et al., 2002; Marqués et al., 2002; McCabe et al., 2003). *Wit* is expressed by MNs (Aberle et al., 2002; Marqués et al., 2002) during development, and its excision during development causes a reduction in mEJP frequency, EJP amplitude, increased failure rate, and decrease in quantal content (Aberle et al., 2002; Marqués et al., 2002). Interestingly, neurotransmission in the *wit* mutants can be rescued by expression of the *wit* transgene in MNs, but not muscle (Marqués et al., 2002). Similarly, *gbb* mutant larvae have a reduced frequency of mEJPs, smaller EJP amplitudes, and lower quantal content. Further, all of these phenotypes can be rescued when the *gbb* transgene is expressed in muscle (McCabe et al., 2003). All of the electrophysiological phenotypes reported in the *Drosophila* mutants are more severe than those found in the present study.This difference could simply be due to species differences. However, it could also be due to the fact that *wit* and *gbb* were knocked out from the onset of larval develoment while BMP4 expression in our study was not eliminated until P30. Furthermore, the present study only eliminated BMP4 from skeletal muscle, while the *Drosophila* studies mutated all *wit* and *gbb*.

In agreement with our results, previous studies in mice have shown that the signaling pathway downstream of BMPRII activation regulates skeletal muscle fibre cross-sectional area. Using a muscle-specific knock out of Smad4, Sartori et al., (2013)

found a slight, but significant, decrease in cross-sectional area of oxidative (type I and type IIa) and glycolytic (type IIb) muscle fibres in the TA muscle (Sartori et al., 2013). This study did not differentiate oxidative muscles into type I vs type IIa, as performed in our study, so they could not determine whether type IIa fibre cross sectional area was altered in the Smad4 mutants. Furthermore, regulation of muscle fibre size through the BMPRII signaling pathway appears to be more influential under pathological conditions because the loss of muscle size was significantly greater in Smad4 mutant mice compared to WT mice when muscles were denervated for up to a month (Sartori et al., 2013; Winbanks et al., 2013).

The increase in endplate area observed in this study differs from those reported in *Drosophila*, where decreased NMJ size was observed (Aberle et al., 2002). However, the observed increase in our study is likely attributed to the observed increase in fragmentation and dispersion on AChR clusters within single endplates. Interestingly, BMP4 staining at the NMJ appears to be localized around the perimeter of the post-synaptic density (Chou et al., 2013). It has previously been speculated that this localization could function to maintain AChR clustering at the synaptic site, and inhibit clustering outside the NMJ (Osses and Henríquez, 2015). The perimeter of the post-synaptic rich in polymerized f-actin and LL5β, both have which have been implicated in limiting AChR clustering at the NMJ (Kishi et al., 2003; Lee et al., 2010). It is therefore possible that BMP4-mediated signaling is involved in regulating the structure of AChRs at the endplate, and in its absence, there is dismantlement of this system leading to NMJ fragmentation.

Somewhat surprising was the relatively small decrease in contractile force, and no change in fatigue index, in the $HSA^{Cre}BMP4^{fl/fl}$ mice considering the poor performance on the rotarod. However, a similar reduction in medial gastrocnemius muscle contractile force was reported in muscle specific Smad4 knockouts (Sartori et al., 2013) indicating that loss of BMP4-dependent signaling does not regulate muscle force, or fibre size, to a great extent. The discrepancy between loss of force and rotarod performance prompted us to investigate changes in proprioception because HSA, the promoter used to drive the cre recombinase activity in our study, is also expressed in intrafusal fibres within muscle spindles (Leu et al., 2003). Within the spinal cord, locomotion is regulated through the

integrated actions of interneuronal circuits that ultimately drive patterned activity of flexor and extensor muscles involved in walking (Rossignol et al., 2006). However, sensory mediated feedback from cutaneous and proprioceptive inputs are required for normal locomotion. For example, there is a significant degradation in locomotor pattern when sensory feedback from muscle spindles is genetically ablated in mice (Akay et al., 2014). Furthermore, like the results in the present study, there was reduced precision in rear foot placement in the horizontal ladder walking test (Akay et al., 2014). The similarity in these results with the present study suggest that the significant decline in rotarod performance by the $HSA^{Cre}BMP4^{fl/fl}$ mice is due, in part, to attenuated proprioceptive feedback.

An interesting hypothesis to consider is that BMP4 knockdown is contributing to an accelerated, premature ageing phenotype. Sarcopenia, which can be observed in mice by decreased rotarod performance, decreased muscle strength, and muscle atrophy, is a hallmark of ageing (Nair, 2005; Franceshi et al., 2018; Graber and Fandrey, 2019). The average number of fragments per NMJ also tends to increase with ageing, correlating with our results (Willadt et al., 2018). Neurotransmission has been shown to be altered in aged mice compared to young, with mEPP frequency decreasing with ageing, as we have shown in our $HSA^{Cre}BMP4^{fl/fl}$ mice (Banker et al., 1983). However, our findings that EPP amplitudes and quantal content are decreased in $HSA^{Cre}BMP4^{fl/fl}$ mice are opposite to what is typically observed during ageing (Banker et al., 1983) (Fig. 3.7B,C).

Axon growth potential has also been well documented to decline with age (Moore et al., 2009; Park et al., 2009), and Smad1, a downstream effector of BMP4, is induced after peripheral axotomy (Parikh et al., 2011). It has also been shown both in culture and *in vivo*, that administration of BMP4 activates Smad1 and enhances axon regeneration in dorsal root ganglion (DRG) neurons, and is essential for axonal regeneration (Zou et al., 2009; Parikh et al., 2011). Furthermore, phosphorylated Smad1 is upregulated during development and axon outgrowth, and downregulated in the adult, and administration of BMP4 via AAV in the adult DRG following injury improves regeneration (Parikh et al., 2011). Considering an increase in BMP4 can improve adult axon outgrowth, decreased BMP4 signaling could be involved in the age-related decline in axon growth potential. It is therefore possible that the loss of muscular BMP4 in our model is accelerating a

mechanism that occurs during normal ageing. This notion also agrees with our finding that $HSA^{Cre}BMP4^{fl/fl}$ are more denervated than WT controls (Fig. 3.5E,F).

Together, this study provides the first evidence that BMP4 has similar roles in adult vertebrate NMJ homeostasis as previously reported in *Drosophila* larvae. The smaller phenotype in the $HSA^{Cre}BMP4^{fl/fl}$ mice compared to *Drosophila* could be due to differences in species, time when BMP4 signaling was eliminated, or compensation by SC derived BMP4. Furthermore, our results indicate that BMP4 signaling occurs within muscle spindles and is required for proprioceptive feedback for normal locomotion.

Chapter 3 Figures

Figure 3.1. BMP4 expression in WT and HSA^{Cre}BMP4$^{fl/fl}$ soleus muscle. **A**, WT soleus muscle cross-sections, immunostained for BMP4 (red) and labeled with BTX (cyan), shows BMP4 expression along the cell membrane and BTX^{+} endplates (arrowheads). Scale bar = 50 µm **B**, Fluorescence intensity measurements (mean ±SD, arbitrary units) from WT muscle immunostained with BMP4 and labeled with BTX indicates that BMP4 fluorescence is higher at BTX^{+}, endplate-rich regions compared to the surrounding muscle membrane. ***p<0.0001, Unpaired t-test. **C**, Soleus muscle cross-section from an adult HSA^{cre}ROSATomato$^{fl/fl}$ mouse stained for DsRed (red) shows high tdTomato expression throughout individual skeletal muscle fibres. Scale bar = 100 µm **D**, BMP4 immunolabeled soleus muscle cross-sections from an adult WT (left) and HSA^{cre}BMP4$^{fl/fl}$ (right) mouse show abundant expression in WT fibres and no expression in the HSA^{cre}BMP4$^{fl/fl}$ fibres. Scale bar = 50 µm.

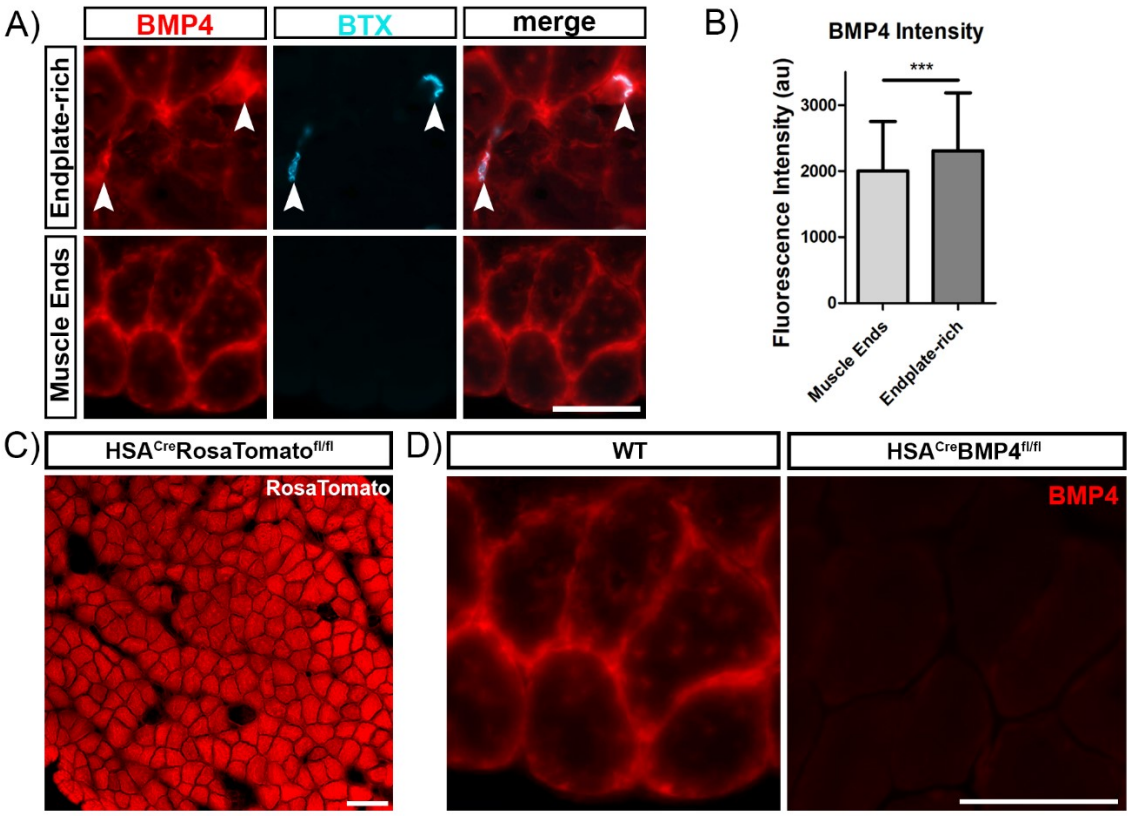
A)
BMP4
BTX
merge
Endplate-rich
Muscle Ends
B)
BMP4 Intensity
***
Fluorescence Intensity (au)
3000
2000
1000
0
Muscle Ends
Endplate-rich
C)
HSA^CreRosaTomato^fl/fl
RosaTomato
D)
WT
HSA^CreBMP4^fl/fl
BMP4

Figure 3.2. Motor tasks deteriorates over time in $HSA^{Cre}BMP4^{fl/fl}$ mice. **A**, Forelimb grip tests from WT and $HSA^{Cre}BMP4^{fl/fl}$ mice prior to, and after, doxycycline administration (values shown as mean ± SEM) shows a significant decline in force overtime in $HSA^{Cre}BMP4^{fl/fl}$ mice ($P<0001$, two-way ANOVA). Post hoc analysis showed significant difference after 19 days of treatment ($p<0.05$ Bonferroni test). **B**, Latency to fall off the rotarod at 20 rpm was significantly different between WT and $HSA^{Cre}BMP4^{fl/fl}$ mice (values equal mean ± SEM) ($p<0.002$, Two-Way ANOVA) and post hoc analysis showed differences at 28 days (*$p <0.05$, Bonferroni post analysis test). **C**, Rotarod performance of the $HSA^{Cre}BMP4^{fl/fl}$ mice declined over time compared to WT littermates ($p<0.0001$; Two-Way ANOA) and post hoc analysis showed differences at 23, 26-28 days (*$p <0.05$, **$p<0.01$; Bonferroni post test).

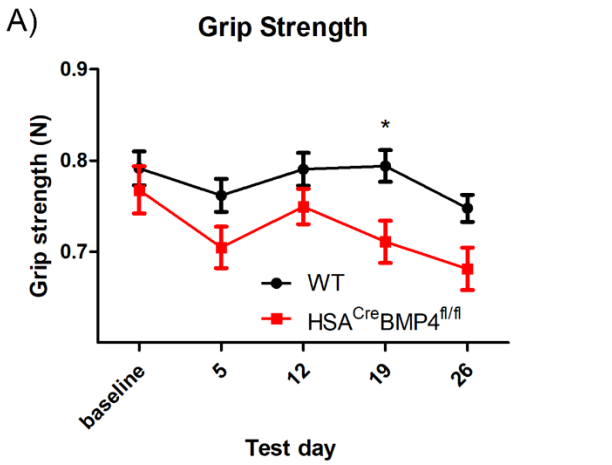
A)
Grip Strength
Grip strength (N)
0.9
0.8
0.7
*
WT
HSA^Cre BMP4^fl/fl
baseline
5
12
19
26
Test day

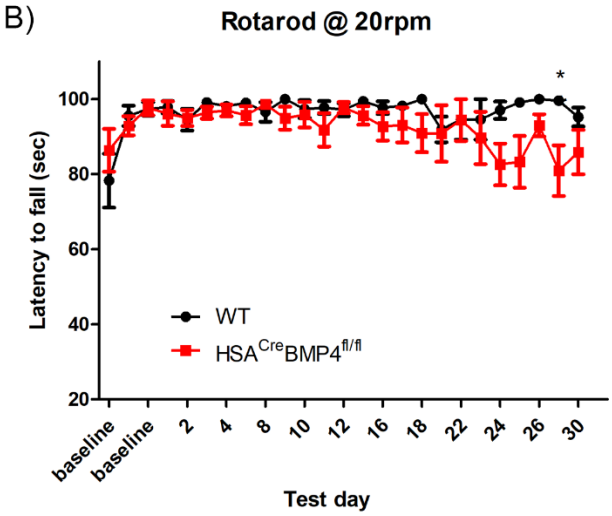
B)
Rotarod @ 20rpm
Latency to fall (sec)
100
80
60
40
20
*
WT
HSA^Cre BMP4^fl/fl
baseline
baseline
2
4
8
10
12
16
18
22
24
26
30
Test day

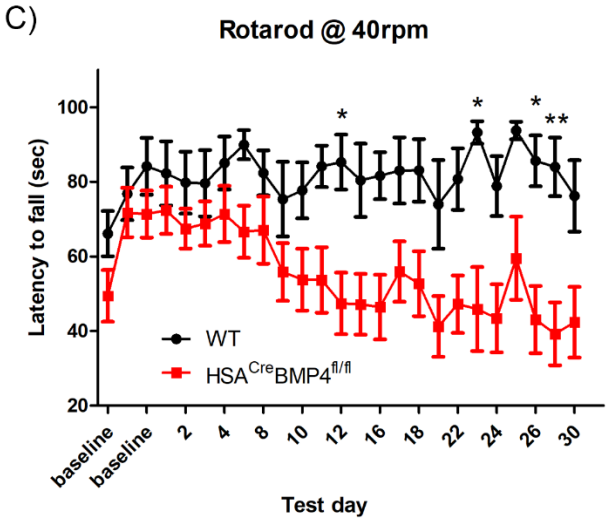
C)
Rotarod @ 40rpm
Latency to fall (sec)
100
80
60
40
20
*
*
*
**
WT
HSA^Cre BMP4^fl/fl
baseline
baseline
2
4
8
10
12
16
18
22
24
26
30
Test day

Figure 3.3. Soleus muscles lacking BMP4 lose contractile force over time. **A,C** Representative soleus twitch (A) and tetanic (C) forces (50 Hz, 1 s duration) from WT and $HSA^{Cre}BMP4^{fl/fl}$ mice 2 and 4 months of doxycycline administration. **B,D** Mean (± SD) soleus twitch (B) and tetanic (D) forces 2 month and 4 months after doxycycline treatment. *p=0.0338 WT 2 mo twitch vs $HSA^{Cre}BMP4^{fl/fl}$ 2 mo twitch, *p=0.0329 WT 4 mo twitch vs $HSA^{Cre}BMP4^{fl/fl}$ 4 mo twitch, *p=0.0204 WT 4 mo tetanus vs $HSA^{Cre}BMP4^{fl/fl}$ 4 mo tetanus, Unpaired t-test. **E,** $HSA^{Cre}BMP4^{fl/fl}$ and WT soleus muscle fatigue index 2 and 4 months after doxycycline administration.

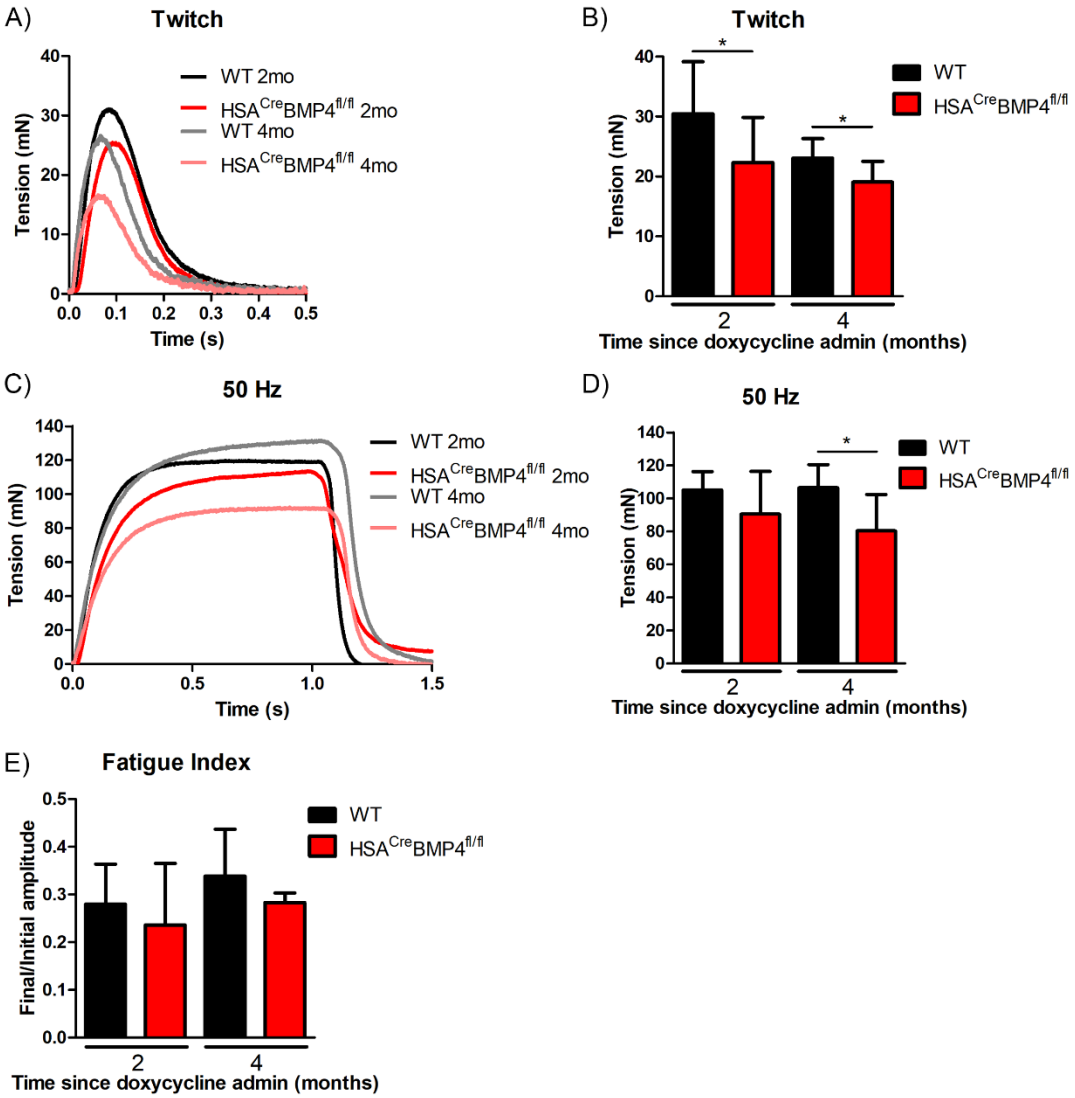
A)
Twitch
WT 2mo
HSACreBMP4fl/fl 2mo
WT 4mo
HSACreBMP4fl/fl 4mo
Tension (mN)
Time (s)
B)
Twitch
WT
HSACreBMP4fl/fl
Tension (mN)
Time since doxycycline admin (months)
C)
50 Hz
WT 2mo
HSACreBMP4fl/fl 2mo
WT 4mo
HSACreBMP4fl/fl 4mo
Tension (mN)
Time (s)
D)
50 Hz
WT
HSACreBMP4fl/fl
Tension (mN)
Time since doxycycline admin (months)
E)
Fatigue Index
WT
HSACreBMP4fl/fl
Final/Initial amplitude
Time since doxycycline admin (months)

Figure 3.4. Loss of BMP4 in adult skeletal muscle causes atrophy of type I muscle fibres 4 months after doxycycline administration. **A,** Mean (± SD) whole soleus muscle cross-sectional areas from WT and $HSA^{Cre}BMP4^{fl/fl}$ mice. **B,** Mean (± SD) muscle fibre number at the midbelly of soleus muscles from WT and $HSA^{Cre}BMP4^{fl/fl}$ mice. **C,** Representative WT soleus muscle cross-section immunolabeled for type I and type IIa fibres. **D,** Mean (± SD) cross-sectional areas of type I and type in soleus muscles from WT and $HSA^{Cre}BMP4^{fl/fl}$ mice 4 months after treatment. ***p=0.0003, Mann-Whitney test.

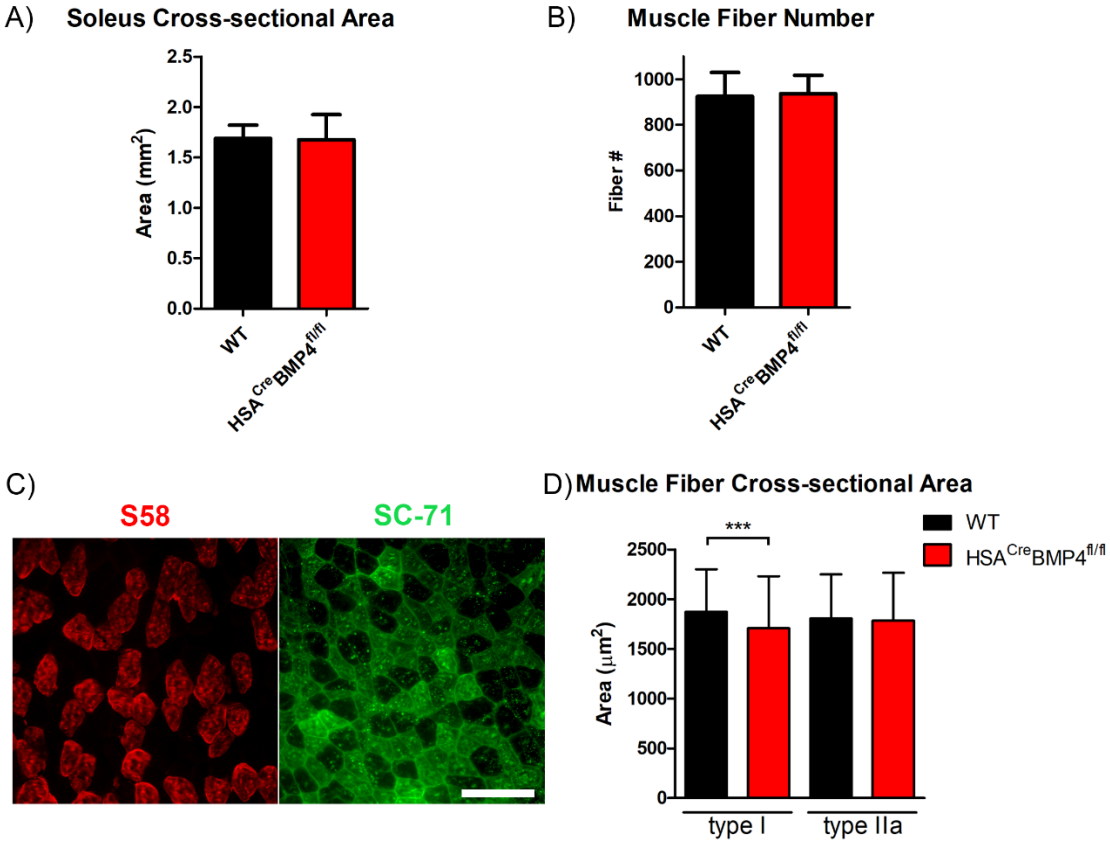
A)
Soleus Cross-sectional Area
Area (mm2)
2.5
2.0
1.5
1.0
0.5
0.0
WT
HSACreBMP4fl/fl
B)
Muscle Fiber Number
Fiber #
1000
800
600
400
200
0
WT
HSACreBMP4fl/fl
C)
S58
SC-71
D)
Muscle Fiber Cross-sectional Area
***
WT
HSACreBMP4fl/fl
Area (μm2)
2500
2000
1500
1000
500
0
type I
type IIa

Figure 3.5. NMJ morphology is altered in $HSA^{Cre}BMP4^{fl/fl}$ mice 4 months after doxycycline administration. **A,** Representative examples of BTX^{+} endplate morphologies in soleus muscles from WT and $HSA^{Cre}BMP4^{fl/fl}$ mice. Hashed yellow lines indicate how area measurements were obtained. Scale bar = 10 µm. **B,** Mean (± SD) endplate areas from soleus muscles in WT (n=4) and $HSA^{Cre}BMP4^{fl/fl}$ (n=4) mice, approximately 50 endplates measured per animal. *p= 0.0309, Unpaired t-test. **C,** Volumetric, three-dimensional reconstructions of BTX^{+} endplates rendered from z-stacks of whole-mounted WT and $HSA^{Cre}BMP4^{fl/fl}$ soleus muscle fibres shows greater fragmentation in the mutant mouse. Scale bar = 10 µm. **D,** Mean (± SD) number of AChR fragments in WT and $HSA^{Cre}BMP4^{fl/fl}$ mice. ***p=0.0004, Mann-Whitney test. **E,** Percentage (Mean ± SD) of innervated soleus muscle endplates in WT and $HSA^{Cre}BMP4^{fl/fl}$ mice. p=0.0143. **F,** Percentage (Mean ± SD) of partially innervated soleus muscle endplates in WT and $HSA^{Cre}BMP4^{fl/fl}$ mice. p=0.0286. Mann-Whitney test.

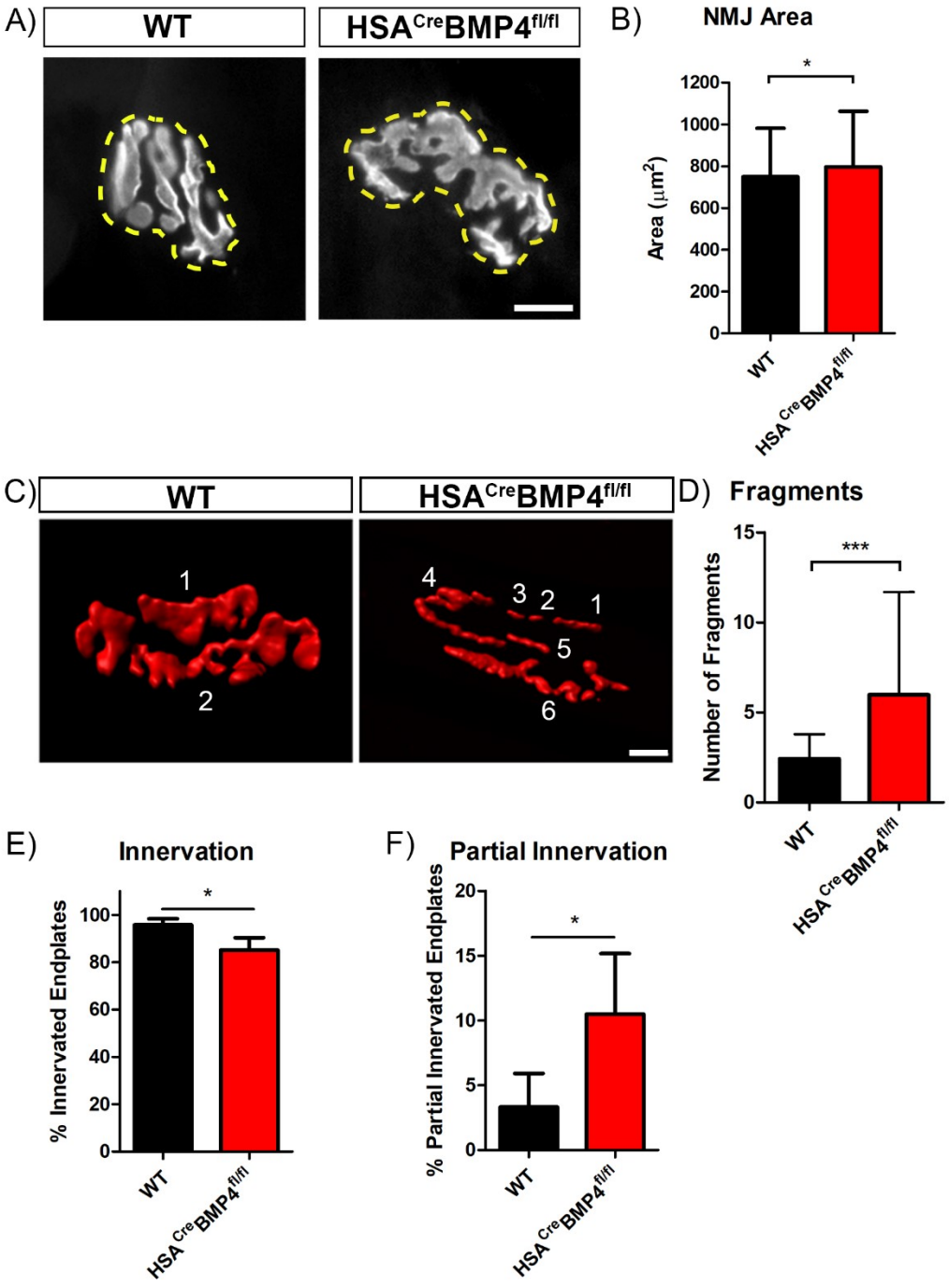
A)
WT
HSA^CreBMP4^fl/fl
B)
NMJ Area
Area (μm²)
1200
1000
800
600
400
200
0
*
WT
HSA Cre BMP4 fl/fl
C)
WT
HSA^CreBMP4^fl/fl
1
2
4
3
2
1
5
6
D)
Fragments
Number of Fragments
15
10
5
0
***
WT
HSA Cre BMP4 fl/fl
E)
Innervation
% Innervated Endplates
100
80
60
40
20
0
*
WT
HSA Cre BMP4 fl/fl
F)
Partial Innervation
% Partial Innervated Endplates
20
15
10
5
0
*
WT
HSA Cre BMP4 fl/fl

Figure 3.6. Spontaneous transmitter release is altered in $HSA^{Cre}BMP4^{fl/fl}$ mice 4 months after doxycycline administration. **A,** Representative traces of mEPPs recorded from soleus NMJs in WT and $HSA^{Cre}BMP4^{fl/fl}$ mice. **B-D,** Mean (± SD) MEPP amplitude (B) (p=0.004, t-test), frequency (C) (p=0.005, Mann-Whitney test) and rise time (D) (p=0.0025, t-test) recorded from soleus NMJs in WT and $HSA^{Cre}BMP4^{fl/fl}$ mice.

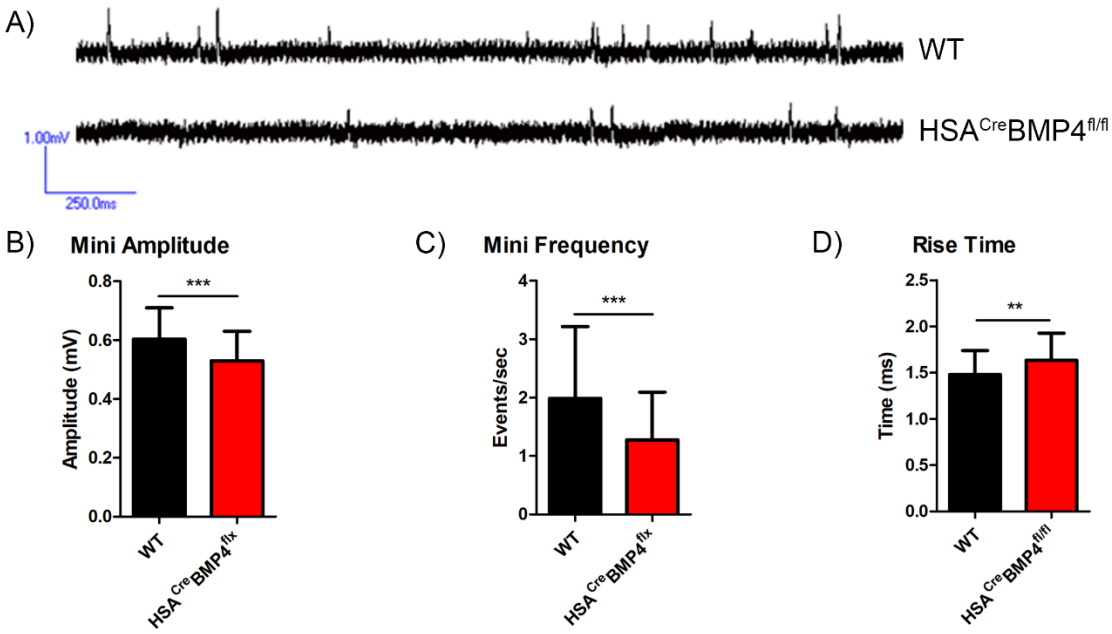
A)
WT
HSA^CreBMP4^fl/fl
1.00mV
250.0ms
B)
Mini Amplitude
Amplitude (mV)
0.8
0.6
0.4
0.2
0.0
***
WT
HSA Cre BMP4 flx
C)
Mini Frequency
Events/sec
4
3
2
1
0
***
WT
HSA Cre BMP4 flx
D)
Rise Time
Time (ms)
2.5
2.0
1.5
1.0
0.5
0.0
**
WT
HSA Cre BMP4 fl/fl

Figure 3.7. Neurotransmission is altered in $HSA^{Cre}BMP4^{fl/fl}$ mice 4 months after doxycycline administration. **A,** Representative traces of evoked EPPs recorded from soleus NMJs in WT and $HSA^{Cre}BMP4^{fl/fl}$ mice. **B,** Mean (± SD) EPP amplitude recorded from soleus NMJs from WT and $HSA^{Cre}BMP4^{fl/fl}$ mice. ***$p<0.0001$, Mann-Whitney test. **C,** Mean (± SD) quantal content for soleus NMJs in WT and $HSA^{Cre}BMP4^{fl/fl}$ mice ($p=0.0011$, Mann-Whitney test. **D,** Quantal content from NMJs from WT and $HSA^{Cre}BMP4^{fl/fl}$ mice plotted as a frequency histogram and cumulative distribution shows a parallel shift to smaller values in the mutant mice. **E,** Representative traces of evoked EPPs (100Hz, 1 second duration) recorded from soleus NMJs in WT and $HSA^{Cre}BMP4^{fl/fl}$ mice shows multiple failures (gaps) in the mutant mice. **F,** Mean (± SD) percentage of failures per cell in WT and $HSA^{Cre}BMP4^{fl/fl}$ soleus muscles.

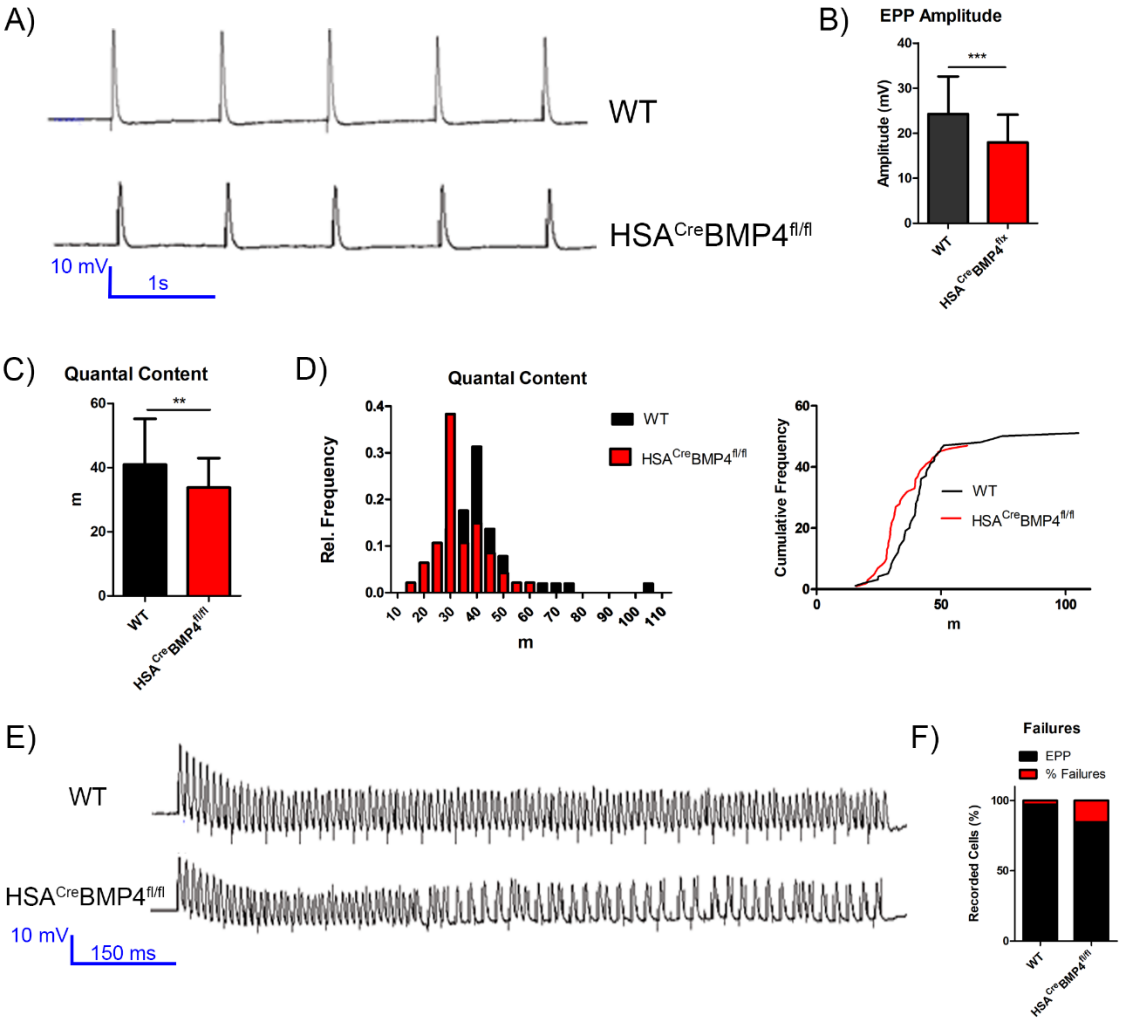
A)
WT
HSA^CreBMP4^fl/fl
10 mV
1s
B)
EPP Amplitude
***
Amplitude (mV)
WT
HSA CreBMP4 flx
C)
Quantal Content
**
m
WT
HSA CreBMP4 fl/fl
D)
Quantal Content
Rel. Frequency
WT
HSA^CreBMP4^fl/fl
m
Cumulative Frequency
WT
HSA^CreBMP4^fl/fl
m
E)
WT
HSA^CreBMP4^fl/fl
10 mV
150 ms
F)
Failures
EPP
% Failures
Recorded Cells (%)
WT
HSA CreBMP4 fl/fl

Figure 3.8. $HSA^{Cre}BMP4^{fl/fl}$ mice have morphological and behavioural deficits associated with proprioceptive function. **A,B** Mean (± SD) number of misses per trial on the horizontal ladder task for WT and $HSA^{Cre}BMP4^{fl/fl}$ mice on the first (B) and fifth (C) days of doxycycline administration. *p=0.0426, Mann-Whitney test. Scale = 500 μm.

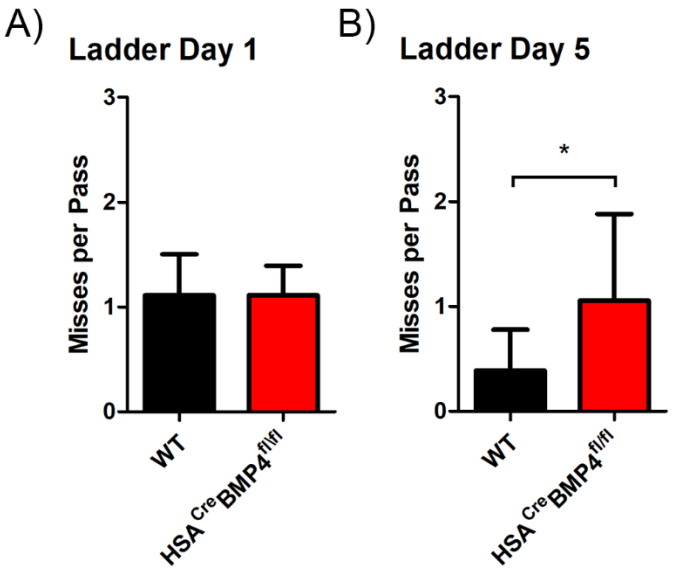
A)
Ladder Day 1
Misses per Pass
3
2
1
0
WT
HSA Cre BMP4 fl/fl
B)
Ladder Day 5
Misses per Pass
*
3
2
1
0
WT
HSA Cre BMP4 fl/fl

CHAPTER 4: NEUROMUSCULAR REINNERVATION IN THE ABSENCE OF MUSCLE-DERIVED BMP4

Abstract

Injuries to peripheral nerves are highly common and have limited recovery potential. This is due, in part, to the relatively slow regeneration rate of peripheral axons (~1mm/day), and the degeneration of muscle fibres in the absence of innervation. Therefore, improving functional recovery following peripheral nerve injury has remained elusive. Bone morphogenic protein 4 (BMP4) has been shown to contribute to *Drosophila* NMJ formation during development, and studies in dorsal root ganglion (DRG) neurons both *in vitro* and *in vivo* point to the BMP4 signaling pathway as being critical in axon outgrowth in development and after injury. We therefore sought to determine the involvement of muscle-derived BMP4 on neuromuscular reinnervation following Tibial n. crush, in mice. To do so, we utilized $HSA^{Cre}BMP4^{fl/fl}$ mice, where skeletal muscle specific BMP4 can be knocked down in adulthood following the administration of doxycycline food pellets. We fed mice with doxycycline for one month prior a unilateral Tibial n. crush, followed by 21, 30, or 90 days of recovery. We found that while whole-muscle tetanic force in reinnervated $HSA^{Cre}BMP4^{fl/fl}$ soleus muscles was not affected, these muscles varied in their fatigue and contraction kinetics over time. There was also evidence of muscle atrophy in both type I and type IIa muscle fibres, which led to an overall reduction in muscle cross-sectional area in reinnervated muscles lacking BMP4. At the NMJ, reinnervated $HSA^{Cre}BMP4^{fl/fl}$ endplates were less innervated, more partially innervated, and more denervated at all timepoints. Further, we observed delayed withdrawal of polyneuronal innervation in these endplates. Together, these results indicate that muscular BMP4 contributes to the maturation of reinnervated endplates following Tibial n. crush. Enhancing BMP4 signaling following peripheral nerve injury could therefore improve the rate of functional reinnervation.

Introduction

Peripheral nerves are highly susceptible to a range of injuries and have limited recovery potential. Peripheral nerve injuries can arise from a wide variety of events including both traumatic and non traumatic events. These injuries vary greatly in severity, from a mild compression injury where axon conduction is typically restored, to complete axon transection. Recovery potential following peripheral nerve injuries varies greatly depending on the severity of the damage and the proximity of the injury site to the target muscle. Nerve regeneration in mice occurs at a rate of ~1 mm/day (Sunderland, 1946), and, given that muscle fibres that remain denervated for as little as 3 days begin to atrophy (Sunderland and Ray, 1950), increasing the speed of peripheral axon regeneration while maintaining muscle health are of paramount importance to recovery. While the mechanisms underlying peripheral nerve regeneration have been extensively studied, there are currently no therapies that significantly improve nerve repair and functional outcomes in patients (Caillaud et al., 2019). One recent study has reported that a conditioning electrical stimulus prior to nerve transection significantly improves axonal regeneration and functional recovery (Senger et al., 2019). Though this technique is promising, an effective therapy that can be applied after the injury has already taken place remains elusive.

Many developmental mechanisms have been shown to re-activate following injury, including previous work from this laboratory on the role of NCAM following Tibial n. crush (Chipman et al., 2010, 2014a). Another developmentally significant protein, BMP4, has well-documented roles in development including neural tube patterning and tissue specification, and has previously been shown in *Drosophila* to be critical in healthy NMJ stability and function (Aberle et al., 2002; Marqués et al., 2002; McCabe et al., 2003). More recent work from our lab in mice has also revealed similar roles of BMP4 at the adult vertebrate NMJ, however, it is currently poorly understood whether BMP4 signaling influences peripheral nerve regeneration and the re-establishment of NMJs following injury.

Evidence to suggest the BMP4 pathway has a role in nerve regeneration comes from studies performed on DRG injury models both *in vitro* and *in vivo*. Cultured DRG neurons display upregulation of Smad1, a downstream effector of BMP4, in response to

axotomy (Zou et al., 2009), indicating increased activity of this pathway in response to injury. Upon knockdown of Smad1, these neurons also had impaired axonal outgrowth (Zou et al., 2009). *In vivo*, it has been shown that noggin, an inhibitor of the BMP4 pathway, is downregulated following injury to DRG neurons (Ma et al., 2011). Further, Smad1 activation seems to be necessary for axon outgrowth both in development and after injury (Parikh et al., 2011; Kelly et al., 2013). Mice with a DRG-specific knockout of Smad1 had impaired axonal regeneration after dorsal-column transection compared to controls, and, importantly, this impairment was rescued via AAV administration of BMP4 (Parikh et al., 2011). These studies revealed the necessity of the BMP4/Smad pathway in axon regeneration, however, the question remains whether BMP4 has a role in NMJ reinnervation following injury.

BMP4 at the mouse NMJ is derived from two different sources: muscle and terminal TSCs. In this study, we sought to determine the impact of the absence of muscular BMP4 in recovery following Tibial n. crush. It is also not known whether BMP4 derived from muscles or TSCs have similar or different roles following injury. So, we utilized mice harboring an inducible mutation resulting in a knockdown of BMP4 specifically in skeletal muscle ($HSA^{Cre}BMP4^{fl/fl}$), induced a Tibial n. crush, and allowed 21, 30, and 90 days of recovery. Electrophysiological recordings as well as anatomical analyses were performed on the reinnervated (TC) and unoperated (unop) soleus muscles to determine the relative capabilities of these mice to recover following Tibial n. crush.

Methods

Mice and Surgery

All protocols were in accordance with the criteria by the Canadian Council on Animal Care and Dalhousie University. HSA tet Cre::BMP4 flox/flox mice (designated throughout as $HSA^{Cre}BMP4^{fl/fl}$) were generated by breeding BMP4-floxed ($BMP4^{fl/fl}$) mice (Jackson Laboratories) with mice expressing inducible tetracycline cre-recombinase under the control of the HSA promoter (HSA tet Cre mice, Jackson Laboratories). Cre-negative littermates were used as WT controls. These mice were administered doxycycline food pellets (Bio-Serv) at ~P30 to induce the skeletal muscle specific

knockdown of BMP4. Following 30 days (P60) to allow for complete BMP4 knockdown, mice were anesthetized with a combination of isoflurane and oxygen and the dorsal aspect of the lower hindlimb shaved. An incision (~1 cm) was made along the length of the leg, slightly medial to the ankle, to expose the muscle and fat behind the knee. Tissue were separated using retractors or hooks to expose the Tibial n. where it enters between the medial and lateral gastrocnemius muscles. The Tibial n. was unilaterally crushed (10s) with large forceps and the incisions were closed. Mice were allowed periods of 21, 30, and 90 days of recovery which are designated throughout as the TC21, TC30, and TC90 timepoints, respectfully, at which points the mice were sacrificed and the soleus muscles of the TC and unoperated (unop) legs were removed and used for electrophysiology experiments and anatomy.

Ex vivo *isometric force recordings*

Mice were anesthetized with isoflurane and oxygen and the soleus, and its nerve supply were quickly removed and transferred to oxygenated Tyrodes solution (125 mM NaCl, 24 mM $NaHCO_3$,5.37 mM KCl, 1 mM $MgCl_2$, 1.8 mM CaCl2, and 27.75 mM dextrose). The proximal tendon was pinned in place in a Sylgard (Dow Corning)-coated recording chamber and the distal tendon was attached to a force transducer (FT 03; Grass Technologies). Measurements of twitch and tetanic forces were obtained as previously described (Chapters 2 and 3). Fatigue indices were obtained by stimulating soleus muscles at 40 Hz for 325 ms, every second, for 2 minutes.

Immunofluorescence and imaging

Muscles to be fixed and stained whole-mount were pinned at physiological length and fixed in 4% paraformaldehyde (PFA) for 20 minutes. Muscles were then washed 3x5 minutes in phosphate buffered saline (PBS), permeabilized in cold methanol for 6 minutes, and washed again, as before. Fixed muscles were transferred to a Sylgard-coated dish, pinned in place, and the distal tendon removed, under a dissecting microscope. Using fine forceps, small bundles of muscle fibres were carefully teased apart, leaving them attached to the proximal tendon. Teased muscles were then incubated in cocktails of

primary antibodies (mouse anti SV2, 1:50, Developmental Studies Hybridoma Bank; chicken anti Tuj1, 1:250, Abcam) in 10% goat serum and 0.3% Triton in PBS overnight on a gentle shaker at room temperature. Muscles were then rinsed 3x5 minutes in PBS prior to incubation in secondary antibodies (goat anti mouse Cy2, 1:500, Jackson Laboratories; goat anti chicken Alexa Fluor 488, 1:500, Invitrogen; Alexa Fluor 647-conjugated α-bungarotoxin (BTX), 1:250, Invitrogen), 10% goat serum, and 0.3% Triton for 2 hours at room temperature. Muscles were rinsed once more, as before, and transferred to a microscope slide with lab-made mounting media (50% Glycerol in PBS and 0.03 mg/mL phenylene diamine), the remaining tendon removed, and the bundles of muscle fibres carefully arranged prior to coverslipping.

Muscles to be used for cross-sectional area measurements were flash frozen in liquid nitrogen-cooled isopentane in a mixture of 1:2 20% sucrose in O.C.T Compound (Tissue Tek). Frozen tissue blocks were then stored at least overnight at -80 °C. Cross-sections were obtained at 30 µm using a cryostat (Leica), rinsed 3x10 minutes in PBS and incubated in mouse anti S58 antibody (IgA,1:5, Developmental Studies Hybridoma Bank) in 10% goat serum and 0.01% Triton in PBS overnight in a humid environment at room temperature. Sections were then rinsed 3x10 minutes in 0.01% PBS-T, fixed in 4% PFA for 15 minutes, and rinsed again. Sections then received a second primary antibody incubation in mouse anti SC-71 (IgG,1:5, Developmental Studies Hybridoma Bank) in 10% goat serum and 0.01% Triton in PBS overnight at room temperature. Sections were then rinsed 3x10 minutes in 0.01% PBS-T and incubated in secondary antibodies (1:500 DyLight 594 goat anti-mouse IgA, Abcam; 1:500 Cy2 goat anti mouse, Jackson Laboratories) in 10% goat serum and 0.01% PBS-T for 2 hours in a dark, humid environment, and rinsed once more. Stained cross-sections were fluoroprotected using mounting media (50% Glycerol in PBS containing 0.03 mg/ml phenylene diamine) and covered with coverslips.

Z-stacks were obtained using a laser-scanning confocal microscope (Zeiss) utilizing Zen 2009 software (Zeiss). Collapsed z-stacks were obtained using Zen 2009 software and then compiled into figures using Adobe Photoshop CC 2015.

Quantification of innervation/polyneuronal innervation

Whole mounts of soleus muscles stained for SV2 and BTX were used to quantify innervation. The degree of colabeling between the pre and postsynaptic markers were categorized as either fully innervated (complete or nearly complete colocalization between SV2 and BTX), partially innervated (a significant portion of SV2 labelling was absent), or denervated (no SV2 colabeling at a BTX-positive site), with approximately 150 endplates counted per muscle.

To quantify polyneuronal innervation, approximately 150 innervated endplates stained for the axonal marker, Tuj1, as well as BTX, were counted. For each endplate, the microscope was focused up and down to determine the number of innervating axons. Polyneuronally innervated endplates were then represented as a percentage of total innervated endplates counted per muscle.

Cross-sectional area measurements

Cross-sections of soleus muscles were imaged using an upright fluorescence microscope (Leica) and ZenBlue software (Zeiss). Cross-sectional area measurements of 50 S58 and SC-71-positive muscle fibres per muscle were obtained utilizing the software's contour function. Similarly, whole-muscle cross sectional area measurements were obtained by measuring the largest (mid-belly) sections. Muscle fibre number estimates were obtained using mean cross-sectional area measurements for both fibre-types and mean mid-belly cross sectional area (muscle fibre number ≈ mean csa of soleus mid-belly/mean csa of S58 and SC-71 positive fibres).

Statistical analysis

Data were first compiled in Microsoft Excel prior to transferring to GraphPad Prism software to generate figures and perform statistical analyses. Means were considered to be statistically significant at $p<0.05$. Unpaired t-tests were used to determine statistical significance unless the result of the F test revealed unequal variances, in that case, Mann-Whitney tests were used. Mann-Whitney tests were also used when comparing data sets

with n's <10 considering these samples were too low to accurately determine whether the data were normally distributed.

Results

Muscular force and fatigue following Tibial n. crush in muscles lacking BMP4

Previous work from our lab revealed that $HSA^{Cre}BMP4^{fl/fl}$ soleus muscles have decreased strength of twitch and tetanic contraction over time since BMP4 knockdown (see chapter 3). Therefore, we first sought to determine whether the lack of muscular BMP4 impacts the re-establishment of muscular force following Tibial n. crush at 21, 30, and 90 days of recovery, termed TC21, TC30, and TC90, respectfully. Peripheral nerve regeneration progresses at a rate of ~1 mm/day (Sunderland, 1946), and, given the location of the Tibial n. crush was ~1cm from the soleus muscle, we anticipated that WT TC muscles will have been reinnervated well-before 21 days.

After 21 and 30 days of recovery, there were no differences in twitch (data not shown) or tetanic forces (Fig. 4.1A,B,D,E) across groups (WT unop, WT TC, $HSA^{Cre}BMP4^{fl/fl}$ unop, $HSA^{Cre}BMP4^{fl/fl}$ TC). These findings in the WT were unsurprising given the well-documented rate of peripheral nerve regeneration in mice (Sunderland, 1946). By TC30, mice had only undergone doxycycline administration for two months, therefore, our finding that unoperated $HSA^{Cre}BMP4^{fl/fl}$ soleus muscles did not have a reduction in force relative to WT agrees with previous results for the same time point ($p=0.2704$). Further, by TC90, there was a significant reduction in tetanic force in the $HSA^{Cre}BMP4^{fl/fl}$ unoperated soleus muscles relative to WT ($p=0.0204$), though there was no impact of Tibial n. crush on the restoration of force in $HSA^{Cre}BMP4^{fl/fl}$ muscles (Fig. 4.1C,F; $p=0.1320$ $HSA^{Cre}BMP4^{fl/fl}$ unop vs TC). Interestingly, at every time point examined, there was no difference in force generated between $HSA^{Cre}BMP4^{fl/fl}$ TC soleus muscles and unoperated $HSA^{Cre}BMP4^{fl/fl}$ controls. These findings suggest that the absence of muscular BMP4 does not impair axon regeneration or reinnervation to the extent that whole-muscle tetanic force is affected.

We further examined fatigue index and contraction kinetics to determine if muscular BMP4 has more subtle effects on muscle contraction following Tibial n. crush. We found no differences across groups at TC21 (Fig. 4.2A), however, at TC30,

$HSA^{Cre}BMP4^{fl/fl}$ TC soleus muscles were significantly less fatigable compared to $HSA^{Cre}BMP4^{fl/fl}$ unoperated and WT TC controls, as evidenced by an increase in fatigue index (Fig. 4.2B; p=0.0018 and p=0.0031, respectfully). In contrast, by TC90, $HSA^{Cre}BMP4^{fl/fl}$ TC muscles were significantly more fatigable (lesser fatigue index) than their unoperated counterparts (Fig. 4.2C; p=0.0464). We also observed that the contraction profile in $HSA^{Cre}BMP4^{fl/fl}$ TC muscles in unfused tetani (10 Hz) were slower and similar to controls at TC30 (Fig. 4.2D,E) and TC90 (Fig. 4.2F,G), respectfully. This indicates significant alterations in contraction kinetics in $HSA^{Cre}BMP4^{fl/fl}$ TC muscles over recovery time, indicating that there could be continuous remodeling ongoing in these reinnervated muscles.

Muscle atrophy in regenerated soleus muscles lacking BMP4

Another measure to determine regeneration efficacy is to examine denervation-induced atrophy of muscle fibres after Tibial n. crush. Muscle fibres that have remained denervated for too long will atrophy, which will be reflected in cross-sectional area (CSA). Therefore, we measured the CSA of type I and type IIa muscle fibres in WT and $HSA^{Cre}BMP4^{fl/fl}$ soleus muscles 30 and 90 days after Tibial n. crush. At TC30, we found a significant reduction in CSA in type I muscle fibres in $HSA^{Cre}BMP4^{fl/fl}$ TC muscles compared to unoperated ($p<0.0001$) and WT TC (p=0.0021) soleus muscles (Fig. 4.3A). There was a reduction in the CSA of type IIa muscle fibres of $HSA^{Cre}BMP4^{fl/fl}$ TC muscles compared to WT TC muscles (p=0.0012), however there was no difference compared to unoperated $HSA^{Cre}BMP4^{fl/fl}$ controls (Fig. 4.3B; p=0.4128). These reductions in individual fibre type CSA was also reflected in significant reductions in overall muscle CSA and muscle fibre number compared to WT TC ($p<0.0001$ and p=0.0108, respectfully) and muscle CSA compared to $HSA^{Cre}BMP4^{fl/fl}$ unoperated (Fig. 4.3C,D; p=0.0234).

At TC90, there was no difference in CSA of type I muscle fibres in $HSA^{Cre}BMP4^{fl/fl}$ TC muscles compared to unoperated (Fig. 4.3E; p=0.1405). However, type I muscle fibres in unoperated $HSA^{Cre}BMP4^{fl/fl}$ muscles do show reductions in CSA over time since doxycycline administration (Fig. 4.3E), therefore, this effect of time is likely confounding the effects of the crush injury. Interestingly, the reduction seen

previously at TC30 in type IIa muscle fibre CSA was not observed at TC90, rather a modest increase in $HSA^{Cre}BMP4^{fl/fl}$ TC IIa muscle fibre CSA compared to unoperated (Fig. 4.3F; p=0.0066). However, similar to what was observed with the type I muscle fibres, there was evidence that unoperated $HSA^{Cre}BMP4^{fl/fl}$ muscle fibres had a decrease in type IIa muscle fibre CSA relative to WT which was not observed at TC30 (p<0.0001). Further, mean whole-muscle CSA was reduced in $HSA^{Cre}BMP4^{fl/fl}$ TC muscles at TC90, however, this was not significantly different from unoperated $HSA^{Cre}BMP4^{fl/fl}$ soleus muscles (p=0.2209) considering this group had a significant reduction in whole muscle CSA relative to WT (Fig. 4.3G; p=0.0249).

The finding that muscle fibres are lost in muscles lacking BMP4 following Tibial n. crush indicates that reinnervation was unsuccessful at least in a subset of muscle fibre types. We immunostained cross sections of soleus muscles with the myosin type I specific antibody, S58, and found that not only did $HSA^{Cre}BMP4^{fl/fl}$ TC muscles have reduced intensity of S58 staining, but there was an apparent increase in the proportion of S58 positive muscle fibres relative to WT TC muscles at TC30 (Fig. 4.3I,J; p=0.0108). This was possibly due to a loss of the S58-negative type IIa fibres. By TC90, we did not observe a similar significant increase in type I fibres, although the means were similar to those observed at TC30 (Fig. 4.3K). These results could indicate that BMP4 could have differential effects on type I vs type IIa muscle fibres following Tibial n. crush, and that there is more atrophy in reinnervated muscles lacking BMP4 than in WT.

Soleus muscles lacking BMP4 fail to recover innervation following Tibial n. crush

Given the evidence of muscle atrophy in $HSA^{Cre}BMP4^{fl/fl}$ TC muscles, we next wanted to determine if there were any alterations in NMJ innervation between groups following Tibial n. crush. At TC21, WT TC muscles were slightly, yet significantly, less innervated than unoperated controls (p=0.0143), and while $HSA^{Cre}BMP4^{fl/fl}$ TC muscles tended towards being less innervated than $HSA^{Cre}BMP4^{fl/fl}$ unoperated muscles, this result was not significant (Fig. 4.5A; p=0.0571). Correspondingly, there was a higher percentage of partially innervated endplates in the WT TC muscles compared to unoperated (p=0.0143), and the same trend was observed in the $HSA^{Cre}BMP4^{fl/fl}$ muscles but was not significant (Fig. 4.4D; p=0.0571). Denervation at TC21 tended to be highest in the

$HSA^{Cre}BMP4^{fl/fl}$ TC muscles, however there were no significant differences between groups (Fig. 4.4G).

Interestingly, one week later at TC30, $HSA^{Cre}BMP4^{fl/fl}$ TC muscles were significantly less innervated than unoperated and WT TC groups (Fig. 4.4B; p=0.0002 and p=0.0005, respectfully). There was also evidence of denervation in $HSA^{Cre}BMP4^{fl/fl}$ unoperated muscles compared to WT unoperated controls (p=0.0002), indicating that $HSA^{Cre}BMP4^{fl/fl}$ muscles are overall less innervated than WT controls (Fig. 4.4B,H). The proportion of partially innervated endplates in both TC groups were significantly greater than their unoperated counterparts (WT p=0.0002 and $HSA^{Cre}BMP4^{fl/fl}$ p=0.0009), though there were more partially innervated endplates in the $HSA^{Cre}BMP4^{fl/fl}$ TC than the WT TC muscles (Fig. 4.4E; p=0.0190). In accordance with the pattern observed with innervation, the unoperated $HSA^{Cre}BMP4^{fl/fl}$ muscles had more partially innervated endplates than WT unoperated controls (Fig. 4.4E; p=0.0003). There were also significantly more denervated endplates in $HSA^{Cre}BMP4^{fl/fl}$ TC muscles compared to both unoperated and WT TC controls (p=0.0005 and p=0.0015, respectfully), corresponding with innervation and partial innervation results (Fig. 4.4H). These results were particularly interesting because $HSA^{Cre}BMP4^{fl/fl}$ TC axons appear to be undergoing considerable remodeling given that endplates were less innervated and more denervated at TC30 compared to TC21. This indicates that muscular BMP4 must act trans-synaptically on the reinnervating axon.

By TC90, reinnervation had progressed further in the WT TC group such that there was a lesser difference in innervation compared to unoperated controls than at TC30 (Fig. 4.4B,C). Still at this time point, however, $HSA^{Cre}BMP4^{fl/fl}$ TC muscles were significantly less innervated compared to $HSA^{Cre}BMP4^{fl/fl}$ unoperated (p=0.0143) and WT TC muscles (Fig. 4.4C; p=0.0143). There was also still considerable evidence of partial innervation in the $HSA^{Cre}BMP4^{fl/fl}$ TC group relative to unoperated (p=0.0286) and WT TC (p=0.0143), which was reduced with respect to values obtained at TC30 (Fig. 4.4E,F). Importantly, the degree of partial innervation at TC90 in the WT TC group was not statistically significant from unoperated (Fig. 4.4F; p=0.1714). Finally, there were still significantly more denervated endplates in the $HSA^{Cre}BMP4^{fl/fl}$ TC muscles compared to the other groups (p=0.0143 vs WT TC, and p=0.0143 vs $HSA^{Cre}BMP4^{fl/fl}$

unop), and numbers were similar to those obtained at TC30 (Fig. 4.4H,I). These results indicate that neuromuscular remodelling is persisting even 90 days after Tibial n. crush in the $HSA^{Cre}BMP4^{fl/fl}$ soleus muscle, and that reinnervation is less successful in these muscles than in WT. Therefore, muscular BMP4 is involved in reinnervation following peripheral nerve injury.

Delayed withdrawal of polyneuronal innervation in muscles lacking BMP4 after Tibial n. crush

Our results, thus far, indicate that $HSA^{Cre}BMP4^{fl/fl}$ TC endplates could be immature compared to their unoperated and WT controls. Another process that contributes to the maturation of the NMJ during development is the withdrawal of polyneuronal innervation. When the early NMJ is forming, more than one axon typically innervates each endplate. Eventually, these redundant connections are lost such that a single axon innervates each endplate. The rate at which polyneuronal innervation disappears depends on the relative activity of the competing inputs, among other mechanisms (Sanes and Lichtman, 1999). In the rat diaphragm, it has been reported that endplates are singly innervated by P14 (Redfern et al., 1970; Rosenthal and Taraskevich, 1977), though some polyneuronally innervated endplates can persist longer (Sanes and Lichtman, 1999). Similar to development, polyneuronal innervation occurs following axonal injury during the re-establishment of NMJs and is ultimately withdrawn (Ostberg et al., 1986; Rich and Lichtman, 1989b; Werle and Herrera, 1991; Barry and Ribchester, 1995). So, a determinant of whether an NMJ has matured following injury is whether a given endplate is innervated by one or more axons.

We therefore quantified polyneuronal innervation in whole-mounted muscle sections from WT and $HSA^{Cre}BMP4^{fl/fl}$ TC soleus muscles stained with Tuj1 and BTX. We found that a significant proportion of $HSA^{Cre}BMP4^{fl/fl}$ TC endplates were polyneuronally innervated (21.98% ± 3.852) compared to WT TC endplates (1.971% ± 1.526) at TC21 (Fig. 4.5A,B; $p=0.0143$). By TC30, these numbers had declined in $HSA^{Cre}BMP4^{fl/fl}$ TC muscles (8.919% ± 4.180), though were still significantly greater than in WT (2.413% ± 2.165) (Fig. 4.5A,B; $p=0.0286$). Finally, at TC90, there was no

difference in the proportion of polyneuronally innervated endplates between groups (WT 4.009% ± 3.272 vs HSA^{Cre}BMP4$^{fl/fl}$ 4.248% ± 2.300, p=0.5000), indicating that HSA^{Cre}BMP4$^{fl/fl}$ TC endplates were similarly mature to WT controls at this time-point (Fig. 4.5A,B). Together, these results further provide evidence that maturation of reinnervated endplates in HSA^{Cre}BMP4$^{fl/fl}$ TC soleus muscles is delayed compared to WT, meaning that muscular BMP4 must play a role in the re-establishment and maturation of NMJs following injury.

Discussion

This study sought to determine whether adult knockdown of muscular BMP4 impaired neuromuscular reinnervation following Tibial n. crush. We found that tetanic force was largely unaffected by the absence of muscular BMP4. However, we did observe significant anatomical findings of muscle atrophy, impaired NMJ innervation, and delayed withdrawal of polyneuronal innervation in soleus muscles lacking BMP4 following Tibial n. crush. These results suggest that HSA^{Cre}BMP4$^{fl/fl}$ NMJs take longer to mature following injury than WT NMJs with normal levels of BMP4. It is also important to note that these NMJs are not devoid of BMP4, given the expression of BMP4 in TSCs. Therefore, future experiments will seek to determine the effect of knocking down SC-derived BMP4 on NMJ reinnervation, in addition to muscle and SC double-knockdown experiments. We anticipate that the absence of SC-derived BMP4 will have a significant impact on axonal regeneration following Tibial n. crush given that SCs guide and facilitate axon regrowth following injury (Son and Thompson, 1995b), and that double knockdown of both sources of BMP4 at the NMJ will have severe consequences following injury.

Our finding that tetanic force was not significantly reduced in HSA^{Cre}BMP4$^{fl/fl}$ TC muscles at any timepoint was somewhat surprising, however, we believe that the tendency of unoperated HSA^{Cre}BMP4$^{fl/fl}$ soleus muscles to lose force over time since doxycycline administration may be confounding these results. Furthermore, it has been previously reported in the context of ALS, as well as in peripheral nerve injury models, that nerve crush injuries act as conditioning lesions that accelerate healing and promote the formation of more resilient NMJs (Richardson and Verge, 1987; Torigoe et al., 1999;

Gordon et al., 2010; Sharp et al., 2018). It is also important to note that axonal regeneration, a major determinant of the re-establishment of muscular force, was likely unaffected in these mice considering BMP4 was only knocked down in skeletal muscle, and distant BMP4 signals from the soleus would likely not impact axon regeneration at the crush site. It is more likely that SC loss of BMP4 would have a more significant impact on this stage of repair. Considering BMP4 loss was only present in muscle, it therefore stands to reason that muscular BMP4 signaling would only influence the re-establishment and maturation of the NMJ. Again, $HSA^{Cre}BMP4^{fl/fl}$ NMJs do not lack BMP4 entirely, and it is therefore possible that TSC-derived BMP4 is compensating for BMP4 loss in muscle, resulting in more subtle synaptic changes that were not evident at the whole-muscle force level, discussed below.

Although whole-muscle tetanic force was not impaired in $HSA^{Cre}BMP4^{fl/fl}$ muscles following Tibial n. crush, we did find evidence of significant alterations in contraction kinetics. Namely, a large increase in fatigue index in these muscles at TC30 which was reversed by TC90. An explanation for this result is that $HSA^{Cre}BMP4^{fl/fl}$ TC muscles are slower to contract than unoperated and WT controls, leading to increased potentiation between pulses and thus an increased fatigue index at TC30 (Fig. 4.2D,E). The reversal of this effect 60 days later is evidence of further remodeling that is continuing to occur in these muscles over recovery time. Without muscular BMP4, the developmental mechanisms and remodeling that lead to the establishment of mature contraction kinetics could be slowed. By TC90, this decrease in fatigue index could be evidence of further remodelling occurring even at this late stage of recovery, which is happening more slowly than in WT due to diminished BMP4 levels.

The inconsistency of fatigue index over time was also not the only evidence of delayed or continuing remodeling in $HSA^{Cre}BMP4^{fl/fl}$ muscles. We also observed that the proportion of fully innervated endplates was less in $HSA^{Cre}BMP4^{fl/fl}$ TC muscles at TC30 than at TC90 (Fig. 4.4B,C), which agrees with fatigue index results at these timepoints. Further, our finding that the withdrawal of polyneuronal innervation was delayed in $HSA^{Cre}BMP4^{fl/fl}$ TC muscles supports that these NMJs take longer to mature, supporting the idea that remodeling could be continuously occurring between TC30 and TC90 (Fig. 4.5B).

Following injury to skeletal muscles, satellite cells resident within the muscle activate and repopulate any sites of tissue damage to help maintain muscle mass. It has been previously shown that the Smad pathway, downstream of BMP4 signaling, is upregulated in activated satellite cells after muscle injury (Ono et al., 2011). It is therefore possible that, in the absence of muscular BMP4, activation of these satellite cells is incomplete or perhaps does not occur following injury. In support of this notion, we found that type I, type IIa, and whole soleus midbelly CSAs were all reduced 30 days after Tibial n. crush in $HSA^{Cre}BMP4^{fl/fl}$ soleus muscles (Fig. 4.3A-C). This atrophy not only reduced the CSA of the muscle, but there was also evidence of significant muscle fibre loss in these muscles (Fig. 4.3D). Interestingly, by TC90, these patterns were not as clear. There was a general trend for CSA measurements in $HSA^{Cre}BMP4^{fl/fl}$ TC muscles to be less than controls, however, there were reductions in unoperated $HSA^{Cre}BMP4^{fl/fl}$ CSA measurements that confounded these results. We have shown from our previous work in unoperated $HSA^{Cre}BMP4^{fl/fl}$ soleus muscles that type I CSA, in particular, and, to some extent, type IIa CSA, are reduced over time since doxycycline administration. In support of these findings, previous work has revealed that BMP4 is a key regulator of muscle mass, such that inhibiting BMP4 signaling actually results in muscle atrophy (Sartori et al., 2013; Winbanks et al., 2013). It is therefore likely that the muscle specific knockdown of BMP4, itself, has long-term (TC90) effects on muscle CSA, while the role of BMP4 in activated satellite cells was revealed in $HSA^{Cre}BMP4^{fl/fl}$ TC muscles after only 30 days.

BMP4 has known roles as a retrograde signaling molecule that influences the growth and maturation of the NMJ during development (Aberle et al., 2002; McCabe et al., 2003; Zhang et al., 2017; Politano et al., 2019). Therefore, the absence of muscular BMP4 should negatively influence the size and maturation of new NMJs following injury. Our findings therefore support the literature given our evidence that NMJ denervation is significantly sustained in $HSA^{Cre}BMP4^{fl/fl}$ soleus muscles even 90 days following Tibial n. crush (Fig. 4.4A-I). Another study has reveled that a noncanonical BMP4 signaling pathway actually regulates NMJ maturation via phosphorylated Smad (Sulkowski et al., 2016). Disruption of this pathway resulted in reduced postsynaptic accumulation of glutamate type A receptors in *Drosophila* (Sulkowski et al., 2016).

Although vertebrate NMJs are cholinergic as opposed to glutamatergic, our previous work, in addition to this study, support similar roles for BMP4 in vertebrates. Further, our findings of delayed reinnervation and withdrawal of polyneuronal innervation both further indicate a role of BMP4 signaling on synapse maturation following injury in the mouse.

Overall, this study highlights the role of muscle-derived BMP4 in NMJ maturation during reinnervation following peripheral nerve injury. These results were unsurprising given how, during development, knockout of the *Drosophila* the BMP4 homolog, *wit*, impairs NMJ formation. This study also provides evidence that the BMP4 signaling pathway is another developmentally significant pathway that is reactivated upon injury induced regeneration. We believe that it is possible that a more severe phenotype will be observed following double knockdown of BMP4 in both muscle and SCs, given that SCs guide regenerating axons, which will be the focus of future experiments. Given previous reports that BMP4 is a regulator of muscle mass, promoting BMP4 signaling in denervated muscles may help to maintain muscle mass in the absence of innervation. This could therefore be a valuable therapeutic strategy for improving reinnervation, and, therefore, outcomes, in patients with peripheral nerve injury.

Chapter 4 Figures

Figure 4.1. Lack of muscular BMP4 does not impair the re-establishment of muscle force following Tibial n. crush. Representative isometric tetanic tension recordings obtained at 50 Hz from WT unoperated (unop), WT Tibial n. crushed (TC), $HSA^{Cre}BMP4^{fl/fl}$ unop, and $HSA^{Cre}BMP4^{fl/fl}$ TC soleus muscles taken **A,** 21, **B,** 30, and **C,** 90 days post Tibial n. crush. Quantification (mean + SD) of maximum tetanic forces (mN) obtained from WT unop, WT TC, $HSA^{Cre}BMP4^{fl/fl}$ unop, and $HSA^{Cre}BMP4^{fl/fl}$ TC soleus muscles at **D,** 21(n=4), **E,** 30 (n=10), and **F,** 90 days (WT unop n=6, WT TC n= 6, $HSA^{Cre}BMP4^{fl/fl}$ unop n=5, $HSA^{Cre}BMP4^{fl/fl}$ TC n=6) post Tibial n. crush. *p=0.0204, Unpaired t-test.

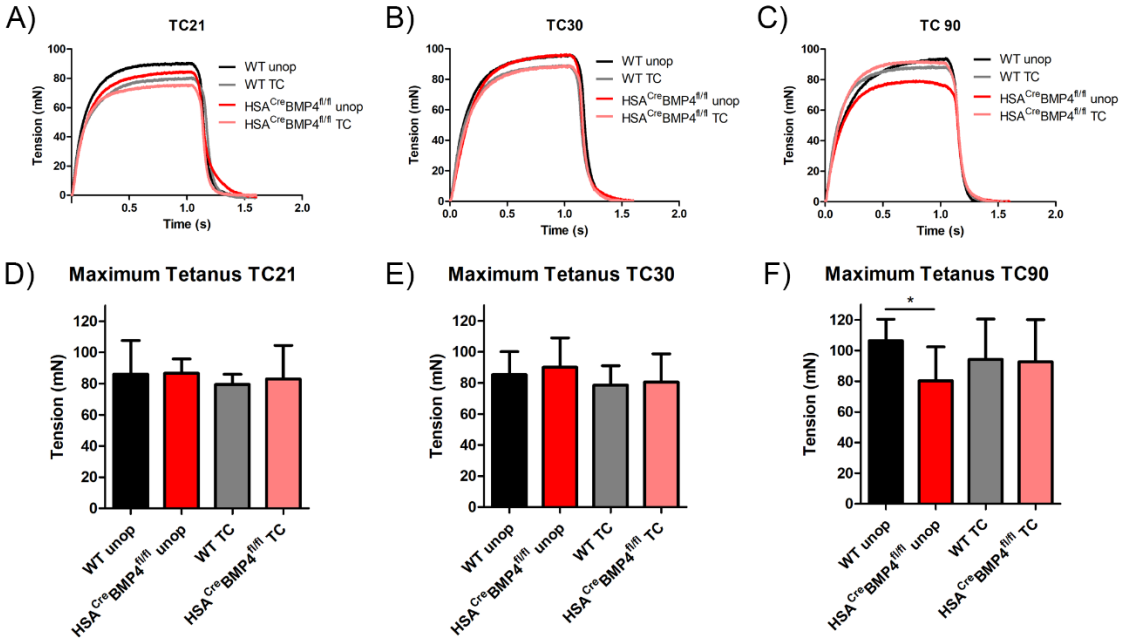
A)
TC21
Tension (mN)
Time (s)
WT unop
WT TC
HSA^Cre BMP4^fl/fl unop
HSA^Cre BMP4^fl/fl TC
B)
TC30
C)
TC 90
D)
Maximum Tetanus TC21
E)
Maximum Tetanus TC30
F)
Maximum Tetanus TC90
*

Figure 4.2. Soleus muscles lacking BMP4 vary in fatigue and contraction kinetics over recovery time. Fatigue indices (mean + SD) obtained by dividing the peak of the last peak after 2 minutes over the initial peak from recordings taken by stimulating at 40 Hz for 325 ms/s, for 2 minutes **A,** 21 (n=4), **B,** 30 (WT unop n=8, WT TC n= 9, $HSA^{Cre}BMP4^{fl/fl}$ unop n=10, $HSA^{Cre}BMP4^{fl/fl}$ TC n=10), and **C,** 90 days (n=4) following Tibial n. crush. **p=0.0031 WT TC vs $HSA^{Cre}BMP4^{fl/fl}$ TC, and **p=0.0018 $HSA^{Cre}BMP4^{fl/fl}$ unop vs $HSA^{Cre}BMP4^{fl/fl}$ TC; *p=0.0411 WT unop vs WT TC, and *p=0.0464 $HSA^{Cre}BMP4^{fl/fl}$ unop vs $HSA^{Cre}BMP4^{fl/fl}$ TC, Unpaired t-test. Representative traces of tetani obtained at 10 Hz from WT and $HSA^{Cre}BMP4^{fl/fl}$ soleus muscles at **D,E** 30 and **F,G** 90 days, respectfully.

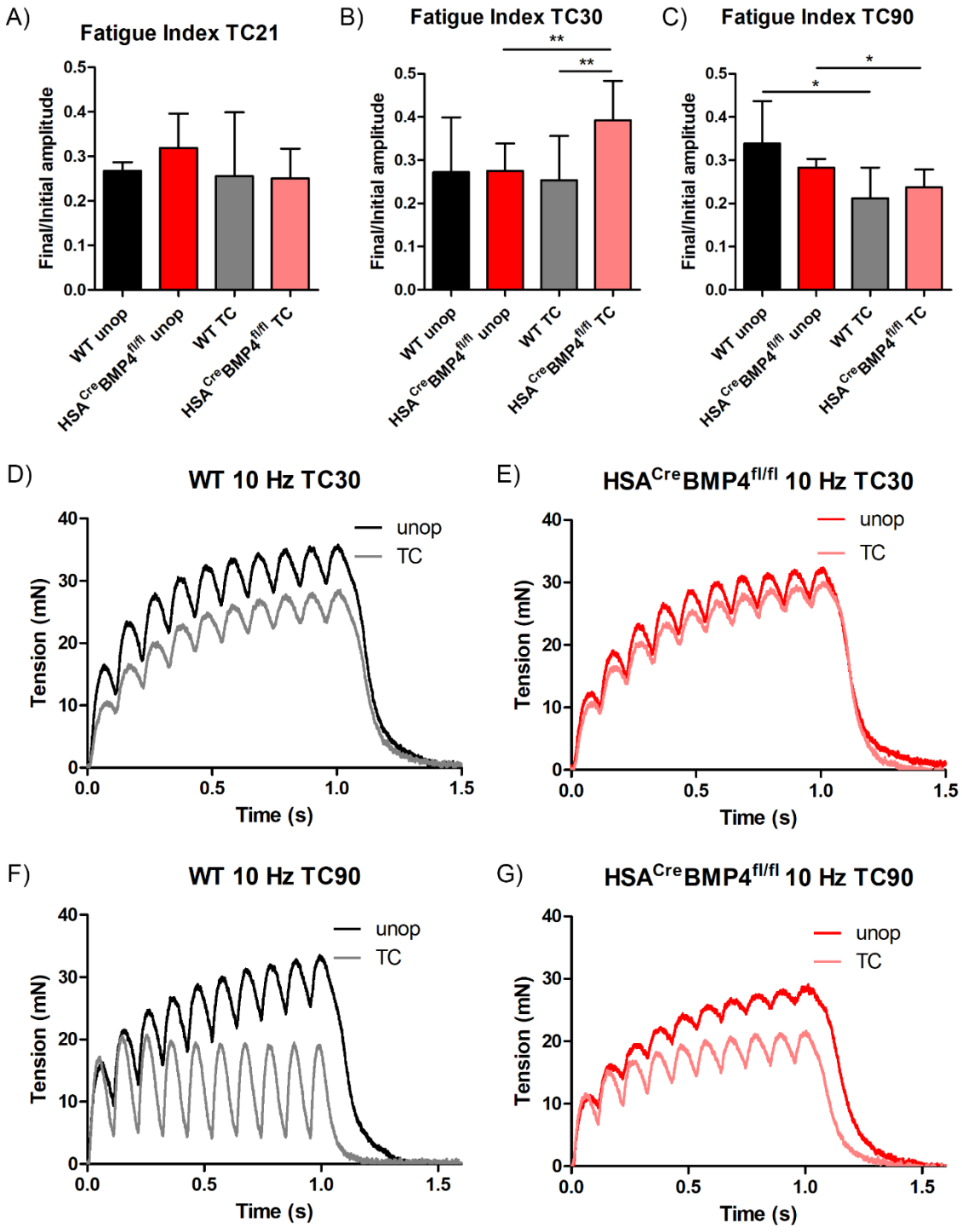
A)
Fatigue Index TC21
Final/Initial amplitude
0.5
0.4
0.3
0.2
0.1
0.0
WT unop
HSA Cre BMP4 fl/fl unop
WT TC
HSA Cre BMP4 fl/fl TC
B)
Fatigue Index TC30
**
**
C)
Fatigue Index TC90
*
*
D)
WT 10 Hz TC30
unop
TC
Tension (mN)
40
30
20
10
0
0.0
0.5
1.0
1.5
Time (s)
E)
HSA Cre BMP4 fl/fl 10 Hz TC30
F)
WT 10 Hz TC90
G)
HSA Cre BMP4 fl/fl 10 Hz TC90

Figure 4.3. Muscle atrophy in regenerated soleus muscles lacking BMP4. Mean CSA (+SD) in **A,** type I and **B,** type IIa muscle fibres from cross sections (30 um) of WT unop, WT TC, $HSA^{Cre}BMP4^{fl/fl}$ unop, and $HSA^{Cre}BMP4^{fl/fl}$ TC soleus muscles after 30 days of recovery, 50 fibres measured per muscle (n=2). **p=0.0021 WT TC vs $HSA^{Cre}BMP4^{fl/fl}$ TC, ***p<0.0001 $HSA^{Cre}BMP4^{fl/fl}$ unop vs $HSA^{Cre}BMP4^{fl/fl}$ TC (type I), and ***p=0.0009 WT unop vs WT TC, **p=0.0012 WT TC vs $HSA^{Cre}BMP4^{fl/fl}$ TC (type IIa), Unpaired t-test. **C,** Mean midbelly CSA (+SD) taken from cross sections (30 um) of soleus muscles, ~4 measurements taken per muscle (n=2). *p=0.0143 WT TC vs $HSA^{Cre}BMP4^{fl/fl}$ TC, Mann-Whitney test. **D,** Muscle fibre number estimates (mean + SD) obtained by dividing the mean midbelly CSA by the mean muscle fibre CSA, per muscle (n=2). *p=0.0108 WT TC vs $HSA^{Cre}BMP4^{fl/fl}$ TC, Unpaired t-test. **E,** CSA (mean +SD) of type I muscle fibres 90 days after Tibial n. crush (WT unop n=4, WT TC n=3, $HSA^{Cre}BMP4^{fl/fl}$ unop n=4, $HSA^{Cre}BMP4^{fl/fl}$ TC n=4). **p=0.0035 WT unop vs $HSA^{Cre}BMP4^{fl/fl}$ unop, Mann-Whitney test. **F,** CSA of type IIa muscle fibres 90 days post Tibial n. crush (WT unop n=4, WT TC n=3, $HSA^{Cre}BMP4^{fl/fl}$ unop n=4, $HSA^{Cre}BMP4^{fl/fl}$ TC n=4). ***p>0.0001 WT unop vs $HSA^{Cre}BMP4^{fl/fl}$ unop, Mann-Whitney test, and **p=0.0066 $HSA^{Cre}BMP4^{fl/fl}$ unop vs $HSA^{Cre}BMP4^{fl/fl}$ TC, Unpaired t-test. **G,** Midbelly CSA (mean+SD) of soleus muscles 90 days after Tibial n. crush (WT unop n=4, WT TC n=3, $HSA^{Cre}BMP4^{fl/fl}$ unop n=4, $HSA^{Cre}BMP4^{fl/fl}$ TC n=4). **p=0.0100 WT unop vs WT TC, *p=0.0249 WT unop vs $HSA^{Cre}BMP4^{fl/fl}$ unop, Mann-Whitney test. **H,** Muscle fibre number (mean+SD) in muscles 90 days after Tibial n. crush (WT unop n=4, WT TC n=3, $HSA^{Cre}BMP4^{fl/fl}$ unop n=4, $HSA^{Cre}BMP4^{fl/fl}$ TC n=4). **I,** Representative images of soleus cross-sections (30 µm) immunostained for S58 (red). Scale = 500 µm. Proportion of S58-positive fibres (mean+SD) taken at the soleus midbelly at **J,** TC30 (n=2) and **K,** TC90 (WT unop n=4, WT TC n=3, $HSA^{Cre}BMP4^{fl/fl}$ unop n=4, $HSA^{Cre}BMP4^{fl/fl}$ TC n=4). *p=0.0500, Mann-Whitney test.

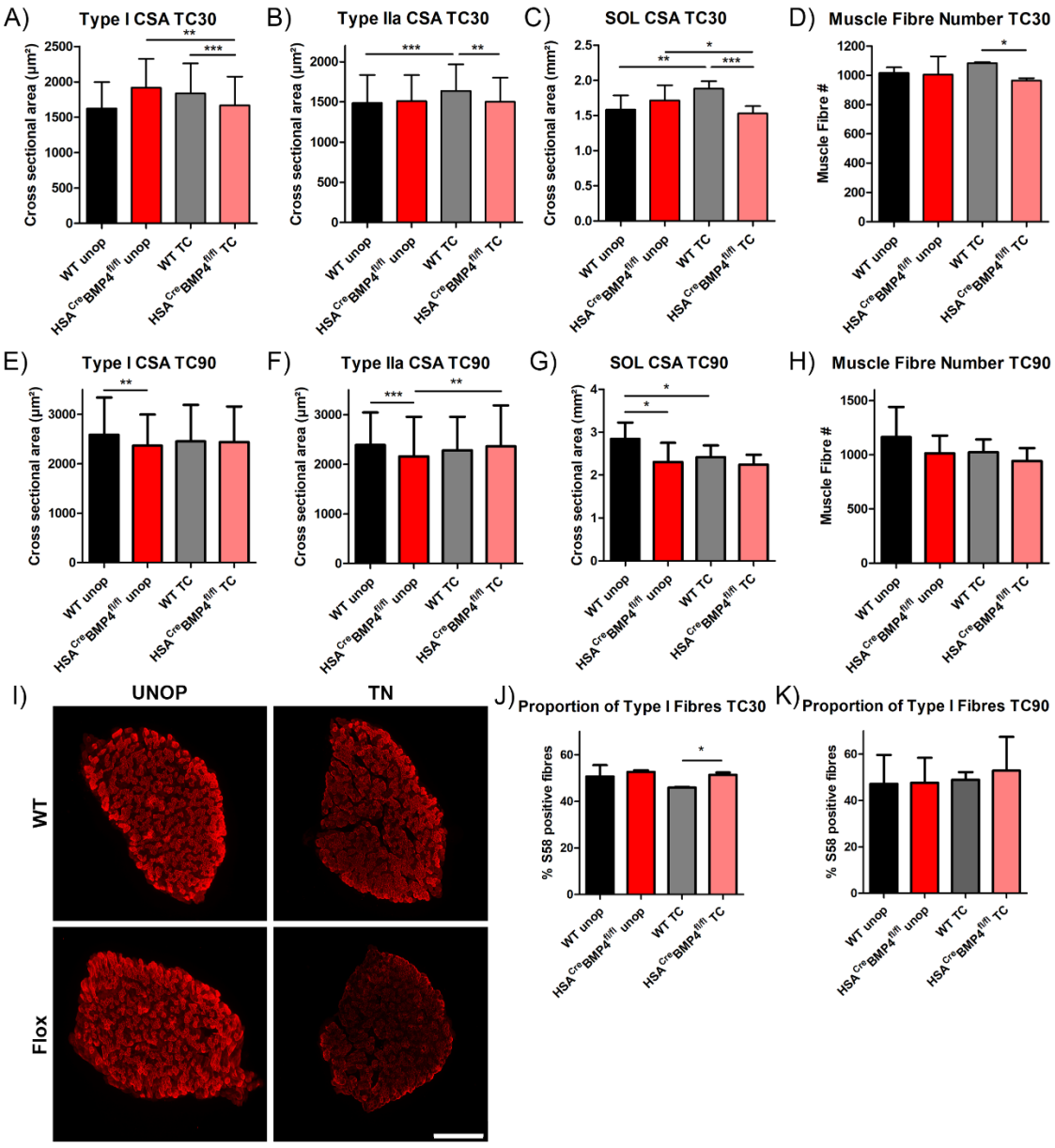
A)
Type I CSA TC30
Cross sectional area (µm²)
B)
Type IIa CSA TC30
Cross sectional area (µm²)
C)
SOL CSA TC30
Cross sectional area (mm²)
D)
Muscle Fibre Number TC30
Muscle Fibre #
E)
Type I CSA TC90
Cross sectional area (µm²)
F)
Type IIa CSA TC90
Cross sectional area (µm²)
G)
SOL CSA TC90
Cross sectional area (mm²)
H)
Muscle Fibre Number TC90
Muscle Fibre #
WT unop
HSA CreBMP4 fl/fl unop
WT TC
HSA CreBMP4 fl/fl TC
I)
UNOP
TN
WT
Flox
J)
Proportion of Type I Fibres TC30
% S58 positive fibres
K)
Proportion of Type I Fibres TC90
% S58 positive fibres

Figure 4.4. Soleus muscles lacking BMP4 fail to recover innervation following Tibial n crush compared to WT. **A,** Quantification of the percentage (mean+SD) of innervated endplates 21 days after Tibial n. crush (TC21). *p=0.0143 WT unop vs WT TC. **B,** Percentage of innervated (mean+SD) endplates after 30 days of recovery (TC30). ***p=0.0002 WT unop vs $HSA^{Cre}BMP4^{fl/fl}$ unop, 0.0005 WT TC vs $HSA^{Cre}BMP4^{fl/fl}$ TC, 0.0002 $HSA^{Cre}BMP4^{fl/fl}$ TC vs $HSA^{Cre}BMP4^{fl/fl}$ unop, <0.0001 WT TC vs WT unop. **C,** Percentage (mean+SD) of innervated endplates after 90 days of recovery (TC90). *p=0.0143 WT TC vs $HSA^{Cre}BMP4^{fl/fl}$ TC, 0.0143 $HSA^{Cre}BMP4^{fl/fl}$ TC vs $HSA^{Cre}BMP4^{fl/fl}$ unop, 0.0286 WT TC vs WT unop, 0.0143 WT unop vs $HSA^{Cre}BMP4^{fl/fl}$ unop. **D,** Percentage (mean+SD) of partially innervated endplates taken at TC21. *p=0.0143 WT unop vs WT TC. **E,** Percentage of partially innervated endplates (mean+SD) at TC30. *p=0.0190 WT TC vs $HSA^{Cre}BMP4^{fl/fl}$ TC, ***p=0.0003 WT unop vs $HSA^{Cre}BMP4^{fl/fl}$ unop, 0.0009 $HSA^{Cre}BMP4^{fl/fl}$ TC vs $HSA^{Cre}BMP4^{fl/fl}$ unop, 0.0002 WT TC vs WT unop. **F,** Percentage of partially innervated endplates (mean+SD) at TC90. *p=0.0286 WT unop vs $HSA^{Cre}BMP4^{fl/fl}$ unop, 0.0143 WT TC vs $HSA^{Cre}BMP4^{fl/fl}$ TC, 0.0286 $HSA^{Cre}BMP4^{fl/fl}$ TC vs $HSA^{Cre}BMP4^{fl/fl}$ unop. **G,** Percentage of denervated endplates (mean+SD) at TC21. No significant differences between groups (p>0.05). **H,** Percentage of denervated endplates (mean+SD) at TC30. **p=0.0074 WT unop vs $HSA^{Cre}BMP4^{fl/fl}$ unop, 0.0015 WT TC vs $HSA^{Cre}BMP4^{fl/fl}$ TC, ***p=0.0005 $HSA^{Cre}BMP4^{fl/fl}$ TC vs $HSA^{Cre}BMP4^{fl/fl}$ unop, <0.0001 WT TC vs WT unop. **I,** Percentage of denervated endplates (mean+SD) at TC90. *p=0.0143 WT TC vs $HSA^{Cre}BMP4^{fl/fl}$ TC, 0.0143 $HSA^{Cre}BMP4^{fl/fl}$ TC vs $HSA^{Cre}BMP4^{fl/fl}$ unop, 0.0143 WT TC vs WT unop, 0.0143 WT unop vs $HSA^{Cre}BMP4^{fl/fl}$ unop. TC21 n=4, TC30 n=8, TC90 n=4 for all. Mann-Whitney tests used for all.

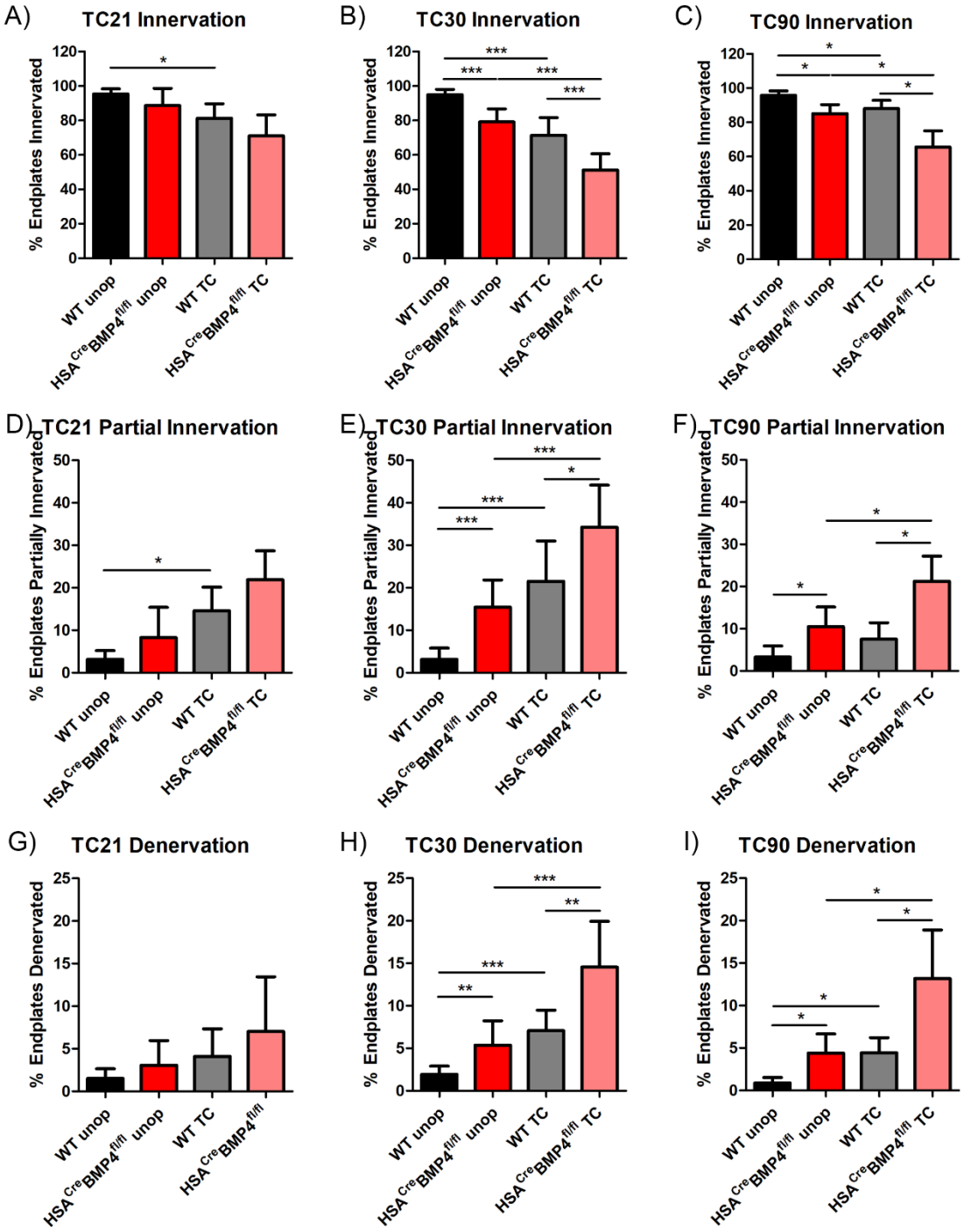
A)
TC21 Innervation
% Endplates Innervated
B)
TC30 Innervation
% Endplates Innervated
C)
TC90 Innervation
% Endplates Innervated
D)
TC21 Partial Innervation
% Endplates Partially Innervated
E)
TC30 Partial Innervation
% Endplates Partially Innervated
F)
TC90 Partial Innervation
% Endplates Partially Innervated
G)
TC21 Denervation
% Endplates Denervated
H)
TC30 Denervation
% Endplates Denervated
I)
TC90 Denervation
% Endplates Denervated
WT unop
HSA CreBMP4 fl/fl unop
WT TC
HSA CreBMP4 fl/fl TC

Figure 4.5. Delayed withdrawal of polyneuronal innervation at reinnervated endplates lacking muscular BMP4. **A,** Representative collapsed z-stack images from WT and $HSA^{Cre}BMP4^{fl/fl}$ TC soleus muscles at 21, 30, and 90 days post Tibial n. crush, stained for Tuj1 (yellow) and BTX (magenta). Arrowheads: examples of polyneuronal innervation. **B,** Quantification of the proportion of endplates innervated by more than one axon (mean+SD) in WT (n=4) and $HSA^{Cre}BMP4^{fl/fl}$ (n=4) TC soleus muscles at 21, 30, and 90 days of recovery. *p=0.0143 WT TC21 vs $HSA^{Cre}BMP4^{fl/fl}$ TC21 and *p=0.0286 WT TC30 vs $HSA^{Cre}BMP4^{fl/fl}$ TC30, Mann-Whitney test.

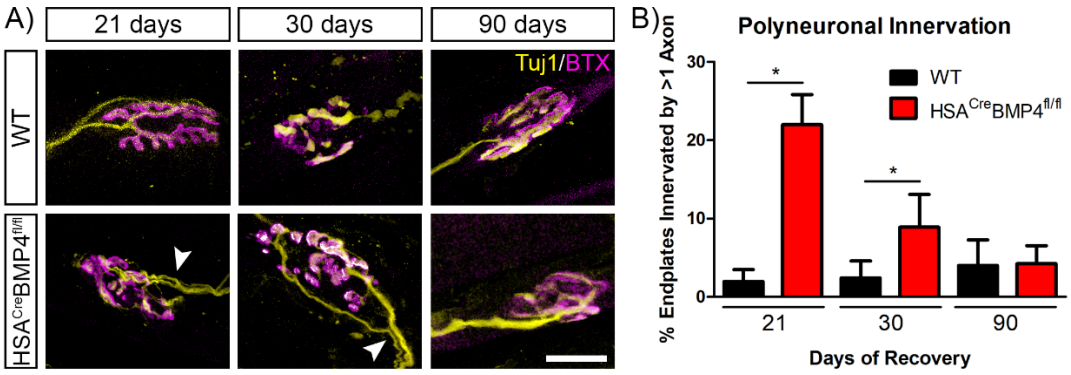
A)
21 days
30 days
90 days
Tuj1/BTX
WT
HSACreBMP4fl/fl
B)
Polyneuronal Innervation
% Endplates Innervated by >1 Axon
30
20
10
0
*
*
WT
HSACreBMP4fl/fl
21
30
90
Days of Recovery

CHAPTER 5: GENERAL DISCUSSION

The results I have presented in this thesis contributes to our understanding of NMJ stability in disease, homeostasis, and injury. I have shown how the rescue of a natural compensation mechanism to denervation can be rescued in ALS by preserving the health of TSCs at the NMJ. Next, I showed that normal NMJ structure and function are disrupted when muscular BMP4 is lost in the adult mouse. Finally, I showed that intact muscular BMP4 is required for efficient maturation of reinnervated synapses. Together, this research can be carried forward to apply to a variety of neuromuscular diseases and injuries to promote the stability and maintenance of these functional connections that are necessary for movement. Greater context, challenges, and future directions pertaining to each chapter are discussed in more detail below.

Muscle specific response to partial denervation in SOD1^{G93A} mice

The objective of this work was to determine whether the impairment in sprouting response in ALS is related to the muscle fibre-type specific pattern of denervation also observed during the disease. If this self-repair mechanism can be recovered, then this could be a viable therapeutic strategy to improve quality of life for ALS patients. I found that, indeed, fast twitch muscles from SOD1^{G93A} mice failed to reinnervate (sprout) denervated endplates relative to controls following a partial denervation injury. This was due to the loss of TSCs associated, specifically, with type IIb muscle fibres, the first to become denervated in ALS. TSCs are responsible for facilitating the sprouting of neighbouring intact MNs following denervation. Therefore, without TSCs, no sprouting can be initiated. These TSCs were shown to be vulnerable to high numbers of infiltrating macrophages, and, upon inhibition of these macrophages, TSC loss was prevented, and reinnervation capacity was restored in fast twitch ALS muscles. Therefore, this work has shown a causative link between impaired sprouting and motor-unit degeneration patterns in ALS. It also proposes the utility of macrophage inhibitors, such as masitinib, as potential therapeutics in ALS.

This study is one of many that further confirms ALS as a non-cell autonomous disease and that glial cells, in particular, contribute to ALS pathogenesis. Although TSCs

have been studied in the context of NMJ stability in ALS, little is known on TSC subtypes. Standard dogma dictates that all TSCs are the same. Though the results here dictate that, at least in the context of ALS, different TSCs respond differently to the stress of infiltrating macrophages. Specifically, TSCs associated with type IIa muscle fibres within the plantaris muscle do not leave the NMJ like the type IIb TSCs do, even though they are exposed to the same microenvironment. Furthermore, TCSs associated with type I muscle fibres, in the soleus, are also unaffected, even there is evidence of greater macrophage density in the soleus compared to the plantaris. It is possible that type IIb TSCs sense early alterations in synaptic transmission that precede denervation, and that the additional stress of macrophage infiltration tips the scale. However, if this were the case, then these TSCs likely would not mount a successful sprouting response after masitinib treatment. Therefore, future work should investigate the differential protein expression patterns and signaling mechanisms that may exist between the TSCs of different muscle fibre types. It would also be interesting to determine whether the expression of mutant SOD1, itself, interacts differently with these different TSC types. One possible strategy for separating TSCs associated with specific fibre types would be to perform laser-capture experiments on muscles stained for various myosin isoforms. Various proteomic and genomic screens could then be carried out on these distinct populations of TSCs, potentially even at different disease stages.

A challenge with implementing masitinib as a therapeutic for ALS is that, by the time a human with ALS has diagnosable symptoms, the disease has already progressed. The type IIb NMJs are already lost, and the remaining MNs have already sprouted to capacity to compensate. This sprouting response that has been shown to occur in ALS patients is likely responsible, in part, for why individuals do not display gross motor deficits even when muscles display significant denervation. In this study, pre-disease-onset mice were chosen specifically to determine whether there is an inherent sprouting deficit in fast twitch muscles in $SOD1^{G93A}$ mice. These results do suggest that $SOD1^{G93A}$ do have a reduced capacity for reinnervation compared to WT controls that is independent of disease progression. Though masitinib did rescue the sprouting response pre-disease-onset, it is still unclear whether masitinib would be capable of rescuing sprouting in symptom-onset mice.

AB Science recently completed a phase 2/3 clinical trial for masitinib in ALS patients. Masitinib, in combination with riluzole, delayed the decline in the ALS functional rating score compared to riluzole treatment alone (Mora et al., 2019). As of their most recent reports, there have been no indications that masitinib increases survival, although quality of life was reported to be maintained longer in patients (Mora et al., 2019). They also reported that the earlier masitinib was administered (i.e. less severe disease stage) the better effects observed in patients (Mora et al., 2019). This agrees with our results, that masitinib could be particularly effective with earlier intervention. The obvious challenge with early intervention, however, is that denervation has already significantly progressed by the time an individual has diagnosable symptoms. It is possible, therefore, that masitinib treatment would be particularly promising as a treatment for individuals with known cases of familial ALS where a parent has already presented with the disease.

A possible challenge with prescribing masitinib could be immune system suppression. In the clinical trial, patients receiving masitinib were more likely to report adverse events than those given placebo (Mora et al., 2019). Among others, adverse events included peripheral edema and urinary or upper respiratory tract infections, all of which could potentially be associated with macrophage inhibition. Overall, however, side affects were minor and the research group deemed the drug safe for use (Mora et al., 2019).

Given that ALS is a multifactorial disease involving pathologies across multiple cell types and systems, it is likely that effective therapies for ALS will combinatorial in nature. However, this work reveals that the stability of the NMJ is of key importance in slowing disease progression in ALS. Also, TSCs associated with type IIb muscle fibres are unable to mount a proper sprouting response due to an increased infiltration of macrophages. Inhibiting macrophages allows TSCs to respond normally to denervation and mount a successful sprouting response. Therefore, TSC loss is the functional link between impaired sprouting and muscle fibre type susceptibility in ALS.

Characterization of a novel mouse model of BMP4 loss in skeletal muscle

BMP4 is an extensively studied protein in the context of development that has also been implicated in NMJ stability and in ALS. In a proteomics screen conducted by our lab on embryonic stem cell derived MNs harbouring a TDP-43 mutation, we found that many Smad proteins were dysregulated. These effectors are all downstream of BMP4 signaling, which led us to investigate the role of BMP4 at the vertebrate NMJ. This work will help inform future work on determining how alterations in BMP4 signaling at the NMJ contribute to ALS disease pathogenesis.

Therefore, in this study, we sought to determine whether mammalian BMP4 has similar roles in NMJ structure and function as its homolog, *wit,* does in *Drosophila.* To investigate this, we utilized a novel mouse model with inducible knockdown of BMP4 in skeletal muscle. We then performed behavioural, physiological, and anatomical methods to determine how mammalian BMP4 derived from muscle contributes to normal NMJ homeostasis. We found that, similar to *Drosophila*, mice lacking muscular BMP4 had motor impairments, deficits in synaptic transmission, and alterations in NMJ morphology. Additionally, BMP4 signaling must have a role in the structure and function of muscle spindles. This is the first study to our knowledge to investigate the functional roles of BMP4 at the vertebrate NMJ.

Though our results are consistent with results in *Drosophila*, the phenotype in mice was less severe. This was an adult knockdown model as opposed to a developmental mutation, so, one explanation for this reduced severity may be because BMP4 was not mutated during development. It is also important to note that muscular BMP4 is not the only contribution of BMP4 at the NMJ. A paper by Chou et al. in 2013 has shown that BMP4 is also present in SCs, including TSCs at the NMJ. It is therefore likely that some BMP4 signaling was still occurring at the NMJs of our mice given that SC-derived BMP4 was unaffected. It is also possible that TSCs even upregulate their BMP4 production in the absence of muscular BMP4, but this will need to be investigated with future experiments. It will also be necessary to perform experiments on mice harbouring double knockdown of BMP4 in both skeletal muscle and SCs to determine how NMJ structure and function are affected in the total absence of BMP4.

Additionally, given BMP4 expression in satellite cells, it would be interesting to determine how BMP4 signaling contributes to muscle regeneration following injury. $BMP4^{fl/fl}$ mice could be crossed with mice harboring an inducible Cre recombinase under the control of the Pax7 promoter, yielding an adult model of BMP4 knockdown in satellite cells. We could then induce a muscle injury with, for example, snake venom injection, and determine how BMP4-null satellite cells are able to proliferate, differentiate, and ultimately repopulate the degenerated muscle site.

Overall, vertebrate BMP4 does appear to be important in maintaining normal synaptic transmission and structure at the NMJ. What remains to be determined is whether changes in BMP4 contribute to pathology in ALS. This study to investigate the role of BMP4 at the adult NMJ came from results from a proteomics screen of ESCMNs harbouring an ALS-inducing TDP-43 mutation. This study showed that various Smad proteins, downstream of BMP4 signaling, were dysregulated. Therefore, given the evidence presented here that mammalian BMP4 does contribute to NMJ stability in the otherwise healthy adult mouse, the next steps will be to further examine how BMP4 signaling contributes to ALS pathology at the NMJ. One possible experiment would be to knock down muscular and/or SC-derived BMP4 in $SOD1^{G93A}$ mice and examine NMJ structural and functional alterations throughout disease progression.

Neuromuscular reinnervation in the absence of muscle-derived BMP4

Many developmentally regulated mechanisms are reactivated during disease and injury. Understanding these mechanisms are, therefore, central to developing therapies to improve repair or delay degeneration. There is evidence in DRG models of axotomy that the BMP4/Smad1 pathway is essential to repair (Zou et al., 2009; Parikh et al., 2011; Zhong and Zou, 2014). Understanding how BMP4 signaling contributes to repair following injury could therefore provide insight into how dysregulation of Smad proteins contributes to ALS. So, we examined whether BMP4 loss in muscle impairs neuromuscular reinnervation and repair following Tibial n. crush. We utilized mice with selective knockdown of BMP4 in skeletal muscle, performed a unilateral Tibial n. crush, and allowed various recovery times (21, 30, and 90 days) to examine reinnervation in the absence of BMP4.

We found that while contractile force was unaffected in the regenerated muscles lacking BMP4, there was evidence of altered contractile properties over recovery time. We also found that muscle lacking BMP4 failed to reinnervate to the degree of WT controls after Tibial n. crush. This led to increased muscle atrophy, which was evident in decreases in cross-sectional area. Finally, we found that reinnervated endplates lacking muscular BMP4 are less mature than their WT counterparts, indicating that BMP4 signaling does act to re-establish NMJs following peripheral nerve injury.

If contractile force is unaffected, then it would stand to reason that axonal outgrowth was not impaired in $HSA^{Cre}BMP4^{fl/fl}$ mice. Given that these mice only lacked BMP4 in skeletal muscle, this finding was unsurprising. However, muscular BMP4 did play in NMJ reinnervation and synapse maturation following injury. Since SCs are known to provide the scaffolding for regenerating axons (Son and Thompson, 1995b), we anticipate that BMP4 knockdown in SCs may lead to a more severe phenotype following Tibial n. crush. Therefore, we will be pursuing the role of SC-derived BMP4 in axonal regeneration following Tibial n. crush in future experiments.

The finding that reinnervated $HSA^{Cre}BMP4^{fl/fl}$ soleus muscles did not have reduced strength compared to unoperated controls was somewhat surprising when, as shown in Chapter 3, that $HSA^{Cre}BMP4^{fl/fl}$ soleus muscles are weaker over time since doxycycline administration. A potential explanation for this phenomenon is the tendency for reinnervated endplates to be more stable than their original counterparts (Sharp et al., 2018). Similar nerve injuries as that performed in this study have previously been shown to have a conditioning effect that prevents further degeneration of NMJs in mouse models of ALS (Gordon et al., 2010; Sharp et al., 2018). It therefore stands to reason that although these reinnervated endplates displayed delayed maturity, they may be more stable over time and prevent further endplate dismantling and instability due to the lack of muscular BMP4. As has been previously discussed, there is also evidence to suggest that BMP4 dysregulation at the NMJ is occurring in ALS (Duval et al., 2014; Deshpande et al., 2016; Held et al., 2019). Both muscular BMP4 loss and ALS lead to progressive motor impairments over time, so it is possible that, as has been reported in ALS studies, the Tibial n. crush performed here could be acting as a conditioning lesion to protect against future NMJ instability caused by muscular BMP4 loss. It would be interesting to

follow up this notion with long-term BMP4 knockdown experiments and determine whether Tibial n. crush protects against future degeneration.

BMP4 has well documented roles in NMJ development and stability in *Drosophila*. Therefore, upon disruption of this pathway, it was unsurprising that reinnervated NMJs were less mature. To further determine how synapse maturity is impaired in these mice, it will be important to conduct intracellular recordings at various time points throughout recovery to determine how the function of the NMJ changes over time. In the future, we hope to determine whether enhanced BMP4 signaling in muscle and/or SCs can be exploited to improve the rate of axonal outgrowth and reinnervation in models of peripheral nerve injury.

Conclusion

Diseases or injuries of the neuromuscular system pose a significant threat to the health and independence of those afflicted. These conditions can be devastating and severely impact quality of life. While no outright cures are proposed in this thesis, I believe I have highlighted the utility of the NMJ as a therapeutic target, both in disease and injury. By identifying and understanding mechanisms of NMJ instability in ALS we take essential steps at designing effective therapies to treat that instability. This is of key importance to treating the disease considering that NMJ denervation occurs before MN death. Additionally, by perturbing NMJ reinnervation following injury, we better understand what molecular mechanisms contribute to repair at the NMJ that could be enhanced during healing. Translating invertebrate results into vertebrate models is also a key step in the translation of scientific findings to human health. Potential hope could lie in enhancing the signaling of known endogenous NMJ stabilizing proteins, such as BMP4, to improve reinnervation in injury or disease. In conclusion, understanding the various components that contribute to NMJ stability is vital to be able to treat neuromuscular injuries and diseases.

REFERENCES

Aberle H, Haghighi AP, Fetter RD, McCabe BD, Magalhães TR, Goodman CS (2002) wishful thinking Encodes a BMP Type II Receptor that Regulates Synaptic Growth in Drosophila. Neuron 33:545–558.

Ahmadi M, Liu J-X, Brannstrom T, Andersen PM, Stal P, Pedrosa-Domellof F (2010) Human extraocular muscles in ALS. Invest Ophthalmol Vis Sci 51:3494–3501.

Ajroud-Driss S, Siddique T (2015) Sporadic and hereditary amyotrophic lateral sclerosis (ALS). Biochim Biophys Acta 1852:679–684.

Akay T, Tourtellotte WG, Arber S, Jessell TM (2014) Degradation of mouse locomotor pattern in the absence of proprioceptive sensory feedback. Proc Natl Acad Sci U S A 111:16877–16882.

Alexander GM, Erwin KL, Byers N, Deitch JS, Augelli BJ, Blankenhorn EP, Heiman-Patterson TD (2004) Effect of transgene copy number on survival in the G93A SOD1 transgenic mouse model of ALS. Brain Res Mol Brain Res 130:7–15.

Anderson MJ, Cohen MW (1977) Nerve-induced and spontaneous redistribution of acetylcholine receptors on cultured muscle cells. J Physiol 268:757–773.

Arbour D, Tremblay E, Martineau E, Julien J, Robitaille R (2015) Early and Persistent Abnormal Decoding by Glial Cells at the Neuromuscular Junction in an ALS Model. J Neurosci 35:688–706.

Arbour D, Velde C Vande, Robitaille R (2017) New perspectives on amyotrophic lateral sclerosis : the role of glial cells at the neuromuscular junction. J Physiol 595:647–661.

Baichwal RR, Bigbee JW, DeVries GH (1988) Macrophage-mediated myelin-related mitogenic factor for cultured Schwann cells. Proc Natl Acad Sci U S A 85:1701–1705.

Balice-Gordon RJ, Breedlove SM, Bernstein S, Lichtman JW (1990) Neuromuscular junctions shrink and expand as muscle fiber size is manipulated: in vivo observations in the androgen-sensitive bulbocavernosus muscle of mice. J Neurosci 10:2660–2671.

Balice-Gordon RJ, Lichtman JW (1990) In vivo visualization of the growth of pre- and postsynaptic elements of neuromuscular junctions in the mouse. J Neurosci 10:894–908.

Balice-Gordon RJ, Lichtman JW (1993) In vivo observations of pre- and postsynaptic changes during the transition from multiple to single innervation at developing neuromuscular junctions. J Neurosci 13:834–855.

Banker BQ, Kelly SS, Robbins N (1983) Neuromuscular Transmission and Correlative Morphology in Young and Old Mice. J Physiol 339:355–375.

Bányai L, Sonderegger P, Patthy L (2010) Agrin Binds BMP2 , BMP4 and TGFβ1. PLoS One 5.

Barrette B, Hebert M-A, Filali M, Lafortune K, Vallieres N, Gowing G, Julien J-P, Lacroix S (2008) Requirement of myeloid cells for axon regeneration. J Neurosci 28:9363–9376.

Barry JA, Ribchester RR (1995) Persistent polyneuronal innervation in partially denervated rat muscle after reinnervation and recovery from prolonged nerve conduction block. J Neurosci 15:6327–6339.

Bawa PNS, Jones KE, Stein RB (2014) Assessment of size ordered recruitment. Front Hum Neurosci 8.

Beers DR, Appel SH (2019) Immune dysregulation in amyotrophic lateral sclerosis: mechanisms and emerging therapies. Lancet Neurol 18:211–220.

Beirowski B, Adalbert R, Wagner D, Grumme DS, Addicks K, Ribchester RR, Coleman MP (2005) The progressive nature of Wallerian degeneration in wild-type and slow Wallerian degeneration (WldS) nerves. BMC Neurosci 6:1–27.

Bennett MR, Pettigrew AG (1976) The formation of neuromuscular synapses. Cold Spring Harb Symp Quant Biol 40:409–424.

Berke B, Wittnam J, McNeill E, Van Vactor DL, Keshishian H (2013) Retrograde BMP Signaling at the Synapse: A Permissive Signal for Synapse Maturation and Activity-Dependent Plasticity. J Neurosci 33:17937–17950.

Bewick GS, Reid B, Jawaid S, Hatcher T, Shanley L (2004) Postnatal emergence of mature release properties in terminals of rat fast- and slow-twitch muscles. Eur J Neurosci 19:2967–2976.

Bewick GS, Young C, Slater CR (1996) Spatial relationships of utrophin, dystrophin, beta-dystroglycan and beta-spectrin to acetylcholine receptor clusters during postnatal maturation of the rat neuromuscular junction. J Neurocytol 25:367–379.

Billger M, Wallin M, Karlsson JO (1988) Proteolysis of tubulin and microtubule-associated proteins 1 and 2 by calpain I and II. Difference in sensitivity of assembled and disassembled microtubules. Cell Calcium 9:33–44.

Birchmeier C, Nave K-A (2008) Neuregulin-1, a key axonal signal that drives Schwann cell growth and differentiation. Glia 56:1491–1497.

Bloch-Gallego E (2015) Mechanisms controlling neuromuscular junction stability. Cell Mol Life Sci 72:1029–1043.

Bloch RJ, Steinbach JH, Merlie JP, Heinemann S (1986) Collagenase digestion alters the organization and turnover of junctional acetylcholine receptors. Neurosci Lett 66:113–119.

Bloemberg D, Quadrilatero J (2012) Rapid Determination of Myosin Heavy Chain Expression in Rat , Mouse , and Human Skeletal Muscle Using Multicolor Immunofluorescence Analysis. PLoS One 7.

Bradke F, Fawcett JW, Spira ME (2012) Assembly of a new growth cone after axotomy: the precursor to axon regeneration. Nat Rev Neurosci 13:183–193.

Bragdon B, Moseychuk O, Saldanha S, King D, Julian J, Nohe A (2011) Bone Morphogenetic Proteins : A critical review. Cell Signal 23:609–620.

Brenner HR, Herczeg A, Slater CR (1992) Synapse-specific expression of acetylcholine receptor genes and their products at original synaptic sites in rat soleus muscle fibres regenerating in the absence of innervation. Development 116:41–53.

Brown MC, Ironton R (1978) Sprouting and regression of neuromuscular synapses in partially denervated mammalian muscles. J Physiol 278:325–348.

Burden SJ, Sargent PB, McMahan UJ (1979) Acetylcholine receptors in regenerating muscle accumulate at original synaptic sites in the absence of the nerve. J Cell Biol 82:412–425.

Burke RE (1981) Motor units: anatomy, physiology and functional organization. In: VB Brooks (ed.), Handbook of Physiology, Volume II., pp 345–422. Bethesda, MD: American Physiological Society.

Burke RE, Levine DN, Tsairis P, Zajac FE (1973) Physiological types and histochemical profiles in motor units of the cat gastrocnemius. J Physiol 234:723–748.

Burke RE, Levine DN, Zajac, III FE, Tsairis P, Engel WK (1971) Mammalian Motor Units: Physiological-Histochemical Correlation in Three Types in Cat Gastrocnemius. Science (80-) 174:709–712.

Burke RE, Tsairis P (1973) Anatomy and innervation ratios in motor units of cat gastrocnemius. J Physiol 234:749–765.

Burnett MG, Zager EL (2004) Pathophysiology of peripheral nerve injury: a brief review. Neurosurg Focus 16:E1.

Caillaud M, Richard L, Vallat J-M, Desmoulière A, Billet F (2019) Peripheral nerve regeneration and intraneural revascularization. Neural Regen Res 14:24–33.

Cajal SRY (1928) Degeneration and Regeneration of the Nervous System. Brain 51:525.

Campanelli JT, Roberds SL, Campbell KP, Scheller RH (1994) A role for dystrophin-associated glycoproteins and utrophin in agrin-induced AChR clustering. Cell 77:663–674.

Carrasco DI, Bahr BA, Seburn KL, Pinter MJ (2016a) Abnormal response of distal Schwann cells to denervation in a mouse model of motor neuron disease. Exp Neurol 278:116–126.

Carrasco DI, Seburn KL, Pinter MJ (2016b) Altered terminal Schwann cell morphology precedes denervation in SOD1 mice. Exp Neurol 275:172–181.

Chancellor AM, Warlow CP (1992) Adult onset motor neuron disease: worldwide mortality, incidence and distribution since 1950. J Neurol Neurosurg Psychiatry 55:1106–1115.

Chargé SBP, Rudnicki MA (2004) Cellular and Molecular Regulation of Muscle Regeneration. Physiol Rev 84:209–238.

Chipman PH, Franz CK, Nelson A, Schachner M, Rafuse VF (2010) Neural cell adhesion molecule is required for stability of reinnervated neuromuscular junctions. Eur J Neurosci 31:238–249.

Chipman PH, Schachner M, Rafuse VF (2014a) Presynaptic NCAM is required for motor neurons to functionally expand their peripheral field of innervation in partially denervated muscles. J Neurosci 34:10497–10510.

Chipman PH, Zhang Y, Rafuse VF (2014b) A stem-cell based bioassay to critically assess the pathology of dysfunctional neuromuscular junctions. PLoS One 9.

Chiu AY, Zhai P, Dal Canto MC, Peters TM, Kwon YW, Prattis SM, Gurney ME (1995) Age-dependent penetrance of disease in a transgenic mouse model of familial amyotrophic lateral sclerosis. Mol Cell Neurosci 6:349–362.

Chou H, Lai D, Huang C, McLennan IS, Wang H, Wang Y (2013) BMP4 Is a Peripherally-Derived Factor for Motor Neurons and Attenuates Glutamate-Induced Excitotoxicity In Vitro. PLoS One 8.

Clark JA, Southam KA, Blizzard CA, King AE, Dickson TC (2016) Axonal degeneration, distal collateral branching, and neuromuscular junction architecture alterations occur prior to symptom onset in the SOD1G93A mouse model of amyotrophic lateral sclerosis. J Clin Neuroanat 76:35–47.

Clawson LL, Cudkowicz M, Krivickas L, Brooks BR, Sanjak M, Allred P, Atassi N, Swartz A, Steinhorn G, Uchil A, Riley KM, Yu H, Schoenfeld DA, Maragakis NJ (2018) A randomized controlled trial of resistance and endurance exercise in amyotrophic lateral sclerosis. Amyotroph Lateral Scler Frontotemporal Degener 19:250–258.

Cohen MW, Godfrey EW (1992) Early appearance of and neuronal contribution to agrin-like molecules at embryonic frog nerve-muscle synapses formed in culture. J Neurosci 12:2982–2992.

Colomar A, Robitaille R (2004) Glial Modulation of Synaptic Transmission at the Neuromuscular Junction. Glia 47:284–289.

Courtney J, Steinbach JH (1981) Age changes in neuromuscular junction morphology and acetylcholine receptor distribution on rat skeletal muscle fibres. J Physiol 320:435–447.

Covault J, Sanes JR (1986) Distribution of N-CAM in synaptic and extrasynaptic portions of developing and adult skeletal muscle. J Cell Biol 102:716–730.

Dale HH, Feldberg W, Vogt M (1936) Release of acetylcholine at voluntary motor nerve endings. J Physiol 86:353–380.

Darabid H, Arbour D, Robitaille R, Hc Q (2013) Glial Cells Decipher Synaptic Competition at the Mammalian Neuromuscular Junction. J Neurosci 33:1297–1313.

Day NC, Wood SJ, Ince PG, Volsen SG, Smith W, Slater CR, Shaw PJ (1997) Differential Localization of Voltage-Dependent Calcium Channel α1 Subunits at the Human and Rat Neuromuscular Junction. J Neurosci 17:6226–6235.

de Oliveira GP, Alves CJ, Chadi G (2013) Early gene expression changes in spinal cord from SOD1(G93A) Amyotrophic Lateral Sclerosis animal model. Front Cell Neurosci 7:216.

De Winter F, Vo T, Stam FJ, Wisman LAB, Ba PR, Niclou SP, van Muiswinkel FL, Verhaagen J (2006) The expression of the chemorepellent Semaphorin 3A is selectively induced in terminal Schwann cells of a subset of neuromuscular synapses that display limited anatomical plasticity and enhanced vulnerability in motor neuron disease. Mol Cell Neurosci 32:102–117.

Deisseroth K (2011) Optogenetics. Nat Methods 8:26–29.

DeJesus-Hernandez M et al. (2011) Expanded GGGGCC hexanucleotide repeat in noncoding region of C9ORF72 causes chromosome 9p-linked FTD and ALS. Neuron 72:245–256.

Deng B, Lv W, Duan W, Liu Y, Li Z, Ma Y, Zhang G, Song X, Cui C, Qi X, Li Y, Li C (2018) Progressive Degeneration and Inhibition of Peripheral Nerve Regeneration in the SOD1-G93A Mouse Model of Amyotrophic Lateral Sclerosis. Cell Physiol Biochem 46:2358–2372.

Deshpande M, Feiger Z, Shilton AK, Luo CC, Silverman E, Rodal AA (2016) Role of BMP receptor traffic in synaptic growth defects in an ALS model. Mol Biol Cell 27:2898–2910.

Desseille C, Deforges S, Biondi O, Houdebine L, D'amico D, Lamaziere A, Caradeuc C, Bertho G, Bruneteau G, Weill L, Bastin J, Djouadi F, Salachas F, Lopes P, Chanoine C, Massaad C, Charbonnier F (2017) Specific Physical Exercise Improves Energetic Metabolism in the Skeletal Muscle of Amyotrophic-Lateral- Sclerosis Mice. Front Mol Neurosci 10:332.

Di Giorgio FP, Boulting GL, Bobrowicz S, Eggan KC (2008) Human embryonic stem cell-derived motor neurons are sensitive to the toxic effect of glial cells carrying an ALS-causing mutation. Cell Stem Cell 3:637–648.

Ding C, Hammarlund M (2019) Mechanisms of injury-induced axon degeneration. Curr Opin Neurobiol 57:171–178.

Duclert A, Changeux JP (1995) Acetylcholine receptor gene expression at the developing neuromuscular junction. Physiol Rev 75:339–368.

Duval MG, Gilbert MJH, Watson DE, Zerulla TC, Tierney KB, Allison WT (2014) Growth Differentiation Factor 6 As a Putative Risk Factor in Neuromuscular Degeneration. PLoS One 9.

Edds M V. (1950) Collateral Regeneration of Residual Motor Axons in Partially Denervated Muscles. J Exp Zool 113:517–551.

Fahim MA (1989) Rapid neuromuscular remodeling following limb immobilization. Anat Rec 224:102–109.

Fambrough DM (1979) Control of acetylcholine receptors in skeletal muscle. Physiol Rev 59:165–227.

Feng Z, Ko C (2008) Schwann Cells Promote Synaptogenesis at the Neuromuscular Junction via Transforming Growth Factor-β1. J Neurosci 28:9599–9609.

Fischer LR, Culver DG, Tennant P, Davis AA, Wang M, Castellano-Sanchez A, Khan J, Polak MA, Glass JD (2004) Amyotrophic lateral sclerosis is a distal axonopathy: evidence in mice and man. Exp Neurol 185:232–240.

Fleshman JW, Munson JB, Sypert GW, Friedman WA (1981) Rheobase, input resistance, and motor-unit type in medial gastrocnemius motoneurons in the cat. J Neurophysiol 46:1326–1338.

Flis DJ, Dzik K, Kaczor JJ, Cieminski K, Halon-Golabek M, Antosiewicz J, Wieckowski MR, Ziolkowski W (2019) Swim Training Modulates Mouse Skeletal Muscle Energy Metabolism and Ameliorates Reduction in Grip Strength in a Mouse Model of Amyotrophic Lateral Sclerosis. Int J Mol Sci 20.

Flis DJ, Dzik K, Kaczor JJ, Halon-Golabek M, Antosiewicz J, Wieckowski MR, Ziolkowski W (2018) Swim Training Modulates Skeletal Muscle Energy Metabolism, Oxidative Stress, and Mitochondrial Cholesterol Content in Amyotrophic Lateral Sclerosis Mice. Oxid Med Cell Longev 2018:5940748.

Flucher BE, Daniels MP (1989) Distribution of Na+ channels and ankyrin in neuromuscular junctions is complementary to that of acetylcholine receptors and the 43 kd protein. Neuron 3:163–175.

Fogarty MJ, Mu EWH, Noakes PG, Lavidis NA, Bellingham MC (2016) Marked changes in dendritic structure and spine density precede significant neuronal death in vulnerable cortical pyramidal neuron populations in the SOD1G93A mouse model of amyotrophic lateral sclerosis. Acta Neuropathol Commun 4 Available at: http://dx.doi.org/10.1186/s40478-016-0347-y.

Fogarty MJ, Noakes PG, Bellingham MC (2015) Motor cortex layer V pyramidal neurons exhibit dendritic regression, spine loss, and increased synaptic excitation in the presymptomatic hSOD1G93A mouse model of amyotrophic lateral sclerosis. J Neurosci 35:643–647.

Franceshi C, Garagnani P, Morsiani C, Conte M, Santoro A, Grignolio A, Monti D, Capri M, Salvioli S (2018) The Continuum of Aging and Age-Related Diseases: Common Mechanisms but Different Rates. Front Med 5.

Frank E, Fischbach GD (1979) Early events in neuromuscular junction formation in vitro: induction of acetylcholine receptor clusters in the postsynaptic membrane and morphology of newly formed synapses. J Cell Biol 83:143–158.

Frank E, Gautvik K, Sommerschild H (1976) Persistence of junctional acetylcholine receptors following denervation. Cold Spring Harb Symp Quant Biol 40:275–281.

Frey D, Schneider C, Xu L, Borg J, Spooren W, Caroni P (2000) Early and Selective Loss of Neuromuscular Synapse Subtypes with Low Sprouting Competence in Motoneuron Diseases. J Neurosci 20:2534–2542.

Fukata Y, Itoh TJ, Kimura T, Menager C, Nishimura T, Shiromizu T, Watanabe H, Inagaki N, Iwamatsu A, Hotani H, Kaibuchi K (2002) CRMP-2 binds to tubulin heterodimers to promote microtubule assembly. Nat Cell Biol 4:583–591.

Gámez B, Rodriguez-carballo E, Ventura F (2013) BMP signaling in telencephalic neural cell specification and maturation. Front Cell Neurosci 7:1–13.

Garbugino L, Golini E, Giuliani A, Mandillo S (2018) Prolonged Voluntary Running Negatively Affects Survival and Disease Prognosis of Male SOD1G93A Low-Copy Transgenic Mice. Front Behav Neurosci 12:275.

Gaudet AD, Popovich PG, Ramer MS (2011) Wallerian degeneration: Gaining perspective on inflammatory events after peripheral nerve injury. J Neuroinflammation 8.

George EB, Glass JD, Griffin JW (1995) Axotomy-induced axonal degeneration is mediated by calcium influx through ion-specific channels. J Neurosci 15:6445–6452.

Georgiou J, Robitaille R, Trimble WS, Charlton MP (1994) Synaptic regulation of glial protein expression in vivo. Neuron 12:443–455.

Geraldo S, Gordon-Weeks PR (2009) Cytoskeletal dynamics in growth-cone steering. J Cell Sci 122:3595–3604.

Girouard M, Bueno M, Julian V, Drake S, Byrne AB, Fournier AE (2018) The Molecular Interplay between Axon Degeneration and Regeneration. Dev Neurobiol:978–990.

Gitik M, Kleinhaus R, Hadas S, Reichert F, Rotshenker S (2014) Phagocytic receptors activate and immune inhibitory receptor SIRPalpha inhibits phagocytosis through paxillin and cofilin. Front Cell Neurosci 8:104.

Gitik M, Liraz-Zaltsman S, Oldenborg P-A, Reichert F, Rotshenker S (2011) Myelin down-regulates myelin phagocytosis by microglia and macrophages through interactions between CD47 on myelin and SIRPalpha (signal regulatory protein-alpha) on phagocytes. J Neuroinflammation 8:24.

Glajch KE, Ferraiuolo L, Mueller KA, Stopford MJ, Prabhkar V, Gravanis A, Shaw PJ, Sadri-Vakili G (2016) MicroNeurotrophins Improve Survival in Motor Neuron-Astrocyte Co-Cultures but Do Not Improve Disease Phenotypes in a Mutant SOD1 Mouse Model of Amyotrophic Lateral Sclerosis. PLoS One 11:e0164103.

Goldman D, Brenner HR, Heinemann S (1988) Acetylcholine receptor alpha-, beta-, gamma-, and delta-subunit mRNA levels are regulated by muscle activity. Neuron 1:329–333.

Goldman E, Road J, Grassino A (1991) Recovery of costal and crural diaphragmatic contractility from partial paralysis. Anesthesiology 75:123–129.

Goodearl AD, Yee AG, Sandrock AWJ, Corfas G, Fischbach GD (1995) ARIA is concentrated in the synaptic basal lamina of the developing chick neuromuscular junction. J Cell Biol 130:1423–1434.

Goold CP, Davis GW (2007) The BMP ligand Gbb gates the expression of synaptic homeostasis independent of synaptic growth control. Neuron 56:109–123.

Gordon T, Hegedus J, Tam SL (2004) Adaptive and maladaptive motor axonal sprouting in aging and motoneuron disease. Neurol Res 26:174–185.

Gordon T, Tyreman N, Li S, Putman CT, Hegedus J (2010) Functional over-load saves motor units in the SOD1-G93A transgenic mouse model of amyotrophic lateral sclerosis. Neurobiol Dis 37:412–422.

Gould TW, Buss RR, Vinsant S, Prevette D, Sun W, Knudson CM, Milligan CE, Oppenheim RW (2006) Complete Dissociation of Motor Neuron Death from Motor Dysfunction by Bax Deletion in a Mouse Model of ALS. J Neurosci 26:8774–8786.

Graber TG, Fandrey KR (2019) Novel individualized power training protocol preserves physical function in adult and older mice. GeroScience.

Grady RM, Merlie JP, Sanes JR (1997) Subtle neuromuscular defects in utrophin-deficient mice. J Cell Biol 136:871–882.

Gurney ME et al. (1994) Motor Neuron Degeneration in Mice That Express a Human Cu , Zn Superoxide Dismutase Mutation. Science (80-) 264:1772–1775.

Han SM, Baig HS, Hammarlund M (2016) Mitochondria Localize to Injured Axons to Support Regeneration. Neuron 92:1308–1323.

Harandi VM, Lindquist S, Kolan SS, Brannstrom T, Liu J-X (2014) Analysis of neurotrophic factors in limb and extraocular muscles of mouse model of amyotrophic lateral sclerosis. PLoS One 9:e109833.

Hegedus J, Putman CT, Gordon T (2007) Time course of preferential motor unit loss in the SOD1G93Amouse model of amyotrophic lateral sclerosis. Neurobiol Dis 28:154–164.

Hegedus J, Putman CT, Tyreman N, Gordon T (2008) Preferential motor unit loss in the SOD1 G93A transgenic mouse model of amyotrophic lateral sclerosis. J Physiol 586:3337–3351.

Heiman-Patterson TD, Sher RB, Blankenhorn EA, Alexander G, Deitch JS, Kunst CB, Cox G (2011) Effect of genetic background on phenotype variability in transgenic mouse models of amyotrophic lateral sclerosis : A window of opportunity in the search for genetic modifiers. Amyotroph Lateral Scler 12:79–86.

Held A, Major P, Sahin A, Reenan RA, Lipscombe D, Wharton KA (2019) Circuit Dysfunction in SOD1 - ALS Model First Detected in Sensory Feedback Prior to Motor Neuron Degeneration Is Alleviated by BMP Signaling. J Neurosci 39:2347–2364.

Henneman E (1957) Relation between size of neurons and their susceptibility to discharge. Science (80-) 126:1345–1347.

Henneman E, Somjen G, Carpenter D (1965a) Functional significance of cell size in spinal motoneurons. J Neurophysiol 28:560–580.

Henneman E, Somjen G, Carpenter DO (1965b) Excitability and inhibitability of motoneurons of different sizes. J Neurophysiol 28:599–620.

Hines HM, Wehrmacher WH, Thomson JD (1945) Functional changes in nerve and muscle after partial denervation. Am J Physiol 145:48–53.

Hoffman H (1950) Local re-innervation in partially denervated muscle; a histophysiological study. Aust J Exp Biol Med Sci 28:383–397.

Horton WA, Eldridge R, Brody JA (1976) Familial motor neuron disease. Evidence for at least three different types. Neurology 26:460–465.

Jimenez CR, Stam FJ, Li KW, Gouwenberg Y, Hornshaw MP, De Winter F, Verhaagen J, Smit AB (2005) Proteomics of the injured rat sciatic nerve reveals protein expression dynamics during regeneration. Mol Cell Proteomics 4:120–132.

Jo SA, Burden SJ (1992) Synaptic basal lamina contains a signal for synapse-specific transcription. Development 115:673–680.

Jones KE, Berry TR, Merali AS, Dal Bello-Haas V (2019) Intentions of Canadian health professionals towards recommending exercise for people living with ALS. BMC Neurol 19.

Kamakura K, Ishiura S, Sugita H, Toyokura Y (1983) Identification of Ca2+-activated neutral protease in the peripheral nerve and its effects on neurofilament degeneration. J Neurochem 40:908–913.

Kang H, Tian L, Mikesh M, Lichtman JW, Thompson WJ (2014) Terminal Schwann cells participate in neuromuscular synapse remodeling during reinnervation following nerve injury. J Neurosci 34:6323–6333.

Katz B (1966) Nerve, Muscle and Synapse. New York, NY: McGraw-Hill.

Kelly CE, Thymiakou E, Dixon JE, Tanaka S, Godwin J, Episkopou V (2013) Rnf165 / Ark2C Enhances BMP-Smad Signaling to Mediate Motor Axon Extension. 11.

Kernell D (2006) The Motoneurone and its Muscle Fibres. New York, NY: Oxford University Press Inc.

Kiryu-Seo S, Tamada H, Kato Y, Yasuda K, Ishihara N, Nomura M, Mihara K, Kiyama H (2016) Mitochondrial fission is an acute and adaptive response in injured motor neurons. Sci Rep 6:28331.

Kishi M, Kummer TT, Eglen SJ, Sanes JR (2003) LL5β : a regulator of postsynaptic differentiation identified in a screen for synaptically enriched transcripts at the neuromuscular junction. J Cell Biol 169:355–366.

Kostic V, Jackson-Lewis V, de Bilbao F, Dubois-Dauphin M, Przedborski S (1997) Bcl-2: prolonging life in a transgenic mouse model of familial amyotrophic lateral sclerosis. Science 277:559–562.

Krejci E, Thomine S, Boschetti N, Legay C, Sketelj J, Massoulie J (1997) The mammalian gene of acetylcholinesterase-associated collagen. J Biol Chem 272:22840–22847.

Lee CW, Han J, Bamburg JR, Han L, Lynn R, Zheng JQ (2010) Regulation of Acetylcholine Receptor Clustering by ADF/Cofilin-Directed Vesicular Trafficking. Nat Neurosci 12:848–856.

Lee Y Il, Thompson WJ, Harlow ML (2017) Schwann cells participate in synapse elimination at the developing neuromuscular junction. Curr Opin Neurobiol 47:176–181.

Lee S-H, Kim Y-J, Choi S-Y (2016) BMP signaling modulates the probability of neurotransmitter release and readily releasable pools in Drosophila neuromuscular junction synapses. Biochem Biophys Res Commun 479:440–446.

Leu M, Bellmunt E, Schwander M, Fariñas I, Brenner HR, Müller U (2003) Erbb2 regulates neuromuscular synapse formation and is essential for muscle spindle development. Development 130:2291–2301.

Lichtman JW, Magrassi L, Purves D (1987) Visualization of neuromuscular junctions over periods of several months in living mice. J Neurosci 7:1215–1222.

Liu F, Ventura F, Doody J, Massagué J (1995) Human type II receptor for bone morphogenic proteins (BMPs): extension of the two-kinase receptor model to the BMPs. Mol Cell Biol 15:3479–3486.

Liu W, Selever J, Wang D, Lu M-F, Moses KA, Schwartz RJ, Martin JF (2004) Bmp4 signaling is required for outflow-tract septation and branchial-arch artery remodeling. Proc Natl Acad Sci U S A 101:4489–4494.

Liz MA, Mar FM, Santos TE, Pimentel HI, Marques AM, Morgado MM, Vieira S, Sousa VF, Pemble H, Wittmann T, Sutherland C, Woodgett JR, Sousa MM (2014) Neuronal deletion of GSK3beta increases microtubule speed in the growth cone and enhances axon regeneration via CRMP-2 and independently of MAP1B and CLASP2. BMC Biol 12:47.

Loeb JA, Fischbach GD (1995) ARIA can be released from extracellular matrix through cleavage of a heparin-binding domain. J Cell Biol 130:127–135.

Lomo T, Westgaard RH (1975) Further studies on the control of ACh sensitivity by muscle activity in the rat. J Physiol 252:603–626.

Lorenz C, Jones KE (2014) IH activity is increased in populations of slow versus fast motor axons of the rat. Front Hum Neurosci 8.

Lunn ER, Brown MC, Perry VH (1990) The pattern of axonal degeneration in the peripheral nervous system varies with different types of lesion. Neuroscience 35:157–165.

Ma CHE, Brenner GJ, Omura T, Samad OA, Costigan M, Inquimbert P, Niederkofler V, Salie R, Sun CC, Lin HY, Arber S, Coppola G, Woolf CJ, Samad TA (2011) The BMP coreceptor RGMb promotes while the endogenous BMP antagonist noggin reduces neurite outgrowth and peripheral nerve regeneration by modulating BMP signaling. J Neurosci 31:18391–18400.

Madisen L, Zwingman TA, Sunkin SM, Oh SW, Zariwala HA, Gu H, Ng LL, Palmiter RD, Hawrylycz MJ, Jones AR, Lein ES, Zeng H (2010) A robust and high-throughput Cre reporting and characterization system for the whole mouse brain. Nat Neurosci 13:133–140.

Malik MN, Fenko MD, Iqbal K, Wisniewski HM (1983) Purification and characterization of two forms of Ca2+-activated neutral protease from calf brain. J Biol Chem 258:8955–8962.

Marqués G, Bao H, Haerry TE, Shimell MJ, Duchek P, Zhang B, O'Connor MB (2002) The Drosophila BMP Type II Receptor Wishful Thinking Regulates Neuromuscular Synapse Morphology and Function. Neuron 33:529–543.

Martineau É, Di Polo A, Vande Velde C, Robitaille R (2018) Dynamic neuromuscular remodeling precedes motor-unit loss in a mouse model of ALS. Elife 7.

Martinez-Muriana A, Mancuso R, Francos-Quijorna I, Olmos-Alonso A, Osta R, Perry VH, Navarro X, Gomez-Nicola D, Lopez-Vales R (2016) CSF1R blockade slows the progression of amyotrophic lateral sclerosis by reducing microgliosis and invasion of macrophages into peripheral nerves. Sci Rep 6:25663.

Mason MRJ, Lieberman AR, Grenningloh G, Anderson PN (2002) Transcriptional upregulation of SCG10 and CAP-23 is correlated with regeneration of the axons of peripheral and central neurons in vivo. Mol Cell Neurosci 20:595–615.

Massenzio F, Pena-Altamira E, Petralla S, Virgili M, Zuccheri G, Miti A, Polazzi E, Mengoni I, Piffaretti D, Monti B (2018) Microglial overexpression of fALS-linked mutant SOD1 induces SOD1 processing impairment, activation and neurotoxicity and is counteracted by the autophagy inducer trehalose. Biochim Biophys acta Mol basis Dis 1864:3771–3785.

McCabe BD, Hom S, Aberle H, Fetter RD, Marques G, Haerry TE, Wan H, O'Connor MB, Goodman CS, Haghighi AP (2004) Highwire regulates presynaptic BMP signaling essential for synaptic growth. Neuron 41:891–905.

McCabe BD, Marqués G, Haghighi AP, Fetter RD, Crotty ML, Haerry TE, Goodman CS, O'Connor MB (2003) The BMP Homolog Gbb Provides a Retrograde Signal that Regulates Synaptic Growth at the Drosophila Neuromuscular Junction. Neuron 39:241–254.

McCann CM, Nguyen QT, Santo Neto H, Lichtman JW (2007) Rapid synapse elimination after postsynaptic protein synthesis inhibition in vivo. J Neurosci 27:6064–6067.

McComas AJ, Quartly C, Griggs RC (1997) Early and late losses of motor units after poliomyelitis. Brain 120:1415–1421.

McComas AJ, Sica RE, Campbell MJ, Upton AR (1971) Functional compensation in partially denervated muscles. J Neurol Neurosurg Psychiatry 34:453–460.

McMahan UJ (1990) The agrin hypothesis. Cold Spring Harb Symp Quant Biol 55:407–418.

Meyer K, Ferraiuolo L, Miranda CJ, Likhite S, McElroy S, Renusch S, Ditsworth D, Lagier-Tourenne C, Smith RA, Ravits J, Burghes AH, Shaw PJ, Cleveland DW, Kolb SJ, Kaspar BK (2014) Direct conversion of patient fibroblasts demonstrates non-cell autonomous toxicity of astrocytes to motor neurons in familial and sporadic ALS. Proc Natl Acad Sci U S A 111:829–832.

Miles GB, Yohn DC, Wichterle H, Jessell TM, Rafuse VF, Brownstone RM (2004) Functional Properties of Motoneurons Derived from Mouse Embryonic Stem Cells. J Neurosci 24:7848–7858.

Miyazono K, Maeda S, Imamura T (2005) BMP receptor signaling: Transcriptional targets, regulation of signals, and signaling cross-talk. Cytokine Growth Factor Rev 16:251–263.

Moloney EB, de Winter F, Verhaagen J (2014) ALS as a distal axonopathy: molecular mechanisms affecting neuromuscular junction stability in the presymptomatic stages of the disease. Front Neurosci 8:252.

Moore DL, Blackmore MG, Hu Y, Kaestner KH, Bixby JL, Lemmon VP, Goldberg JL (2009) NIH Public Access. Science (80-) 326:298–301.

Mora JS et al. (2019) Masitinib as an add-on therapy to riluzole in patients with amyotrophic lateral sclerosis : a randomized clinical trial. Amyotroph Lateral Scler Front Degener 0:1–10.

Morii H, Shiraishi-Yamaguchi Y, Mori N (2006) SCG10, a microtubule destabilizing factor, stimulates the neurite outgrowth by modulating microtubule dynamics in rat hippocampal primary cultured neurons. J Neurobiol 66:1101–1114.

Morris DD (1953) Recovery in partly paralysed muscles. J Bone Joint Surg Br 35-B:650–660.

Nagai M, Re DB, Nagata T, Chalazonitis A, Jessell TM, Wichterle H, Przedborski S (2007) Astrocytes expressing ALS-linked mutated SOD1 release factors selectively toxic to motor neurons. Nat Neurosci 10:615–622.

Nair KS (2005) Aging muscle. Am J Clin Nutr 81:953–963.

Namba T, Scheller RH (1996) Inhibition of agrin-mediated acetylcholine receptor clustering by utrophin C-terminal peptides. Genes Cells 1:755–764.

Nardo G, Trolese MC, Vito G De, Cecchi R, Riva N, Dina G, Heath PR, Quattrini A, Shaw PJ, Piazza V, Bendotti C (2016) Immune response in peripheral axons delays disease progression in SOD1 G93A mice. J Neuroinflammation 13.

Noakes PG, Gautam M, Mudd J, Sanes JR, Merlie JP (1995) Aberrant differentiation of neuromuscular junctions in mice lacking s-laminin/laminin beta 2. Nature 374:258–262.

Nohe A, Keating E, Knaus P, Petersen NO (2004) Signal transduction of bone morphogenetic protein receptors. Cell Signal 16:291–299.

Nystrom B (1968) Histochemical studies of end-plate bound esterases in “slow-red” and “fast-white” cat muscles during postnatal development. Acta Neurol Scand 44:295–317.

O’Malley JP, Waran MT, Balice-Gordon RJ (1999) In vivo observations of terminal Schwann cells at normal, denervated, and reinnervated mouse neuromuscular junctions. J Neurobiol 38:270–286.

Ogata T (1988) Structure of motor endplates in the different fiber types of vertebrate skeletal muscles. Arch Histol Cytol 51:385–424.

Ono Y, Calhabeu F, Morgan JE, Katagiri T, Amthor H, Zammit PS (2011) BMP signalling permits population expansion by preventing premature myogenic differentiation in muscle satellite cells. Cell Death Differ 18:222–234.

Osses N, Henrí-quez JP (2015) Bone morphogenetic protein signaling in vertebrate motor neurons and neuromuscular communication. Front Cell Neurosci 8:1–10.

Ostberg AJ, Vrbova G, O’Brien RA (1986) Reinnervation of fast and slow mammalian muscles by a superfluous number of motor axons. Neuroscience 18:205–213.

Osterloh JM et al. (2012) dSarm/Sarm1 is required for activation of an injury-induced axon death pathway. Science 337:481–484.

Pachter BR, Spielholz NI (1990) Tenotomy-induced motor endplate alterations in rat soleus muscle. Anat Rec 228:104–108.

Parikh P, Hao Y, Hosseinkhani M, Patil SB, Huntley GW, Tessier-Lavigne M, Zou H (2011) Regeneration of axons in injured spinal cord by activation of bone morphogenetic protein/Smad1 signaling pathway in adult neurons. Proc Natl Acad Sci 108:E99–E107.

Park KK, Liu K, Hu Y, Smith PD, Wang C, Cai B, Xu B, Connolly L, Kramvis I, Sahin M, He Z (2009) Promoting Axon Regeneration in the Adult CNS by Modulation of the PTEN/mTOR Pathway. Science (80-) 322:963–966.

Patton BL, Chiu AY, Sanes JR (1998) Synaptic laminin prevents glial entry into the synaptic cleft. Nature 393:698–701.

Peters MF, Sadoulet-Puccio HM, Grady MR, Kramarcy NR, Kunkel LM, Sanes JR, Sealock R, Froehner SC (1998) Differential membrane localization and intermolecular associations of alpha-dystrobrevin isoforms in skeletal muscle. J Cell Biol 142:1269–1278.

Pette D, Staron RS (2000) Myosin Isoforms , Muscle Fiber Types , and Transitions. Microsc Res Tech 50:500–509.

Pinelli P, Pisano F, Ceriani F, Miscio G (1991) EMG evaluation of motor neuron sprouting in amyotrophic lateral sclerosis. Ital J Neurol Sci 12:359–367.

Politano SF, Salemme RR, Ashley J, López-Rivera JA, Bakula TA, Puhalla KA, Quinn JP, Juszczak MJ, Phillip LK, Carrillo RA, Vanderzalm PJ (2019) Tao Negatively Regulates BMP Signaling During Neuromuscular Junction Development in Drosophila. Dev Neurobiol 79:335–349.

Pun S, Santos AF, Saxena S, Xu L, Caroni P (2006) Selective vulnerability and pruning of phasic motoneuron axons in motoneuron disease alleviated by CNTF. Nat Neurosci 9:408–419.

Rafuse VF, Gordon T, Orozco R (1992) Proportional enlargement of motor units after partial denervation of cat triceps surae muscles. J Neurophysiol 68:1261–1276.

Rao P, Monks DA (2009) A tetracycline-inducible and skeletal muscle-specific Cre recombinase transgenic mouse. Dev Neurobiol 69:401–406.

Reaume AG, Elliott JL, Hoffman EK, Kowall NW, Ferrante RJ, Siwek DF, Wilcox HM, Flood DG, Beal MF, Brown RHJ, Scott RW, Snider WD (1996) Motor neurons in Cu/Zn superoxide dismutase-deficient mice develop normally but exhibit enhanced cell death after axonal injury. Nat Genet 13:43–47.

Reddy L V, Koirala S, Sugiura Y, Herrera AA, Ko C (2003) Glial Cells Maintain Synaptic Structure and Function and Promote Development of the Neuromuscular Junction In Vivo. Neuron 40:563–580.

Redfern P, Lundh H, Thesleff S (1970) Tetrodotoxin resistant action potentials in denervated rat skeletal muscle. Eur J Pharmacol 11:263–265.

Redfern PA (1970) Neuromuscular transmission in new-born rats. J Physiol 209:701–709.

Reist NE, Smith SJ (1992) Neurally evoked calcium transients in terminal Schwann cells at the neuromuscular junction. Proc Natl Acad Sci U S A 89:7625–7629.

Reist NE, Werle MJ, McMahan UJ (1992) Agrin released by motor neurons induces the aggregation of acetylcholine receptors at neuromuscular junctions. Neuron 8:865–868.

Renton AE et al. (2011) A hexanucleotide repeat expansion in C9ORF72 is the cause of chromosome 9p21-linked ALS-FTD. Neuron 72:257–268.

Reynolds ML, Woolf CJ (1992) Terminal Schwann cells elaborate extensive processes following denervation of the motor endplate. J Neurocytol 21:50–66.

Ribas VT, Koch JC, Michel U, Bahr M, Lingor P (2017) Attenuation of Axonal Degeneration by Calcium Channel Inhibitors Improves Retinal Ganglion Cell Survival and Regeneration After Optic Nerve Crush. Mol Neurobiol 54:72–86.

Rich M, Lichtman JW (1989a) Motor nerve terminal loss from degenerating muscle fibers. Neuron 3:677–688.

Rich MM, Lichtman JW (1989b) In vivo visualization of pre- and postsynaptic changes during synapse elimination in reinnervated mouse muscle. J Neurosci 9:1781–1805.

Richardson PM, Verge VM (1987) Axonal regeneration in dorsal spinal roots is accelerated by peripheral axonal transection. Brain Res 411:406–408.

Riederer BM, Pellier V, Antonsson B, Di Paolo G, Stimpson SA, Lutjens R, Catsicas S, Grenningloh G (1997) Regulation of microtubule dynamics by the neuronal growth-associated protein SCG10. Proc Natl Acad Sci U S A 94:741–745.

Riethmacher D, Sonnenberg-Riethmacher E, Brinkmann V, Yamaai T, Lewin GR, Birchmeier C (1997) Severe neuropathies in mice with targeted mutations in the ErbB3 receptor. Nature 389:725–730.

Roberts-Lewis JM, Savage MJ, Marcy VR, Pinsker LR, Siman R (1994) Immunolocalization of calpain I-mediated spectrin degradation to vulnerable neurons in the ischemic gerbil brain. J Neurosci 14:3934–3944.

Robitaille R (1998) Modulation of Synaptic Efficacy and Synaptic Depression by Glial Cells at the Frog Neuromuscular Junction. Neuron 21:847–855.

Robitaille R, Garcia ML, Kaczorowski GJ, Charlton MP (1993) Functional colocalization of calcium and calcium-gated potassium channels in control of transmitter release. Neuron 11:645–655.

Rochon D, Rousse I, Robitaille R (2001) Synapse – Glia Interactions at the Mammalian Neuromuscular Junction. J Neurosci 21:3819–3829.

Ronchi G, Nicolino S, Raimondo S, Tos P, Battiston B, Papalia I, Varejão ASP, Giacobini-Robecchi MG, Perroteau I, Geuna S (2009) Functional and morphological assessment of a standardized crush injury of the rat median nerve. J Neurosci Methods 179:51–57.

Rosen DR, Siddique T, Patterson D, Figlewicz DA, Sapp P, Hentati A, Donaldson D, Goto J, O'Regan JP, Deng HX (1993) Mutations in Cu/Zn superoxide dismutase gene are associated with familial amyotrophic lateral sclerosis. Nature 362:59–62.

Rosenheimer JL, Smith DO (1985) Differential changes in the end-plate architecture of functionally diverse muscles during aging. J Neurophysiol 53:1567–1581.

Rosenthal JL, Taraskevich PS (1977) Reduction of multiaxonal innervation at the neuromuscular junction of the rat during development. J Physiol 270:299–310.

Rossignol S, Dubuc R, Gossard J-P (2006) Dynamic sensorimotor interactions in locomotion. Physiol Rev 86:89–154.

Rousse I, St.-Amour A, Darabid H, Robitaille R (2010) Synapse-glia interactions are governed by synaptic and intrinsic glial properties. Neuroscience 167:621–632.

Şahin A, Held A, Bredvik K, Major P, Achilli T-M, Kerson AG, Wharton K, Stilwell G, Reenan R (2017) Human SOD1 ALS Mutations in a Drosophila Knock-In Model Cause Severe Phenotypes and Reveal Dosage-Sensitive Gain- and Loss-of-Function Components. Genetics 205:707–723.

Sakaguchi S, Shono J, Suzuki T, Sawano S, Anderson JE, Do MQ, Ohtsubo H, Mizunoya W, Sato Y, Nakamura M, Furuse M, Yamada K, Ikeuchi Y, Tatsumi R (2014) Implication of anti-inflammatory macrophages in regenerative moto-neuritogenesis : Promotion of myoblast migration and neural chemorepellent semaphorin 3A expression in injured muscle. Int J Biochem Cell Biol 54:272–285.

Salpeter MM, Loring RH (1985) Nicotinic acetylcholine receptors in vertebrate muscle: properties, distribution and neural control. Prog Neurobiol 25:297–325.

Sandrock AWJ, Dryer SE, Rosen KM, Gozani SN, Kramer R, Theill LE, Fischbach GD (1997) Maintenance of acetylcholine receptor number by neuregulins at the neuromuscular junction in vivo. Science 276:599–603.

Sanes JR, Lichtman JW (1999) Development of the vertebrate neuromuscular junction. Annu Rev Neurosci 22:389–442.

Sanes JR, Lichtman JW (2001) Induction, assembly, maturation and maintenance of a postsynaptic apparatus. Nat Rev Neurosci 2:791–805.

Saris CGJ, Groen EJN, van Vught PWJ, van Es MA, Blauw HM, Veldink JH, van den Berg LH (2013) Gene expression profile of SOD1-G93A mouse spinal cord, blood and muscle. Amyotroph Lateral Scler Frontotemporal Degener 14:190–198.

Sartori R, Schirwis E, Blaauw B, Bortolanza S, Zhao J, Enzo E, Stantzou A, Mouisel E, Toniolo L, Ferry A, Stricker S, Goldberg AL, Dupont S, Piccolo S, Amthor H, Sandri M (2013) BMP signaling controls muscle mass. Nat Genet 45:1309–1318.

Sasaki Y, Milbrandt J (2010) Axonal Degeneration Is Blocked by Nicotinamide Mononucleotide Adenylyltransferase (Nmnat) Protein Transduction into Transected Axons. J Biol Chem 285:41211–41215.

Schaefer AM, Sanes JR, Lichtman JW (2005) A Compensatory Subpopulation of Motor Neurons in a Mouse Model of Amyotrophic Lateral Sclerosis. J Comp Neurol 490:209–219.

Schafer DP, Jha S, Liu F, Akella T, McCullough LD, Rasband MN (2009) Disruption of the axon initial segment cytoskeleton is a new mechanism for neuronal injury. J Neurosci 29:13242–13254.

Schlaepfer WW, Zimmerman UJ (1985) Calcium-activated proteolysis of intermediate filaments. Ann N Y Acad Sci 455:552–562.

Scott LJ, Bacou F, Sanes JR (1988) A synapse-specific carbohydrate at the neuromuscular junction: association with both acetylcholinesterase and a glycolipid. J Neurosci 8:932–944.

Sealock R, Wray BE, Froehner SC (1984) Ultrastructural localization of the Mr 43,000 protein and the acetylcholine receptor in Torpedo postsynaptic membranes using monoclonal antibodies. J Cell Biol 98:2239–2244.

Senger J-L, Chan KM, Macandili H, Chan AWM, Verge VMK, Jones KE, Webber CA (2019) Conditioning electrical stimulation promotes functional nerve regeneration. Exp Neurol 315:60–71.

Sharp PS, Tyreman N, Jones KE, Gordon T (2018) Crush injury to motor nerves in the G93A transgenic mouse model of amyotrophic lateral sclerosis promotes muscle reinnervation and survival of functionally intact nerve-muscle contacts. Neurobiol Dis 113:33–44.

Shefner JM, Cudkowicz M, Brown RHJ (2006) Motor unit number estimation predicts disease onset and survival in a transgenic mouse model of amyotrophic lateral sclerosis. Muscle Nerve 34:603–607.

Shi Y, Massagué J (2003) Mechanisms of TGF-Signaling from Cell Membrane to the Nucleus have been observed in both TGF-family receptors and the Smad proteins. The TGF-type II receptor is inacti-vated by mutation in most human gastrointestinal can. Cell 113:685–700.

Shijo T, Warita H, Suzuki N, Ikeda K, Mitsuzawa S, Akiyama T, Ono H, Nishiyama A, Izumi R, Kitajima Y, Aoki M (2018) Antagonizing bone morphogenic protein 4 attenuates disease progression in a rat model of amyotrophic lateral sclerosis. Exp Neurol 307:164–179.

Shin JE, Geisler S, DiAntonio A (2014) Dynamic regulation of SCG10 in regenerating axons after injury. Exp Neurol 252:1–11.

Sieber C, Kopf J, Hiepen C, Knaus P (2009) Cytokine & Growth Factor Reviews Recent advances in BMP receptor signaling. Cytokine Growth Factor Rev 20:343–355.

Slater CR (1982) Postnatal maturation of nerve-muscle junctions in hindlimb muscles of the mouse. Dev Biol 94:11–22.

Smith DO, Rosenheimer JL (1982) Decreased sprouting and degeneration of nerve terminals of active muscles in aged rats. J Neurophysiol 48:100–109.

Son Y-J, Thompson WJ (1995a) Nerve Sprouting in Muscle Is Induced and Guided by Processes Extended by Schwann Cells. Neuron 14:133–141.

Son Y-J, Thompson WJ (1995b) Schwann Cell Processes Guide Regeneration of Peripheral Axons. Neuron 14:125–132.

Song S, Miranda CJ, Braun L, Meyer K, Frakes AE, Ferraiuolo L, Likhite S, Bevan AK, Foust KD, McConnell MJ, Walker CM, Kaspar BK (2016) Major histocompatibility complex class I molecules protect motor neurons from astrocyte-induced toxicity in amyotrophic lateral sclerosis. Nat Med 22:397–403.

Spira ME, Oren R, Dormann A, Gitler D (2003) Critical calpain-dependent ultrastructural alterations underlie the transformation of an axonal segment into a growth cone after axotomy of cultured Aplysia neurons. J Comp Neurol 457:293–312.

Statland JM, Barohn RJ, McVey AL, Katz JS, Dimachkie MM (2015) Patterns of Weakness, Classification of Motor Neuron Disease, and Clinical Diagnosis of Sporadic Amyotrophic Lateral Sclerosis. Neurol Clin 33:735–748.

Steinbach JH (1981) Developmental changes in acetylcholine receptor aggregates at rat skeletal neuromuscular junctions. Dev Biol 84:267–276.

Stoll G, Griffin JW, Li CY, Trapp BD (1989) Wallerian degeneration in the peripheral nervous system: participation of both Schwann cells and macrophages in myelin degradation. J Neurocytol 18:671–683.

Stratton JA, Holmes A, Rosin NL, Sinha S, Vohra M, Burma NE, Trang T, Midha R, Biernaskie J (2018) Macrophages Regulate Schwann Cell Maturation after Nerve Injury. Cell Rep 24:2561-2572.e6.

Sugiura Y, Mori N (1995) SCG10 expresses growth-associated manner in developing rat brain, but shows a different pattern to p19/stathmin or GAP-43. Brain Res Dev Brain Res 90:73–91.

Sugiura Y, Woppmann A, Miljanich GP, Ko CP (1995) A novel omega-conopeptide for the presynaptic localization of calcium channels at the mammalian neuromuscular junction. J Neurocytol 24:15–27.

Sulkowski MJ, Han TH, Ott C, Wang Q, Verheyen EM, Lippincott-Schwartz J, Serpe M (2016) A Novel , Noncanonical BMP Pathway Modulates Synapse Maturation at the Drosophila Neuromuscular Junction. PLoS Genet 1.

Sunderland S (1946) Course and rate of regeneration of motor fibers following lesions of the radial nerve. Arch Neurol Psychiatry 56:133–157.

Sunderland S, Ray LJ (1950) Denervation changes in mammalian striated muscle. J Neurol Neurosurg Psychiatry 13:159–177.

Suzuki Y, Nakagomi S, Namikawa K, Kiryu-Seo S, Inagaki N, Kaibuchi K, Aizawa H, Kikuchi K, Kiyama H (2003) Collapsin response mediator protein-2 accelerates axon regeneration of nerve-injured motor neurons of rat. J Neurochem 86:1042–1050.

Tam SL, Archibald V, Jassar B, Tyreman N, Gordon T (2001) Increased Neuromuscular Activity Reduces Sprouting in Partially Denervated Muscles. J Neurosci 21:654–667.

Tam SL, Gordon T (2003) Mechanisms controlling axonal sprouting at the neuromuscular junction. J Neurocytol 32:961–974.

Thonhoff JR, Simpson EP, Appel SH (2018) Neuroinflammatory mechanisms in amyotrophic lateral sclerosis pathogenesis. Curr Opin Neurol 31:635–639.

Todd KJ, Darabid H, Robitaille R (2010) Perisynaptic Glia Discriminate Patterns of Motor Nerve Activity and Influence Plasticity at the Neuromuscular Junction. J Neurosci 30:11870–11882.

Toews AD, Barrett C, Morell P (1998) Monocyte chemoattractant protein 1 is responsible for macrophage recruitment following injury to sciatic nerve. J Neurosci Res 53:260–267.

Torigoe K, Hashimoto K, Lundborg G (1999) A role of migratory Schwann cells in a conditioning effect of peripheral nerve regeneration. Exp Neurol 160:99–108.

Traxinger K, Kelly C, Johnson BA, Lyles RH, Glass JD (2013) Prognosis and epidemiology of amyotrophic lateral sclerosis: Analysis of a clinic population, 1997-2011. Neurol Clin Pract 3:313–320.

Tremblay E, Martineau É, Robitaille R (2017) Opposite Synaptic Alterations at the Neuromuscular Junction in an ALS Mouse Model : When Motor Units Matter. J Neurosci 37:8901–8918.

Trias E, Ibarburu S, Barreto-Núñez R, Babdor J, Maciel TT, Guillo M, Gros L, Dubreuil P, Díaz-Amarilla P, Cassina P, Martínez-Palma L, Moura IC, Beckman JS, Hermine O, Barbeito L (2016) Post-paralysis tyrosine kinase inhibition with masitinib abrogates neuroinflammation and slows disease progression in inherited amyotrophic lateral sclerosis. J Neuroinflammation 13.

Trias E, Ibarburu S, Barreto-Núñez R, Varela V, Moura IC, Dubreuil P, Hermine O, Beckman JS, Barbeito L (2017) Evidence for mast cells contributing to neuromuscular pathology in an inherited model of ALS. JCI Insight 2.

Trias E, King PH, Si Y, Kwon Y, Varela V, Ibarburu S, Kovacs M, Moura IC, Beckman JS, Hermine O, Barbeito L (2018) Mast cells and neutrophils mediate peripheral motor pathway degeneration in ALS Graphical abstract Find the latest version : Mast cells and neutrophils mediate peripheral motor pathway degeneration in ALS. JCI Insight 3.

Van Dyke JM, Smit-Oistad IM, Macrander C, Krakora D, Meyer MG, Suzuki M (2016) Macrophage-mediated inflammation and glial response in the skeletal muscle of a rat model of familial amyotrophic lateral sclerosis (ALS). Exp Neurol 277:275–282.

Van Harreveld A (1945) Re-innervation of denervated muscle fibers by adjacent functioning motor units. Am J Physiol 144:477–493.

Van Harreveld A (1952) Re-innervation of paretic muscle by collateral branching of the residual motor innervation. J Comp Neurol 97:385–407.

Verma P, Chierzi S, Codd AM, Campbell DS, Meyer RL, Holt CE, Fawcett JW (2005) Axonal protein synthesis and degradation are necessary for efficient growth cone regeneration. J Neurosci 25:331–342.

Vilalta A, Brown GC (2018) Neurophagy, the phagocytosis of live neurons and synapses by glia, contributes to brain development and disease. FEBS J 285:3566–3575.

Vrbova G, Mehra N, Shanmuganathan H, Tyreman N, Schachner M, Gordon T (2009) Chemical communication between regenerating motor axons and Schwann cells in the growth pathway. Eur J Neurosci 30:366–375.

Wakatsuki S, Saitoh F, Araki T (2011) ZNRF1 promotes Wallerian degeneration by degrading AKT to induce GSK3B-dependent CRMP2 phosphorylation. Nat Cell Biol 13:1415–1423.

Waller A (1851) Experiments on the Section of the Glossopharyngeal and Hypoglossal Nerves of the Frog, and observations of the alterations produced thereby in the Structure of their Primitive Fibres. Edinburgh Med Surg J 76:369–376.

Wang HA, Lee JD, Lee KM, Woodruff TM, Noakes PG (2017) Complement C5a-C5aR1 signalling drives skeletal muscle macrophage recruitment in the hSOD1(G93A) mouse model of amyotrophic lateral sclerosis. Skelet Muscle 7:10.

Wang J, Farr GW, Hall DH, Li F, Furtak K, Dreier L, Horwich AL (2009) An ALS-linked mutant SOD1 produces a locomotor defect associated with aggregation and synaptic dysfunction when expressed in neurons of Caenorhabditis elegans. PLoS Genet 5:e1000350.

Weiss P, Edds MVJ (1946) Spontaneous Recovery of Muscle Following Partial Denervation. Am J Physiol 145:587–607.

Werle MJ, Herrera AA (1991) Elevated levels of polyneuronal innervation persist for as long as two years in reinnervated frog neuromuscular junctions. J Neurobiol 22:97–103.

Wichterle H, Lieberam I, Porter JA, Jessell TM (2002) Directed Differentiation of Embryonic Stem Cells into Motor Neurons. Cell 110:385–397.

Wigston DJ (1990) Repeated in vivo visualization of neuromuscular junctions in adult mouse lateral gastrocnemius. J Neurosci 10:1753–1761.

Willadt S, Nash M, Slater C (2018) Age-related changes in the structure and function of mammalian neuromuscular junctions. Ann N Y Acad Sci 1412:41–53.

Williams PR, Marincu B-N, Sorbara CD, Mahler CF, Schumacher A-M, Griesbeck O, Kerschensteiner M, Misgeld T (2014) A recoverable state of axon injury persists for hours after spinal cord contusion in vivo. Nat Commun 5:5683.

Winbanks CE, Chen JL, Qian H, Liu Y, Bernardo BC, Beyer C, Watt KI, Thomson RE, Connor T, Turner BJ, McMullen JR, Larsson L, McGee SL, Harrison CA, Gregorevic P (2013) The bone morphogenic protein axis is a positive regulator of skeletal muscle mass. J Cell Biol 203:345–357.

Wohlfart G (1957) Collateral Regeneration from Residual Motor Nerve Fibers in Amyotrophic Lateral Sclerosis. Neurology 7:124 LP – 124.

Wohlfart G, Hoffman H (1956) Reinnervation of muscle fibers in partially denervated muscle in Theiler's encephalo-myelitis of mice (mouse poliomyelitis). Acta Psychiatr Scand 31:345–365.

Wong PC, Pardo CA, Borchelt DR, Lee MK, Copeland NG, Jenkins NA, Sisodia SS, Cleveland DW, Price DL (1995) An adverse property of a familial ALS-linked SOD1 mutation causes motor neuron disease characterized by vacuolar degeneration of mitochondria. Neuron 14:1105–1116.

Wood SJ, Slater CR (1998) beta-Spectrin is colocalized with both voltage-gated sodium channels and ankyrinG at the adult rat neuromuscular junction. J Cell Biol 140:675–684.

Wu H, Xiong WC, Mei L (2010) To build a synapse: signaling pathways in neuromuscular junction assembly. Development 137:1017–1033.

Xiao Q, Zhao W, Beers DR, Yen AA, Xie W, Henkel JS, Appel SH (2007) Mutant SOD1(G93A) microglia are more neurotoxic relative to wild-type microglia. J Neurochem 102:2008–2019.

Xiong F, Tentner AR, Huang P, Gelas A, Mosaliganti KR, Souhait L, Rannou N, Swinburne I a, Obholzer ND, Cowgill PD, Schier AF, Megason SG (2013) Specified neural progenitors sort to form sharp domains after noisy Shh signaling. Cell 153:550–561.

Xu C, Tabebordbar M, Iovino S, Ciarlo C, Liu J (2013) A Zebrafish Embryo Culture System Defines Factors that Promote Vertebrate Myogenesis across Species. Cell 155:909–921.

Xu R, Salpeter MM (1997) Acetylcholine receptors in innervated muscles of dystrophic mdx mice degrade as after denervation. J Neurosci 17:8194–8200.

Yamashita H, Ten Dijke P, Franzén P, Miyazono K, Heldin CH (1994) Formation of hetero-oligomeric complexes of type I and type II receptors for transforming growth factor-β. J Biol Chem 269:20172–20178.

Yoshida H, Murachi T, Tsukahara I (1984) Degradation of actin and vimentin by calpain II, a Ca2+-dependent cysteine proteinase, in bovine lens. FEBS Lett 170:259–262.

Zengel JE, Reid SA, Sypert GW, Munson JB (1985) Membrane electrical properties and prediction of motor-unit type of medial gastrocnemius motoneurons in the cat. J Neurophysiol 53:1323–1344.

Zhang M, McLennan IS (1995) During secondary myotube formation, primary myotubes preferentially absorb new nuclei at their ends. Dev Dyn 204:168–177.

Zhang X, Rui M, Gan G, Huang C, Yi J, Lv H, Xie W (2017) Neuroligin 4 regulates synaptic growth via the bone morphogenetic protein (BMP) signaling pathway at the Drosophila neuromuscular junction. J Biol Chem 292:17991–18005.

Zhong J, Zou H (2014) BMP signaling in axon regeneration. Curr Opin Neurobiol 27:127–134.

Zhou B, Yu P, Lin M-Y, Sun T, Chen Y, Sheng Z-H (2016) Facilitation of axon regeneration by enhancing mitochondrial transport and rescuing energy deficits. J Cell Biol 214:103–119.

Zochodne DW (2000) The microenvironment of injured and regenerating peripheral nerves. Muscle Nerve Suppl 9:S33-8.

Zou H, Ho C, Wong K, Tessier-Lavigne M (2009) Axotomy-induced Smad1 Activation Promotes Axonal Growth in Adult Sensory Neurons. J Neurosci 29:7116–7123.

APPENDIX A: GENERATION OF AN EMBRYONIC STEM CELL DERIVED MUSCLE PROTOCOL IN VITRO

Introduction

ALS is a devastating, progressive neuromuscular disease characterized by distal neuropathy resulting in NMJ denervation prior to MN death (Hegedus et al., 2007). There is a stereotypical pattern of NMJ denervation and MN death such that type IIb, or fast-fatigable muscle fibres become denervated first, leaving the slow, or type I muscle fibres the most resilient to disease progression (Frey et al., 2000; Hegedus et al., 2007).

The understanding that ALS disease progression is motor unit-dependent also suggests that MN and/or muscle activity have roles in NMJ instability, considering different motor units have relative differences in activity. To fully understand how MN activity vs muscle activity independently contribute to NMJ stability in ALS, we need a model system where both MN and muscle activity can be controlled independently of one another. Tissue culture poses the most promising method to obtain this level of control, considering specific MN/muscle activity in a freely behaving mouse cannot be fully controlled. Additionally, a reliable co-culture system would allow for large-scale early drug screening experiments that are not feasible *in vivo.* In our lab, the current *in vitro* model system for studying MN-muscle interaction utilizes mouse embryonic stem (ES) cell-derived MNs (ESCMNs) harboring a variety of mutations and fluorescent reporters, cultured on a substrate of myotubes obtained from chick embryos. Though this system is highly reproducible and results in the development of functioning synapses (Miles et al., 2004; Chipman et al., 2014b), it is limited considering the muscle activity cannot be directly controlled, the genotype of the muscle cannot be altered, and the culture system utilizes tissue from two different donor organisms.

The discovery of optogenetic technology has allowed for researchers to control the activity of excitable cell types using transgenic expression of light-activated ion channels, such as channelrhodopsin (ChR2) (Deisseroth, 2011). In this laboratory, we currently use ESCMNs that express ChR2, a light-sensitive ion channel that opens in response to stimulation with 488 nm light, leading to depolarization of the MN membrane. These cells are currently being used to determine how MN function and activity change over time in healthy cells versus ones harbouring the ALS-causing

$SOD1^{G93A}$ mutation. As another excitable cell type, muscle fibres also have the potential to be controlled with optogenetic technology to manipulate their activity *in vitro.* However, to exploit optogenetic technology in muscle cultures, we needed to develop a method to induce muscle fibre differentiation in our ChR2-expressing ES cells.

A study by Xu et al. in 2013 outlined an ES cell muscle differentiation protocol utilizing zebrafish and human induced pluripotent stem cells (iPSCs). In this study, they tested the impact of 2,400 different chemicals on myogenesis in a zebrafish embryo culture system. Of the compounds tested, they ultimately identified that a combination of bFGF, Forskolin, and a GSK3β inhibitor (BIO) was effective at inducing the differentiation of mature muscle fibres from human iPSCs (Xu et al., 2013). However, this protocol has never been attempted in a mouse model using embryonic stem cells.

To separate the concept of MN versus muscle activity in ALS, we therefore needed to develop a muscle culture system that can be a) of mouse origin, b) genetically manipulatable, and c) activity controlled. In this study, we therefore sought to develop an ES cell-derived muscle culture system by adapting the protocol previously described (Xu et al., 2013). In this way, we would be able to generate mouse muscle that expresses ChR2 and/or the $SOD1^{G93A}$ mutation for use with mouse ESCMNs. This would give us a single-organism culture system where the MN and muscle activity can be independently controlled.

Methods

Preparation of embryoid bodies from embryonic stem cells

This study utilized two different ES cell lines: JCS051 (a kind gift from Gregory L. Cox, The Jackson Laboratory, Bar Harbor, Maine), hereafter referred to as WT; and Ai32H1 (generated in-house), which harbour the skeletal muscle-specific HSA promoter to induce the expression of ChR2-GFP in mature skeletal muscle. ES cells were grown and passaged on feeder layers of primary mouse embryonic fibroblasts as previously described (Wichterle et al., 2002; Miles et al., 2004). ES cells were resuspended and cultured in suspension at 37 °C for two days in ADFNK medium (125 ml Neurobasal media, Invitrogen; 125 ml Advanced DMEM/F12, Invitrogen; 2.85 ml 2-

mercaptoethanol, Embryomax; 2.85 ml Glutamax, Invitrogen; and 28.5 ml Knockout Serum Replacement, Invitrogen) to form embryoid bodies.

Modified muscle differentiation protocol

Following these initial two days in suspension, EBs were transferred to suspension culture dishes containing STEMDiff Apelmedium (Stem Cell Technologies) containing the following: 0.5 μM GSK3β inhibitor (Stem Cell Technologies); 20 μM Forskolin (Stem Cell Technologies); and 10 ng/mL bFGF (Stem Cell Technologies) for five additional days. Treated EBs were then plated on Matrigel (Corning)-coated thermanox coverslips in culture wells containing STEMDiff media and the three factors, as above. Several EBs (~3-4) were plated per well to establish a relatively even distribution across the cover slip. EBs were then incubated, undisturbed, for two to three days to allow for adhesion. Finally, the STEMDiff media was aspirated, and the media was replaced with DMEM containing 2% horse serum (culture day 0). Cultures could then be maintained for several weeks.

Immunofluorescence and imaging

Cultures were fixed for 15 minutes with 37% formaldehyde diluted 1:10 in 1XPBS after 24 hours of incubation in DMEM, and then every subsequent 3 days until 22 days *in vitro* (DIV). Fixed cultures were gently rinsed 3x10 minutes in 1XPBS and then incubated in cocktails of primary antibodies (mouse anti S58 IgA, Developmental Studies Hybridoma Bank, 1:10; mouse anti fast myosin, Sigma-Aldrich, 1:500; rabbit anti desmin, Abcam, 1:500) for one hour at room temperature. Cultures stained for the type I myosin marker, S58, were not immediately fixed, and rather received a 5-minute wash in 100% ethanol prior to incubation in S58 and blocking solution. Following rinsing, these cultures were fixed, as above, and rinsed again prior to incubation in any additional primary antibodies. Following additional rinses, cultures were incubated for one hour in appropriate secondary antibodies (DyLight 594 goat anti-mouse IgA, 1:500; Alexa Fluor 488 goat anti mouse IgG, 1:500; goat anti rabbit Alexa Fluor 488, 1:500) prepared in 0.3% Triton in PBS. Cultures were rinsed a final time before the coverslips were transferred to

microscope slides, immersed in lab-made mounting solution (1:2 Glycerol in 1XPBS and 0.03 mg/ml ρ-phenylenediamine), and covered with microscope slide coverslips. Cultures were imaged using an upright fluorescence microscope (Leica) and images underwent post-processing in Adobe Photoshop Software (Adobe).

Results

Establishment of an ES cell-derived muscle culture system

First, we wanted to establish the utility of the protocol, and to determine the timeline of differentiation of ES cell-derived muscle in culture. To do this, we utilized a WT mouse ES cell line to establish a baseline of muscle development in culture in heathy cells. After 1DIV cultured in DMEM and 2% horse serum, embryoid bodies containing desmin-positive, developing muscle were readily observed, and small puncta within these embryoid bodies positive for mature myosin were also observed (Fig. A.1A). By 4DIV, desmin-positive myoblasts were spread out in patches across the Matrigel with some evidence of myoblast fusion into more elongated cells. Some wispy, elongated myosin-positive cells were also occasionally observed (Fig. A.1A). Over the next week, staining for both desmin and myosin became more confluent. By 10DIV, desmin-positive myoblasts were readily fusing into elongated fibres and even more cells were observed expressing myosin (Fig. A.1A). At 13DIV, mature, striated, and confluent myosin-positive muscle fibres were observed, while the incidence of desmin-positive cells was reduced (Fig. A.1A). Over the next week, desmin immunofluorescence was dim or absent, while myosin staining revealed an abundance of healthy, striated, mature muscle fibres forming a confluent layer (Fig. A.1A). From these observations, we concluded that mature muscle fibres were consistently present by approximately 14DIV with some immature myoblasts still present, while by 22DIV, myoblasts were mostly absent (Fig. A.1A). Therefore, this protocol was effective at inducing muscle development from WT mouse ES cells.

Controlling muscle activity in vitro using optogenetics

To determine how muscle activity contributes to NMJ stability, we next needed to determine whether we could use this ES cell derived muscle protocol to generate muscle expressing ChR2. To generate this cell line, we crossed mice harboring the ChR2-GFP gene downstream of a stop codon flanked by loxP sites with mice expressing Cre recombinase under the control of the skeletal muscle-specific HSA promoter. The offspring of this cross thus express ChR2-GFP in mature skeletal muscle. ES cells, referred to as Ai32H1 cells, were obtained from these mice and cultured using our muscle development protocol.

Ai32H1 muscle developed similarly to WT muscle and were responsive to stimulation with 488 nm light (Supplemental Video). Interestingly, these ChR2 muscle cultures were of mixed muscle fibre type and displayed staining for both fast and slow myosin (Fig. A.2A). This observation contrasted with the WT muscle cultures, which only had fibres expressing fast myosin (Fig. A.2A). Interestingly, the passive activity in Ai32H1 cultures when exposed only to ambient light was also greater than that of the WT muscle cultures. This difference in fibre type composition could be an important distinction to exploit in future experiments that would allow us to investigate MN-muscle interactions *in vitro* in the presence of different muscle fibre types, both in the context of ALS and during normal development.

Discussion

We have shown here that this muscle differentiation protocol, previously described in human iPSCs, is efficient at inducing the differentiation of skeletal muscle from two different mouse ES cell lines. By two weeks in culture, confluent, myosin-expressing muscle fibres were observed that displayed both passive, and light-evoked (in the case of the Ai32H1 muscle) contractile capabilities. This is therefore an encouraging first step towards developing a single-organism neuromuscular model system to investigate the respective roles of MN and muscle activity *in vitro.* Future work in this laboratory will seek to evaluate the function of ESCMN and ES muscle co-cultures in comparison to our previously published work utilizing myotubes isolated from chick embryos.

In comparison to the time course of differentiation reported by Xu and colleagues in 2013 in iPSCs, we found that our cultures matured more quickly. They reported that cultures did not express the gene for myosin heavy chain until approximately day 36 (Xu et al., 2013), whereas we noticed evidence of myosin staining as early as 4 DIV, with confluency achieved by 2 weeks. Further, the previous study observed strong desmin-positive staining in muscle cultures at 36 DIV (Xu et al., 2013), which had vanished in our cultures by 21 DIV. These differences indicate that our cultures were faster to mature *in vitro* than was previously described in iPSCs. This was to be expected based on the known relative differentiation rates of mouse vs human cells *in vitro*. Given that mouse ES cells differentiated more quickly into muscle, we concluded that this protocol was efficient at producing mature muscle *in vitro* and would be feasible to routinely perform in the laboratory.

Our finding that WT ES muscle cultures express predominantly fast myosin, while the more active Ai32H1 muscle cultures express a slower, mixed muscle fibre-type composition is unsurprising considering the relationship between muscle fibre activity and fibre type *in vivo* (Burke et al., 1973). Slow motor units, comprised of a small motor neuron and the slow myosin-expressing muscle fibres that it innervates, are relatively active throughout life given the relatively high input resistance of these MNs (Fleshman et al., 1981; Kernell, 2006). A higher input resistance means that less current is needed to depolarize the cell to threshold, and therefore action potentials are generated much more readily, making these motor units the easiest to recruit (Fleshman et al., 1981; Zengel et al., 1985; Kernell, 2006). Easier generation of action potentials in MNs of slow motor units, therefore, corresponds to greater activity in slow-twitch muscle fibres. In contrast, fast-twitch muscle fibres are relatively inactive given the greater threshold of activation required by their innervating motor neurons (Kernell, 2006). There is a general matching of neuronal and muscular properties, and, given that MNs of slow motor units are small and have thin axons, they are more likely to be associated with relatively weak, slow, and fatigue resistant muscle fibres (Henneman, 1957; Henneman et al., 1965a). These types of motor units are essential for tonic activity such as postural control. It therefore stands to reason that, given the greater activity of the Ai32H1 muscle, that myosin isoform expression would be driven towards a more slow-twitch phenotype. It has also been

previously shown that changes in muscle activity are sufficient to drive these changes in muscle fibre type (Pette and Staron, 2000).

Interestingly, during development and later life, muscle fibre type is largely determined by the innervating MN type and, consequently, its activity (Kernell, 2006). However, most primary myotubes (i.e. the first wave of myotubes to differentiate during development) have slow, myosin type I expression, which they tend to maintain throughout life. Although some do end up switching their fibre type composition (Kernell, 2006). Similarly, many secondary myotubes end up as fast muscle fibre types (Kernell, 2006). Therefore, *in vivo,* there does not necessarily seem to be a default muscle fibre type that develops. However, in our *in vitro* model, fast muscle fibre types seem to be the default given that slow muscle fibres are only achieved in cultures with increased activity. It will be interesting in future experiments to determine whether the fibre-type composition of the WT muscle will change when co-cultured with MNs and synapses are formed.

The primary challenge that may interfere with the utility of this model is that the Ai32H1 muscle, in particular, is highly active. Due to this increased activity, it was not uncommon for cultures to become detached from the Matrigel substrate. This poses a challenge if these ES cell-derived muscle cultures will be used in co-culture with MNs. If the muscle fibres are too active and tear off from the substrate, this will damage the muscle and any axonal outgrowth. Torn muscle fibres also tend to bunch together, posing a challenge for imaging. We are, therefore, currently pursuing strategies to limit uninduced activity in these cultures.

In conclusion, this modified ES cell derived muscle protocol was efficacious at inducing differentiation of mouse ES cells from two different lines into mature, myosin-expressing muscle fibres. This system is therefore a promising candidate for obtaining single-organism co-cultures than could be used to study neuromuscular development and disease. Utilizing ChR2-expressing muscle cultures also allows us to independently activate MNs and muscle fibres to better elucidate whether MN and/or muscle activity are beneficial in ALS.

Appendix A Figures

Figure A.1. Time course of desmin and myosin staining in WT ES cell derived muscle. **A,** Top rows: representative desmin-positive staining from 1 to 22 DIV in WT ES cell derived muscle cultures. Bottom rows: time course of fast myosin-positive staining. Scale = 100 μm.

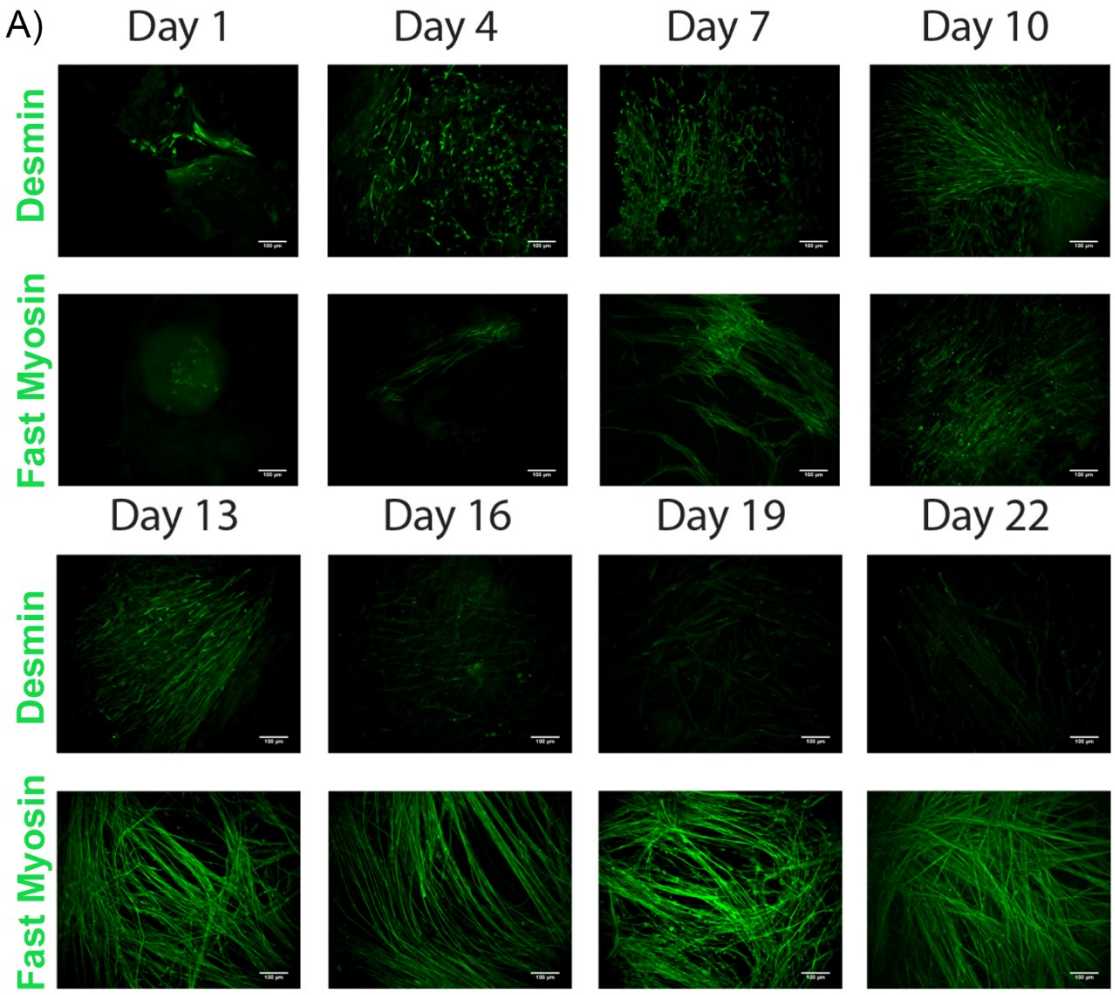
A)
Day 1
Day 4
Day 7
Day 10
Desmin
Fast Myosin
Day 13
Day 16
Day 19
Day 22
Desmin
Fast Myosin

Figure A.2. Expression of fast and slow myosin in WT and Ai32H1 muscle cultures. **A,** Representative images of ES cell derived muscle cultures stained for fast myosin (white) and S58 (slow myosin) (green). Scale = 50 μm.

A)

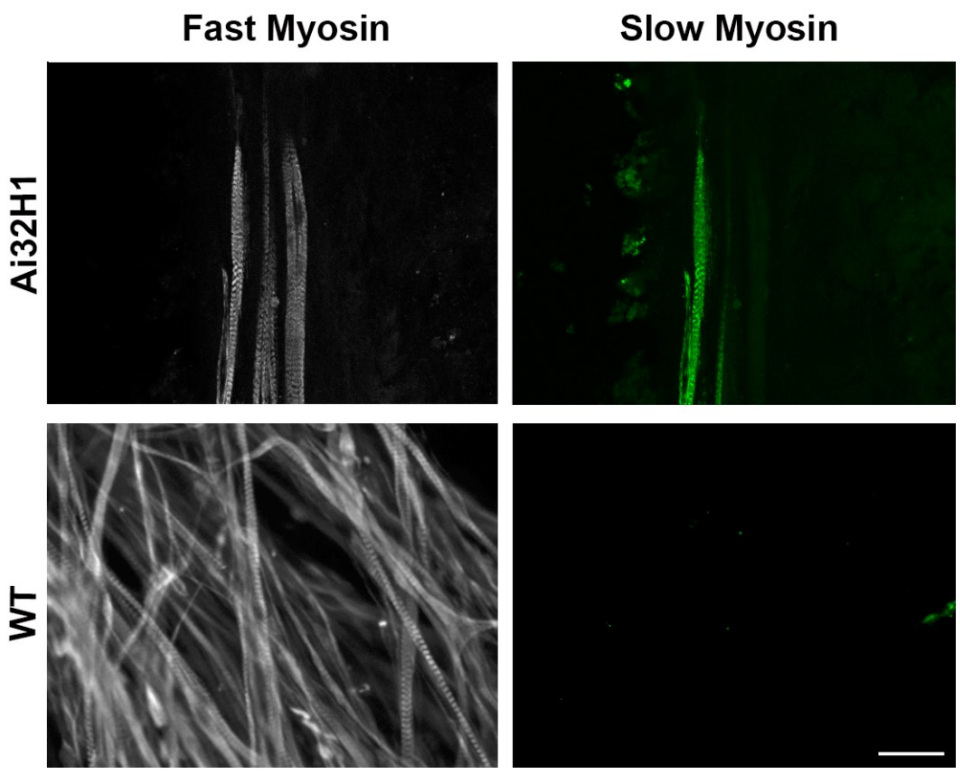

APPENDIX B: SUPPLEMENTAL MATERIAL

Supplemental Video. Light-activated contraction of Ai32H1 muscle cultures. Movie showing contraction of ChR2-expressing ES cell derived muscle in response to pulses of 488 nm LED light. This video is available for viewing on DalSpace.